

# Tractable Reserve Scheduling Formulations for Alternating Current Power Grids with Uncertain Generation

O.A. ter Haar

Master of Science Thesis



# **Tractable Reserve Scheduling Formulations for Alternating Current Power Grids with Uncertain Generation**

MASTER OF SCIENCE THESIS

For the degree of Master of Science in Systems and Control at Delft  
University of Technology

O.A. ter Haar

April 21, 2017

Faculty of Mechanical, Maritime and Materials Engineering (3mE) · Delft University of  
Technology



Copyright © Delft Center for Systems and Control (DCSC)  
All rights reserved.



DELFT UNIVERSITY OF TECHNOLOGY  
DEPARTMENT OF  
DELFT CENTER FOR SYSTEMS AND CONTROL (DCSC)

The undersigned hereby certify that they have read and recommend to the Faculty of  
Mechanical, Maritime and Materials Engineering (3mE) for acceptance a thesis  
entitled

TRACTABLE RESERVE SCHEDULING FORMULATIONS FOR ALTERNATING CURRENT  
POWER GRIDS WITH UNCERTAIN GENERATION

by

O.A. TER HAAR

in partial fulfillment of the requirements for the degree of  
MASTER OF SCIENCE SYSTEMS AND CONTROL

Dated: April 21, 2017

Supervisor(s):

\_\_\_\_\_  
Vahab Rostampour, M.Sc

\_\_\_\_\_  
Dr. ir. Tamás Keviczky

Reader(s):

\_\_\_\_\_  
Prof. ir. Mart A.M.M. van der Meijden

\_\_\_\_\_  
Dr. Jacob W. van der Woude



---

# Abstract

The increasing penetration of wind power generation introduces uncertainty in the behaviour of electric power grids. This work is concerned with the problem of day-ahead reserve scheduling (RS) for power systems with high levels of wind power penetration, and proposes a novel set-up that incorporates an alternating current (AC) Optimal Power Flow (OPF) formulation. The OPF-RS problem is non-convex and in general hard to solve. Using a convex relaxation technique, we focus on systems with uncertain generation and formulate a chance-constrained optimization problem to determine the minimum cost of production and reserves. Following a randomization technique, we approximate the chance constraints and provide a-priori feasibility guarantees in a probabilistic sense. However, the resulting problem is computationally intractable, due to the fact that the computation time complexity grows polynomially with respect to the size of the power network and scheduling horizon.

In this thesis, we first use the so-called scenario approach to approximate a convex set which contains almost surely the probability mass distribution of underlying random events. We rely on the special property of reserve scheduling problems which leads to linear constraint functions with respect to the uncertain parameters. We can therefore formulate a robust problem for only the vertices of the approximated set. Using the proposed approach, the number of scenarios is reduced significantly which is beneficial for the tractability. Such a formulation requires the power network state to only be feasible for all vertices of the convex approximated set. To even further relax such a requirement, we develop a novel RS formulation by considering the network state as a non-linear parametrization function of the uncertainty. By using a conic combination of matrices, only three positive semidefinite constraints per time step are considered. Unlike existing works in RS, our proposed parametrization has a practical meaning and is directly related to the distribution of reserve power. Such a reformulation yields a reduction in computational complexity of OPF-RS problems.

Finally, we extend our results to a more realistic size of power grids, using sparsity pattern and spatiality (multi-area) decomposition of the power networks, leading to a decomposed semidefinite programming (SDP) problem. To solve the SDP in a distributed setting, we formulate a distributed consensus optimization problem, and then the alternating direction method of multipliers (ADMM) algorithm is employed to coordinate local OPF-RS problems between neighbouring areas. The theoretical developments in aforementioned cases were validated on a realistic benchmark system and a discussion on the tractability of the resulting optimization problems by means of computational time analysis is presented.





---

# Table of Contents

<b>1</b>	<b>Introduction</b>	<b>1</b>
1-1	Related work . . . . .	1
1-2	Contributions . . . . .	2
1-3	Structure . . . . .	3
<b>2</b>	<b>Preliminaries</b>	<b>5</b>
2-1	Notation . . . . .	5
2-2	Power system optimization problems . . . . .	5
2-2-1	Lay-out of power systems and frequency control . . . . .	6
2-2-2	Optimization problems in power system operation . . . . .	7
2-2-3	Increasing uncertainty due to renewable energy sources . . . . .	7
2-3	Semidefinite programs . . . . .	9
2-3-1	Definition of a semidefinite program . . . . .	9
2-3-2	Computational complexity of semidefinite programs . . . . .	9
2-4	Optimization under uncertainty . . . . .	10
2-4-1	Uncertain optimization problems . . . . .	11
2-4-2	Reformulating uncertain problems . . . . .	11
2-4-3	The scenario approach for chance constrained problems . . . . .	12
2-5	Alternating direction method of multipliers (ADMM) . . . . .	13
2-5-1	Using algorithms to solve optimization problems . . . . .	13
2-5-2	ADMM algorithm explained . . . . .	13
<b>3</b>	<b>Alternating Current Optimal Power Flow Reserve Scheduling Problem</b>	<b>15</b>
3-1	Optimal power flow (OPF) problem . . . . .	15
3-1-1	Formulation of OPF problem with deterministic wind power . . . . .	15
3-1-2	Computational complexity of the OPF problem . . . . .	18

3-2	Convexification of OPF problem . . . . .	18
3-2-1	Semidefinite relaxation of OPF problem . . . . .	18
3-2-2	Computational complexity of the convexified OPF problem . . . . .	19
3-3	Extending OPF problem to reserve scheduling (OPF-RS) . . . . .	20
3-3-1	Including uncertain wind power in convexified OPF problem . . . . .	20
3-3-2	Reserve power and reserve scheduling . . . . .	21
3-3-3	Formulating OPF-RS as a chance constrained program (CC-OPF-RS) . . . . .	22
3-4	Conclusions . . . . .	23
<b>4</b>	<b>Tractable Approximations for CC-OPF-RS Using the Scenario Approach</b>	<b>25</b>
4-1	Indirect scenario approach using vertex enumeration of uncertainty set . . . . .	25
4-1-1	Approximation of the uncertainty . . . . .	26
4-1-2	Robust OPF-RS by means of vertex enumeration . . . . .	27
4-1-3	Computational complexity of vertex enumerated OPF-RS . . . . .	29
4-2	Direct scenario approach using conic parametrization of network state . . . . .	30
4-2-1	Direct scenario approach and tractability issues . . . . .	30
4-2-2	Tractability through conic parametrization of scenario state . . . . .	31
4-2-3	Conic parametrization of generic network state for OPF-RS . . . . .	32
4-2-4	Scenario approach for parametrization and computational complexity . . . . .	35
4-3	Conclusions . . . . .	36
<b>5</b>	<b>Decomposition of OPF-RS Problems</b>	<b>39</b>
5-1	Sparsity decomposition for OPF-RS problems . . . . .	39
5-1-1	The chordal theorem and matrix completion . . . . .	40
5-1-2	Sparsity decomposition method applied to OPF problem . . . . .	41
5-1-3	Rank-one matrix completion algorithm . . . . .	42
5-2	Multi-area decomposition of OPF-RS problems . . . . .	43
5-2-1	Formulating multi-area OPF problem . . . . .	44
5-2-2	Distributed solving of multi-area OPF problem with ADMM algorithm . . . . .	48
5-2-3	Extension to multi-area OPF-RS problems . . . . .	50
5-3	Conclusions . . . . .	54
<b>6</b>	<b>Simulation Study</b>	<b>57</b>
6-1	Simulation set up . . . . .	57
6-1-1	Modelling wind power and power system . . . . .	57
6-1-2	Running optimization and extracting solutions . . . . .	59
6-1-3	Testing solutions with power flow simulation . . . . .	60
6-1-4	Benchmarking with direct current model . . . . .	60
6-2	Results for tractable approximations of CC-OPF-RS . . . . .	62
6-2-1	Optimization results for tractable approximations . . . . .	62

---

6-2-2	Comparing generator dispatch and reserve distribution . . . . .	64
6-2-3	Violation levels based on power flow simulations . . . . .	68
6-3	Results for sparsity decomposition method . . . . .	72
6-3-1	Optimal solutions for the sparsity decomposed formulations . . . . .	72
6-3-2	Violation levels for sparsity decomposed formulations . . . . .	72
6-4	Simulation results for multi-area networks . . . . .	75
6-4-1	Decomposition set-up . . . . .	75
6-4-2	Selection of step-size for ADMM algorithm . . . . .	76
6-4-3	Simulation results for multi area problems . . . . .	77
6-5	Conclusions . . . . .	81
<b>7</b>	<b>Conclusions</b>	<b>83</b>
<b>8</b>	<b>Future Research Directions</b>	<b>85</b>
8-1	Extensive testing of tractable reformulations . . . . .	85
8-1-1	Testing with different wind models . . . . .	85
8-1-2	Application of indirect scenario approach to different OPF-RS formulations	86
8-1-3	Different approximations of uncertainty set to reduce conservatism . . . . .	86
8-2	Extending application of sparsity decomposition methods . . . . .	86
8-2-1	Sparsity decomposition for large scale OPF-RS problems . . . . .	86
8-2-2	Sparsity decomposition for local matrices of multi-area decomposition . . . . .	87
8-3	Distributed approaches for OPF-RS problems . . . . .	87
8-3-1	Distributed implementation of multi-area decomposition . . . . .	87
8-3-2	Varying wind samples between agents in multi-area decomposition . . . . .	87
8-3-3	Different consensus algorithm for multi-area decomposition . . . . .	88
<b>A</b>	<b>Direct Current Modelling Framework</b>	<b>89</b>
A-1	Classical direct current (DC) OPF . . . . .	89
A-2	Integrating wind power in DC OPF . . . . .	91
	<b>Glossary</b>	<b>95</b>



---

# List of Figures

2-1	Comparison traditional and modern networks . . . . .	8
4-1	Illustration of approximation of the uncertainty . . . . .	28
4-2	$X, P(\delta)$ plot for a (parametrized) scenario program with $d = 1, N_s = 3$ . . . . .	32
4-3	Schematic overview of different scenario approaches . . . . .	36
5-1	Illustration of the maximal cliques of the IEEE 14-bus network . . . . .	40
5-2	Comparison of obtained voltage profile . . . . .	43
5-3	Simple example of a multi-area network: a 4-bus network with two areas . . . . .	45
6-1	Load, wind forecast and wind scenario trajectories as used in optimization . . . . .	58
6-2	Schematic overview of the IEEE 30 bus test system . . . . .	59
6-3	Schematic overview of optimization and simulation process for the (C)DC . . . . .	61
6-4	Schematic overview of optimization and simulation processes for the proposed approaches . . . . .	62
6-5	Average computational time for VE-OPF-RS . . . . .	63
6-6	Generator dispatch per hour for different formulations for the 30-bus test case . . . . .	65
6-7	Up- and downspinning reserve distribution vectors per generator and hour for different formulations for the 30-bus test case . . . . .	66
6-8	Generator dispatch and reserve power for VE-OPF-RS . . . . .	67
6-9	Generator dispatch and reserve power for SP-OPF-RS . . . . .	68
6-10	Relative line loading for all hours and scenarios per line for the 30-bus test case . . . . .	69
6-11	Empirical violation level of lineflow limit for different formulations for the 30-bus test case . . . . .	70
6-12	Relative bus voltages for all hours and scenarios per line for the 30-bus test case . . . . .	71
6-13	Generator dispatch per hour for different sparsity decomposed formulations for the 30-bus test case . . . . .	73

---

6-14	Graphical display of up- and downspinning reserve distribution vectors per generator and hour for different formulations for the 30-bus test case . . . . .	74
6-15	Empirical violation level of lineflow limit for different formulations for the 30-bus test case . . . . .	75
6-16	Schematic overview of the decomposed 28-bus test system . . . . .	76
6-17	Effect of varying step-size $\mu$ on the convergence of ADMM algorithm . . . . .	77
6-18	Generator dispatch per hour for centralized and distributed solutions for the 28-bus test case . . . . .	79
6-19	Graphical display of up- and downspinning reserve distribution vectors per generator and hour for centralized and distributed solutions for the 28-bus test case . . . . .	80

---

# List of Tables

6-1	Cost coefficients used in optimization . . . . .	58
6-2	Optimization times and optimal objectives for the 30-bus test case . . . . .	63
6-3	Optimization times and optimal objectives for the (decomposed) 30-bus test case	72
6-4	Optimization times and optimal objectives for the 28-bus test case . . . . .	77





---

# Acknowledgements

First of all, I would like to thank my direct supervisors Tamás Keviczky and Vahab Rostampour, for the many fruitful discussions we had. I have learned so much from your critical attitude and positive work ethic, and sincerely hope we will stay in touch after my graduation.

My gratitude also goes out to my parents, who supported me throughout my entire education and helped make all this possible. I could not have done it without them.

Also, many thanks for my laborious sister, Carlijn, for proof-reading and understanding most of my work, in spite of her own busy schedule.

Finally, I would like to thank all my friends and girlfriend Emma in particular, for listening to my countless power system optimization stories and practise presentations.



---

# Chapter 1

---

## Introduction

Transmission system operators (TSOs) aim to find an economic operating point to satisfy the power demand and network constraints by solving an optimal power flow (OPF) problem. TSOs have to deal with increasing degrees of uncertainty due to high penetration of wind power generation. While wind power has clear environmental advantages, it is a highly variable and not fully controllable resource. This imposes novel challenges for TSOs, which cannot be solved optimally using traditional decision making tools.

One problem type that has become increasingly challenging is the reserve scheduling (RS) task, which deals with day-ahead scheduling of the reserve power to accommodate possible mismatches between power generation and demand. Due to its uncontrollable and unpredictable nature, the mismatch between forecast and actual wind power adds to the total uncertainty in the RS problem.

### 1-1 Related work

Traditional decision making tools for RS problems with this added uncertainty yield very conservative and costly solutions. Stochastic variants of the RS problem, where violations are allowed with a small probability to achieve better performance, have received a lot of attention in the past few years, see [1, 2, 3, 4, 5, 6] and the references therein. In these approaches, a stochastic RS problem is formulated using a lossless DC model based on the assumption of constant voltage magnitudes and small voltage angles, while ignoring the active power losses [7]. It is worth mentioning that these assumptions do not hold in general and may lead to sub-optimality or even infeasibility when implemented on real world systems, especially for networks under a high degree of stress [8].

The use of an alternating current (AC) representation of the power network enables the stochastic RS formulation to accurately model the effect of large deviations of wind power from its forecast value, and to offer a-priori suitable reserves such that both real and reactive power, and complex-valued voltage are globally optimal. Due to the non-convexity of the OPF problem, identifying such an optimal operating point of a power system may not be

straightforward. In [9], different reformulations and relaxations of the AC OPF problem were presented and their connections were discussed. By means of semidefinite programming (SDP), in [9] a convex relaxation was provided under the existence of a rank-one SDP solution to guarantee the recovery of a globally optimal solution of the power network.

The RS problem incorporated with the OPF formulation has been introduced in [10, 11], where a chance-constrained OPF problem was formulated. With some modifications, motivated by practical observations, the authors in [10] provided a theoretical guarantee that the OPF-RS problem yields a rank-one feasible solution. Using a heuristic Monte Carlo sampling approach, they showed that the resulting optimization problem involves an OPF problem for each wind power profile. Our work is motivated by [10] to provide some results in a more systematic approach.

While preparing the final version of this work, [12] and [13] independently gave an approach to solve OPF-RS problem in each hour separately, based on the results in [11]. OPF-RS formulation in [12] is similar to [10] with some modifications, whereas in [13] the formulation is weaker compared to [10], since they relaxed the condition to distribute reserves among generators. Even though the authors in [10] presented a complete day-ahead OPF-RS formulation with up- and down spinning reserves, the results in the aforementioned references are limited either to heuristic or to a single hourly-based approaches with the relaxed conditions. The major barrier of representing the OPF-RS problem as an SDP is the necessity of defining a square SDP matrix variable, which makes the cardinality of scalar variables of OPF-RS problem quadratic with respect to the number of buses in power network. This may yield a very large-scale SDP problem for realistic large-scale power networks of interest, especially when a large number of operating states (and therefore a large number of matrix variables) need to be considered.

## 1-2 Contributions

Our work in this paper differs from the aforesaid references in two important aspects. We propose a procedure to determine a worst-case reserve requirement in each hour by vertex enumeration (VE) of all possible deviation of wind power scenarios from the forecast value. The outcome of VE determines the up- and down-spinning reserves with a desired level of probability. Using the OPF-RS problem, similarly to [10] with some modifications, we distribute the up- and down-spinning reserves among generators together with the generator dispatch planning for day-ahead schedules. As an alternative to the VE approach, we propose a second tractable reformulation of the OPF-RS problem, where we define the network state as a non-linear parametrization function of the uncertainty which implies positive-semidefiniteness while using only three matrix variables per time step. Unlike existing works in RS, the proposed parametrization has a practical meaning and is directly related to the distribution of reserve power.

Finally, we extend our results to a more realistic size of power grids, using sparsity pattern and spatiality (multi-area) decomposition of the power networks. To address the resulting high-dimensional SDP problem, we leverage the sparsity pattern in power networks to break down the large-scale positive-semidefinite constraints into small-sized constraints, similarly to [14, 15] We then propose a novel recovery algorithm to obtain a rank-one solution based

on the results in [16] to fit in our OPF-RS optimization problem. A spatial decomposition method of the OPF-RS problem for multi-area systems is presented. To solve the resulting SDP problem distributed, the alternating direction method of multipliers (ADMM) algorithm is employed to coordinate OPF-RS problems between neighbouring areas.

The theoretical developments in aforementioned cases were validated on a realistic IEEE test power system and a discussion on the tractability of the resulting optimization problems by means of computational time analysis is presented.

In summary, this work has the following contributions:

- Formulation of the AC OPF-RS problem as a scenario program with a-priori probabilistic feasibility guarantees;
- A tractable formulation of the AC OPF-RS problem using an indirect scenario-based approximation and vertex enumeration;
- A novel parametrization of the network state in the uncertainty, leading to a tractable formulation of the AC OPF-RS problem to which a direct scenario-based approximation is applied;
- The application of sparsity decomposition techniques to both tractable formulations of the AC OPF-RS problem;
- A multi-area decomposition framework for the AC OPF-RS problem, leading to a general consensus problem which is solved using ADMM;
- Validation of all the aforementioned points using power flow simulations on a realistic test case.

## 1-3 Structure

The rest of this work is organized as follows. In Chapter 2, we provide the reader with the preliminaries for the following chapters. Chapter 3 discusses the formulation of the AC OPF problem with reserve scheduling. In Chapter 4, two tractable approximations for this problem (vertex enumeration and conic parametrization) are proposed. In Chapter 5, we explain the different decomposition methods of OPF-RS problems, based on sparsity or control areas. In Chapter 6, we present the simulation results for all the proposed approaches. Finally, Section 7 provides some concluding remarks, and Chapter 8 directions for future work.



---

# Chapter 2

---

## Preliminaries

In this Chapter, some preliminary knowledge is provided, which helps the reader understand the following chapters. First, the notation used throughout this work is presented in Section 2-1. Power system optimization problems are introduced in Section 2-2. A class of optimization problems, the semidefinite programs (SDPs), is presented in Section 2-3. Some background on optimization under uncertainty and the scenario approach is provided in Section 2-4. An algorithm that can be used to solve large optimization problems, the Alternating Direction Method of Multipliers (ADMM), is introduced in Section 2-5.

### 2-1 Notation

$\mathbb{R}$ ,  $\mathbb{R}_+$  denote the set of real and positive real numbers,  $\mathbb{S}$ ,  $\mathbb{S}_+$  denote the set of symmetric matrices and positive-semidefinite matrices, respectively.  $\mathbb{C}$  denotes the set of complex numbers. Vectors are denoted by lower-case bold letters  $\mathbf{a} \in \mathbb{R}^n$ , capitals are reserved for matrices  $A \in \mathbb{R}^{n \times n}$ , and calligraphic letters  $\mathcal{A}$  are used to indicate sets.  $A^T$ ,  $A^*$ , and  $A^H$  are used for the transpose, complex conjugate and conjugate transpose, respectively. The cardinality of a set  $\mathcal{A}$  is denoted by  $|\mathcal{A}| = A$ .

### 2-2 Power system optimization problems

Electric power is used for a wide range of applications, and disruption of its delivery has significant economical and societal impact. Therefore, it is important to safeguard the continuous delivery of power. The economic and secure operation of a power system is key in achieving this. In this section, the basic concepts of power system optimization are introduced, without assuming any prior knowledge of power systems. The general lay-out of a power system is given in Section 2-2-1. After this, the optimization problems which ensure the economic and secure operation of power systems are introduced in Section 2-2-2. Finally, in Section 2-2-3 the added uncertainty due to renewable energy sources is explained.

### 2-2-1 Lay-out of power systems and frequency control

A power system consists of three parts: producers of energy, a transmission network, and consumers of energy. The producers of energy are connected at the ‘generation side’ of the network to the consumers of energy, at the ‘demand side’. Traditionally, power is produced by converting kinetic energy to electric energy with the use of a generator. The kinetic energy is drawn from an energy source, such as thermal energy from fossil or nuclear fuels, or potential energy from water behind a dam. All these forms of traditional power generation are called Hydro-Thermal Generation (HTG). Electric energy is then transported as alternating current over the transmission network, consisting of interconnected overhead lines, underground cables, and transformers. The consumers transform the electric current into a form of energy useful for them. A set of consumers connected to the same point in the grid is aggregated into a single ‘load’. A typical power system has multiple loads, which for example correspond to a urban area or a large industrial customer.

Power systems are organized per geographical region and operated by one Transmission System Operator (TSO) each. TSOs are responsible for the secure delivery of power to the demand side. To do this, they adjust the output of the generators, or the *generator dispatch*. Storage of power in the network is nearly impossible, so every produced Joule must be consumed almost instantaneously. If this is not the case, the frequency of the network will deviate from its nominal value. If the frequency of the network deviates too much, components may fail, causing local outages or even a total black-out. Therefore, it is very important to balance generation and load at all times.

As soon as a frequency deviation occurs, it is the task of a Transmission System Operator to undertake actions to bring the network frequency back the nominal value by issuing corrective actions. This task is called *frequency control*. The frequency control that TSO utilizes can be categorized into three categories: primary, secondary and tertiary frequency control.

Primary control is activated within seconds of the frequency deviation and serves to stop the change of frequency. It is deployed automatically without any intervention of the TSO, and can be seen as the reaction of the system on a frequency deviation. Primary control in traditional power systems consists of the local generator control loops. Because the moving parts of each generator are synchronized with the network frequency, a frequency deviation will cause the generator to rotate at a different speed, which in turn triggers local (mostly proportional) controllers. The local controllers aim to bring the generator back to its original set-point.

After the primary control has reacted to a frequency deviation, the secondary control will be activated. The response time for the secondary control is in the scale of tens of seconds to minutes. Whereas primary frequency control tries to bring the generators back to their original set-point, secondary frequency control changes the generator set-points. This is called providing *reserve* power, because it is not scheduled in advance. The reserve scheduling (RS) task of TSOs deals with the day-ahead scheduling of the reserve power to accommodate possible imbalances in the network. In this work, we consider asymmetric reserve distribution, which means that we distinguish between up- and downspinning reserve. Upspinning reserve is activated in case of a power deficit, downspinning in case of a surplus.

Finally, there is tertiary frequency control, where reserves are deployed that were previously off-line. Because this requires more time, the tertiary control typically takes places in the



scale of tens of minutes to hours or even days. The purpose of the tertiary control is to free the secondary reserve capacity or complement it if it is not enough to restore the frequency.

### 2-2-2 Optimization problems in power system operation

A TSO has to make numerous decisions regarding the network, ranging from long term planning to day-ahead unit commitment, reserve scheduling, and post-contingency safety assessment. On very different time-scales, the TSO wants to know what the effect of his decisions will be on the future state of the network. To help with this decision, several modelling frameworks for a power system have been developed.

Every producing, consuming or transmitting element of a power system has many components that interact with each other. It is therefore hard to model a power system in a very detailed way. However, a very useful model for the power system exists, as for example described by Andersson in [17]. In this model, the power system is represented by a simple connected undirected graph. The nodes of this graph are called buses. The loads and generators of the system are connected to the buses. The edges of the graph connecting the buses represent the transmission lines and transformers, which are aggregated using the so-called  $\Pi$ -model (see [17, §2.2.3]).

A power network is never really in steady state, because all the processes are dynamic. The currents and voltages alternate with the network frequency. Switching actions and changes in load and generation create all kind of transients through the network of transformers and lines. However, the time-scale of these events are usually so small that a steady state model of the network is algebraically justified [17]. A very useful variable to look at the steady state operation is power flow.

Given an operation state of the network, it is possible to find the power flows resulting from that operating state, by solving a Power Flow (PF) problem. This allows the TSO to simulate the behaviour of the network for a given operating state. If the operating state is not given a-priori, but can be chosen from a feasible set of operating states constrained by the electrical laws and operating limits of the network components, the problem is known as the Optimal Power Flow (OPF) [18, 19]. As the name suggests, this is an optimization problem, first formulated in 1962 by Carpentier et al. in [20]. The objective function and constraints can be adapted to formulate a problem for different time-scales and problem types. The OPF problem is involved in all decisions regarding the state of the network, and can be regarded as the key to efficient power system operation. Bienstock provides an extensive survey on the state-of-the-art of the solvers for the traditional (O)PF problems in [21].

### 2-2-3 Increasing uncertainty due to renewable energy sources

To preserve the world for future generations, it is imperative to reduce carbon emissions and the dependence on scarce natural resources. A more sustainable way to electric power generation is necessary. By far the most polluting process in electric power generation is power generation with fossil fuels. Therefore, TSOs are increasing the share of renewable energy sources in the energy mix.

Although many forms of renewable energy sources exist, Wind Power Generation (WPG) [22] has been the most significant form for the past 20 years, and will most likely remain prevalent

in the coming years. Although wind is a resource that cannot be depleted, it also cannot be controlled. Not only is the availability of wind-power sometimes limited and varies with time, it is also hard to predict the availability in the nearby future. Although wind forecasts are available and significantly improving [23], it is still not possible to predict the wind power output with great precision [24]. This makes wind power an uncertain power source, which adds to the total network uncertainty. Because there is more uncertainty, more reserves are necessary to provide enough capabilities for frequency control, as shown in Figure 2-1.

Wind power is modelled as an active power injection on a bus, such that a farm of wind turbines can be aggregated to a single uncertain power injection. This simplification enables the use of existing methods for power system analysis for this new type of energy.

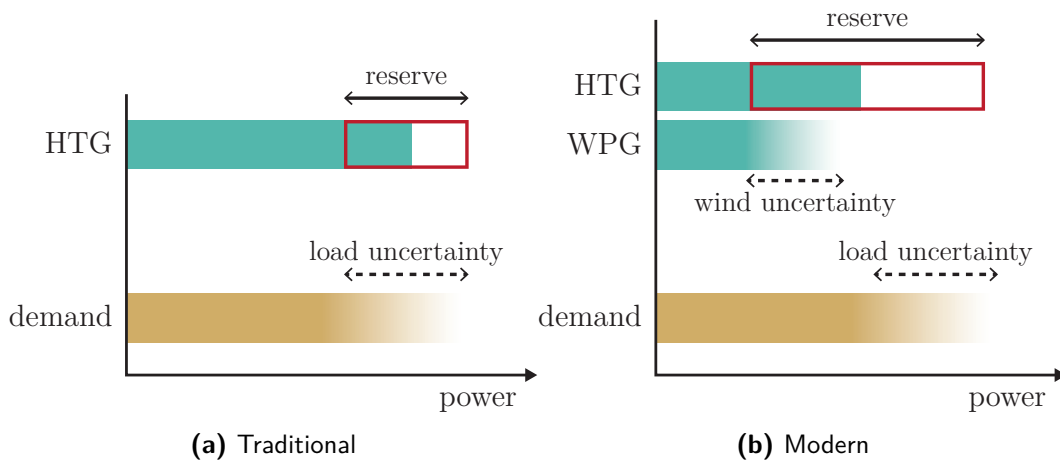


**Figure 2-1:** In traditional networks (left), reserve power is needed to bring balance to the network in the presence of load uncertainty. In modern networks (right), WPG adds more uncertainty to the network, resulting in larger reserve requirements.

The increase in reserve requirement is cause for concern. Extra up-spinning reserves need to come from existing generators, by setting them at a lower set point and thus allowing for more changes in speed. Due to this, the efficiency of the thermal plants might decrease. Another option to provide more reserve is building new controllable generators. This is obviously very costly and most of them would still run on fossil fuels. If reserve requirements are not planned carefully, the two effects described above might negate the positive impact wind energy is suppose to have on the reduction of carbon emissions. Therefore, a modern strategy to reserve planning is needed.

## 2-3 Semidefinite programs

In this section, semidefinite programs (SDPs) are introduced. The general concept and solving methods are given in Section 2-3-1, and the computational complexity of such problems is briefly discussed in Section 2-3-2.

### 2-3-1 Definition of a semidefinite program

A semidefinite program (SDP) is an optimization problem of the following form:

$$\underset{X \in \mathbb{S}^n}{\text{minimize}} \quad \text{Tr}(CX) \quad (2-1a)$$

$$\text{subject to} \quad \text{Tr}(A_i X) \leq b_i \quad i = 1, \dots, m \quad (2-1b)$$

$$X \succeq 0 \quad (2-1c)$$

where  $X$  is a symmetric matrix that is the decision variable, and  $C, A_1, \dots, A_m \in \mathbb{S}^n$  are known data matrices and  $b_1, \dots, b_m \in \mathbb{R}$  are known data vectors. The decision variable is subject to lie in the positive semidefinite cone (see [25], §2.2.5) through the last constraint (2-1c), or simply said, the last constraint encodes that  $X$  is positive-semidefinite (PSD). A matrix  $X$  is PSD when it satisfies the following criterion:

$$y^T X y \geq 0, \quad \forall y \in \mathbb{R}^n,$$

or equivalently, all the eigenvalues of  $X$  are non-negative, or its determinant is non-negative. To solve SDPs, the Interior Point Method (IPM) is used. The IPM works by adding a barrier function that encodes the PSD-cone to the objective. The barrier function increases to infinity when its argument goes outside the cone. In this way, it acts as a barrier that restricts the solution to be within the cone. The most used barrier function for the PSD cone is  $-\log \det X$ , which increases to  $+\infty$  as the determinant of  $X$  goes to zero. A new, unconstrained problem is then formulated, that has the barrier function and the original objective function as its new objective. Using a weight between these two terms, the IPM algorithm iterates by choosing a search direction taking a step in that direction that minimizes the current objective function, and updating the weight and start a minimization that uses the previous iterate as starting point. By starting with zero weight on the original objective, the first iterate will always be inside the cone. As the algorithm progresses, the weight on the original objective is increased (and the weight on the barrier function is thereby decreased), making sure that the final iterate of the algorithm is very close to the optimum of the original problem.

### 2-3-2 Computational complexity of semidefinite programs

To assess the performance of an algorithm, the worst-case computational complexity is examined. This can be used as indication of how the solving-time of a problem scales with the dimensions of that problem. For the IPM, the number of iterations needed to approximate the optimum within a given accuracy  $\alpha$  scales with the problem dimension  $n$  as  $\mathcal{O}(n^{1/2} \log(1/\alpha))$  [26]. This bound is obtained from worst-case complexity analysis, but in practice IPM algorithms can behave better. It has been observed for a wide variety of problems and problem

sizes, the number of iterations grows much slower (see for example [27, §6.4.4]). The number of iterations is typically between 5-50 [28].

The computational cost for each iteration therefore determines the complexity of an SDP algorithm. This is mostly determined by the cost of finding the search direction. In the most basic path-finding algorithm, this is the cost of finding and inverting the Hessian of the barrier function [26]. However, more sophisticated search directions are available. In general, the computational complexity of one iteration, i.e. the number of floating points operations needed, can be characterized by:

$$\beta m^2 n^2 + \gamma m n^3 + \xi m^3 + \mathcal{O}(m^2 n + n^2 m + n^3)$$

with  $\beta, \gamma, \xi > 0$  all (small) constants, depending on the search direction used [29]. See [30] for an overview of the best known values of these constants for various search directions. The last term uses the big-O notation  $\mathcal{O}(\cdot)$ , which denotes all terms that have at most the order of its argument. Since all terms that are of higher order will grow faster than lower order terms, these can be grouped together.

The total worst-case computational complexity to find an  $\alpha$ -solution, i.e. the objective value of the  $\alpha$ -solution is at most  $\alpha > 0$  above the optimum, is then given by the worst-case number of iterations times the worst-case complexity of one iteration:

$$\mathcal{O}((m^2 n^2 + m n^3 + m^3) n^{1/2} \log(1/\alpha)), \quad (2-2)$$

since all lower order terms of  $m$  and  $m$  will drop out<sup>1</sup>. Note that this concerns the worst-case computational complexity for a problem with dense data-matrices. In other words, nothing is assumed on the structure of the problem. Modern day solvers, such as SeDuMi [31], can achieve lower complexities by using sparsity in the problem structure. Whether or not this is the case for our problem, is outside the scope of this thesis. For all IPM solvers, computational complexity scales logarithmic with  $\alpha$ , and polynomial with  $m$  and  $n$ , regardless of whether they make use of the problem structure or not. For all proposed formulations, we will examine how the worst-case computational complexity scales in the number of buses of the network. To see how applicable our proposed algorithm is for the optimization of real-world networks, it must be able to handle a reasonable number of buses.

## 2-4 Optimization under uncertainty

Different approaches to solving optimization problems with uncertainty will be described in this section. A general optimization problem with uncertainty is first formulated in Section 2-4-1. After this, different reformulations of the uncertain constraints are given in Section 2-4-2. A randomization technique called the scenario approach is discussed more in depth in Section 2-4-3.

<sup>1</sup> $m^2 n^2$  and  $m n^3$  are of order four, while  $m^3$  is of order three. This term is however kept in the formulation, since the order of  $m$  might be higher than  $n$ , depending on the problem definition.

### 2-4-1 Uncertain optimization problems

A general optimization program has the following form:

$$\begin{aligned} & \underset{x \in \mathbb{R}^d}{\text{minimize}} && f(x) \\ & \text{subject to} && x \in \mathcal{X}, \end{aligned}$$

where  $f(x) : \mathbb{R}^d \rightarrow \mathbb{R}$  is an objective function which is optimized over the decision variable  $x \in \mathbb{R}^d$ . The decision variable is restricted to lie in the the feasible set  $\mathcal{X} \subseteq \mathbb{R}^d$ . The objective function and the feasible set are both deterministic, i.e. they do not contain uncertain variables, and therefore this program can be solved using various traditional methods, see for example [32] for a survey optimization techniques for deterministic problems.

The feasible set  $\mathcal{X}$  or the objective function  $f(x)$  often contains uncertainty. In the context of the power system optimization, this uncertainty arises in the wind power due to the unpredictability of the weather. In general, an optimization problem with uncertain parameters is called an uncertain program:

$$\text{Uncertain program: } \begin{cases} \underset{x \in \mathbb{R}^n}{\text{minimize}} & f(x) \\ \text{subject to} & x \in \mathcal{X}_\delta, \delta \in \Delta, \end{cases}$$

where  $\delta \in \Delta \subseteq \mathbb{R}^m$  is the uncertain parameter extracted from the (possibly infinite) set values  $\delta$  can take. The uncertain parameters are used to construct  $\mathcal{X}_\delta \subseteq \mathbb{R}^d$ , the uncertain feasible set. Note that the objective function can always be made deterministic with help of the epigraph notation. We assume that  $\mathcal{X}_\delta$  is a convex closed set for all  $\delta \in \Delta$ .

To make the uncertain program as formulated above well-posed, we need to know how  $\delta$  depends on the constraints  $\mathcal{X}_\delta$ . Furthermore, it is unclear if we are aiming for a solution that will be feasible even for the worst-case  $\delta$ , or a solution that will perform best given some realization of  $\delta$ . Different ways of dealing with uncertainty in an optimization problem to formulate a well-posed problem, are presented in the following.

### 2-4-2 Reformulating uncertain problems

One way to make an optimization problem with uncertainty well-posed is to force the solution to satisfy the intersection of *all* the possible constraint sets. This means every element of the set  $\Delta$  will be accounted for. This is called Robust Convex Programming (RCP) [33],

$$\text{RCP: } \begin{cases} \underset{x \in \mathbb{R}^n}{\text{minimize}} & f(x) \\ \text{subject to} & x \in \bigcap_{\delta \in \Delta} \mathcal{X}_\delta. \end{cases}$$

RCP finds a solution which is robust for all possible realizations of  $\delta$ . This can be desirable in the optimization of critical systems, since the solution is extremely conservative. The cost of this conservatism is an increased objective. Since the objective of power systems operation is not only safe, but also economic operation, the conservatism introduced by RCP is deemed undesirable.

A more sophisticated way of looking at uncertain problems is Chance Constrained Programming (CCP). Rather than satisfying all the constraints, CCP seeks for a solution that satisfies most of the constraints, such that only a small fraction of the constraints is violated. This approach is suitable for systems where an ‘occasional’ violation is allowed. One can argue that this is the case for power systems [12]. Every element in  $\Delta$  has a corresponding probability  $\mathbb{P}$  of being drawn. The small fraction of constraints that is violated should have a small probability of being drawn from  $\Delta$ , such that problem is constrained by the probability (chance) of violation. The uncertain parameters are removed from the constraints, and substituted for the probability of infeasibility:

$$\text{CCP: } \begin{cases} \text{minimize} & f(x) \\ \text{subject to} & \mathbb{P}[\delta \in \Delta : x \in \mathcal{X}_\delta] \geq 1 - \varepsilon, \end{cases}$$

where  $\varepsilon \in (0, 1)$  is defined as the violation level. The solution of this program is feasible with a probability  $1 - \varepsilon$  which is chosen a-priori (in advance). The selection of  $\varepsilon$  can be seen as the trade-off between risk aversion and performance. If  $\varepsilon$  is chosen to be very small, the solution is very similar to the solution of the RCP, and thus conservative. If  $\varepsilon$  is increased, the chance of constraint violation increases, but the performance improves.

### 2-4-3 The scenario approach for chance constrained problems

The CCP is in general intractable, due to the probability in the constraint. Therefore, a randomization technique called the scenario approach is introduced in [34]. The formulation of a Scenario Convex Program (SCP) is very similar to the RCP. Rather than satisfying all the possible constraints, a finite number of constraints is considered:

$$\text{SCP: } \begin{cases} \text{minimize} & f(x) \\ \text{subject to} & x \in \bigcap_{i=1}^N \mathcal{X}_{\delta_i}, \quad \{\delta_1, \dots, \delta_{N_s}\} \in \Delta^{N_s}, \end{cases}$$

where a set of independent and identically distributed (i.i.d.) realizations of the uncertain variable  $\{\delta_1, \dots, \delta_{N_s}\}$  is randomly drawn from  $\Delta \times \dots \times \Delta = \Delta^{N_s}$ . The solution should satisfy all constraints constructed from these realizations. Since this program is no longer chance constrained, it can be efficiently solved as long as  $N_s$  is not too large. The set of extractions  $\omega := \{\delta_1, \dots, \delta_{N_s}\} \in \Delta^{N_s}$  is called a multi-extraction and is a random variable. The solution from the SCP,  $x_{N_s}^*(\omega)$ , depends on this multi-extraction, and is thereby a random variable itself.

The authors of [34] show that by randomly selecting an appropriate number of realizations of the uncertain parameter, the solution of the SCP will be feasible for a large share of the unseen constraints. This holds in full generality, so regardless of the structure of the set of the constraints  $\Delta$  and the probability  $\mathbb{P}$ . The authors first showed that the solution of the SCP will be a solution for the CCP with a confidence of at least  $(1 - \beta)$ . In later work [35], the same authors defined a relation between  $N_s$  and the confidence and violation parameters. In [36], an explicit formulation for the lowest bound on  $N_s$  is derived:

$$N_s \geq \left\lceil \frac{2}{\varepsilon} \left( d - 1 + \log \frac{1}{\beta} \right) \right\rceil \quad (2-3)$$

where the  $\lceil \cdot \rceil$  operator denotes the smallest integer greater than or equal to its argument, and  $d$  is the dimension of the decision variables. The number of samples grows logarithmic with the inverse of  $\beta$ . This means that  $\beta$  can be decreased exponentially, and  $N_s$  will only increase linearly. Hence,  $\beta$  can be made almost arbitrarily small, so the confidence  $(1 - \beta)$  of the solution of the SCP can be made very high.

In [37], an extension of the scenario approach is introduced, called the scenario with certificates approach (SwC). This approach discerns between control variables and certificate variables. The latter are introduced for every scenario, and needed to provide a feasibility certificate. The authors prove that the bounds for  $N_s$  still hold for problems with this structure, when the dimension of the control variables is only used for  $d$ .

## 2-5 Alternating direction method of multipliers (ADMM)

The algorithmic approach for optimization problems is introduced in Section 2-5-1 and a specific algorithm, the Alternating Direction Method of Multipliers (ADMM) is discussed in Section 2-5-2.

### 2-5-1 Using algorithms to solve optimization problems

To solve an optimization problem, algorithms are used. An algorithm can be seen as a program that is initialized with some estimate of the solution,  $x^0$ . The program then iterates over a set of rules of the form  $x^{(k+1)} := f(x^{(k)})$  to update the estimate. The superscript  $(k)$  is used here to indicate the iteration number. If the estimate  $x^{(k)} \rightarrow x^*$  as  $k \rightarrow \infty$ , the algorithm is said to be *converging*. After each update step, the convergence criteria are checked, such as the minimum distance between the previous and current estimate or the maximum number of iterations. Once one of these criteria has been satisfied, the program is stopped and the current estimate will be the solution found by the algorithm.

### 2-5-2 ADMM algorithm explained

The alternating direction method of multipliers (ADMM) is an algorithm that solves convex optimization problems by breaking them into smaller pieces, each of which are then easier to handle [38]. It was first proposed by Glowinski et al. in [39] in 1975. It is a combination of the dual ascent method and the method of multipliers. Using this combination, the convergence properties of the method of multipliers are combined with the decomposability of the dual ascent.

To understand the ADMM algorithm, we first define a general separable problem:

$$\underset{x,y}{\text{minimize}} \quad f(x) + g(y) \quad (2-4a)$$

$$\text{subject to} \quad Ax + By = c \quad (2-4b)$$

where  $x \in \mathbb{R}^n, y \in \mathbb{R}^m$  are the optimization variables,  $f(x) : \mathbb{R}^n \rightarrow \mathbb{R}$  and  $g(y) : \mathbb{R}^m \rightarrow \mathbb{R}$  are closed, convex functions, and  $A \in \mathbb{R}^{p \times n}, B \in \mathbb{R}^{p \times m}$  are known matrices and  $c \in \mathbb{R}^p$  is a vector with known data. The problem as defined above is separable in the objective

function and coupled through the linear equality constraints. This is the standard form of an optimization problem, and problems with inequality constraints can be put in the form above by the introduction of slack variables.

The ADMM uses the augmented Lagrangian  $L_\mu(x, y, \lambda) : \mathbb{R}^n \times \mathbb{R}^m \times \mathbb{R}^p \rightarrow \mathbb{R}$ , based on the method of multipliers:

$$L_\mu(x, y, \lambda) = f(x) + g(y) + \lambda^T (Ax + By - c) + \frac{\mu}{2} \|Ax + By - c\|_2^2$$

This is the normal Lagrangian with an extra penalty term on the primal residual (i.e. how infeasible the current estimate is). This reduces to zero if the current estimate is feasible. The weight of this term is called the step size  $\mu \in \mathbb{R}_+$  and is a chosen constant. The advantage of including the extra term is that the problem is differentiable under more conditions than the original problem, and thus converges faster. Each iteration of the ADMM algorithm has the following steps: the primal  $x$ -update,  $y$ -update and the dual update:

$$x^{k+1} := \operatorname{argmin}_x L_\mu(x, y^k, \lambda^k) \quad (2-5a)$$

$$y^{k+1} := \operatorname{argmin}_y L_\mu(x^{k+1}, y, \lambda^k) \quad (2-5b)$$

$$\lambda^{k+1} := \lambda^k + \mu(Ax^{k+1} + By^{k+1} - c) \quad (2-5c)$$

where ‘argmin’ is the operator that returns the argument that minimizes the function. In the  $x$ -update (2-5a), the augmented Lagrangian is minimized over  $x$  using the previous values for  $y$  and  $\lambda$ . The obtained  $x$  is then used to minimize the Lagrangian over  $y$  in (2-5b). The updated versions of the primal variables  $x, y$  are then used to move the dual variable  $\lambda$  using the primal residual weighted by the penalty parameter in (2-5c).

It involves two minimizations of  $L_\mu$ , but each time only on one of the decision variables. Therefore, this optimization is less costly than the optimization of the coupled problem. After this, a closed form for updating  $\lambda$  is available. Depending on the structure of  $f(x), g(y)$ , an algebraic expression of (2-5a) and (2-5b) may be available, allowing for a direct calculation of  $x^{k+1}, y^{k+1}$ . ADMM has a high degree of robustness and a guaranteed convergence under very mild assumptions [38, 40]. This means that as  $k \rightarrow \infty$ , the solutions will converge to:  $x \rightarrow x^*, y \rightarrow y^*$ . In the implementation of ADMM algorithms, a stopping criterion is used on the residual. When these are small enough, the iterations are stopped and the current value for  $x^k, y^k$  is used as the optimal solution.



# Alternating Current Optimal Power Flow Reserve Scheduling Problem

The Optimal Power Flow (OPF) problem aims to find a feasible operating point of the network that minimizes the cost of power generation over the prediction horizon. In the Alternating Current<sup>1</sup>OPF problem, all network dynamics are taken into account. In this section, we first explain the model used, and define the OPF problem with a given wind power as a non-convex problem in Section 3-1. After this, we will apply a relaxation technique to convexify this problem in Section 3-2. The formulation will be extended to include uncertain wind power and reserve scheduling in Section 3-3, where the uncertain problem is transformed to a chance constrained problem. Finally, some concluding remarks are given in Section 3-4.

### 3-1 Optimal power flow (OPF) problem

The OPF problem for a given wind power trajectory is formulated in Section 3-1-1. Then, the computational complexity of this formulation is discussed in Section 3-1-2.

#### 3-1-1 Formulation of OPF problem with deterministic wind power

Consider a power system with a set of buses  $\mathcal{N}$ , a set of lines  $\mathcal{L} \subseteq \mathcal{N} \times \mathcal{N}$  and a set of controllable generator buses  $\mathcal{G} \subseteq \mathcal{N}$  such that  $|\mathcal{N}| = N_b$  and  $|\mathcal{G}| = N_G$ . The set of wind power buses is denoted by  $\mathcal{F} \subseteq \mathcal{N}$  such that  $|\mathcal{F}| = N_w$ . We will assume  $\mathcal{G} \cap \mathcal{F} = \emptyset$ , i.e. no wind in-feed is connected to a generator bus. The set  $\mathcal{T}$  forms the hourly-based prediction horizon and in this work  $|\mathcal{T}| = N_t = 24$ .  $\mathbf{p} \in \mathbb{R}^{N_b}$ ,  $\mathbf{q} \in \mathbb{R}^{N_b}$  and  $\mathbf{s} \in \mathbb{C}^{N_b}$  denote real, reactive and apparent power, respectively. Superscripts  $G, D, w$  are used to indicate generated, demanded and wind power, respectively. The decision variables are the generator dispatch  $\mathbf{p}_t^G, \mathbf{q}_t^G \in \mathbb{R}^{N_G}$  and the

---

<sup>1</sup>In the following, the AC-OPF problem will be referred to as the OPF problem. Any problem using the Direct Current (DC) modelling framework will be explicitly referred to as a DC problem.

complex bus voltages  $\mathbf{v}_t \in \mathbb{C}^{N_b}$  for each time step  $t \in \mathcal{T}$ . For the sake of brevity, a tilde denotes a set of variables over all time steps, such that  $\tilde{\mathbf{a}} := \{\mathbf{a}_t\}_{t \in \mathcal{T}}$ . Using the rectangular voltage notation:  $\mathbf{x}_t := [\text{Re}(\mathbf{v}_t)^\top \text{Im}(\mathbf{v}_t)^\top]^\top \in \mathbb{R}^{2N_b}$ , we follow [9, Lemma 1] to determine the data-matrices  $Y_k, Y_k^*, Y_{lm}, Y_{lm}^*, M_k \in \mathbb{S}^{2N_b}$ .

The objective is the cost of real power generation, expressed as a second order polynomial [41], where the coefficients  $\mathbf{c}^{\text{qu}}, \mathbf{c}^{\text{li}} \in \mathbb{R}_+^{N_G}$  correspond to the quadratic and linear cost of generation, respectively, and  $[\mathbf{c}^{\text{qu}}]$  represents a diagonal matrix with entries  $\mathbf{c}^{\text{qu}}$ . We now formulate the OPF problem with deterministic wind as follows:

$$\underset{\tilde{\mathbf{x}}, \tilde{\mathbf{p}}^G, \tilde{\mathbf{q}}^G}{\text{minimize}} \quad \sum_{t \in \mathcal{T}} (\mathbf{c}^{\text{li}})^\top \mathbf{p}_t^G + (\mathbf{p}_t^G)^\top [\mathbf{c}^{\text{qu}}] \mathbf{p}_t^G \quad (3-1a)$$

**subject to:**

1. **Power generation limits.** The generator dispatch is bounded by the upper and lower limits, such that  $\forall k \in \mathcal{G}, \forall t \in \mathcal{T}$ :

$$\underline{p}_k^G \leq C_k^G \mathbf{p}_t^G \leq \overline{p}_k^G, \quad (3-1b)$$

$$\underline{q}_k^G \leq C_k^G \mathbf{q}_t^G \leq \overline{q}_k^G, \quad (3-1c)$$

where  $\underline{\mathbf{p}}^G, \underline{\mathbf{q}}^G, \overline{\mathbf{p}}^G, \overline{\mathbf{q}}^G \in \mathbb{R}^{N_b}$  are the real and reactive lower and upper generation limits for every bus, and  $C^G \in \{0, 1\}^{N_b \times N_G}$  represents the connection matrix for the generators, for which the  $(i, j)$ -th entry is one if generator  $j$  is located at bus  $i$ , and zero otherwise.  $C_i^G$  represents the  $i$ -th row of the matrix, such that  $C_i^G \mathbf{p}_t^G$  is equal to the scalar  $p_{j,t}^G$  for all  $i \in \mathcal{G}$  and zero for all  $i \in \mathcal{N} \setminus \mathcal{G}$ .

2. **Power balance at every bus.** To achieve balance in every bus, all power generated (either by HTG or WPG) minus the demanded power has to equal the injected power, such that  $\forall k \in \mathcal{N}, \forall t \in \mathcal{T}$ :

$$\mathbf{x}_t^\top Y_k \mathbf{x}_t = C_k^G \mathbf{p}_t^G - p_{k,t}^D + C_k^w \mathbf{p}_t^w, \quad (3-1d)$$

$$\mathbf{x}_t^\top Y_k^* \mathbf{x}_t = C_k^G \mathbf{q}_t^G - q_{k,t}^D, \quad (3-1e)$$

where  $\mathbf{p}_t^w \in \mathbb{R}^{N_w}$  is the wind power and  $\mathbf{p}_t^D, \mathbf{q}_t^D \in \mathbb{R}^{N_b}$  are the real and reactive loads respectively, and  $C^w \in \{0, 1\}^{N_w \times N_b}$  denotes the connection matrix for the wind buses, which is defined in a similar fashion as  $C^G$ , such that  $C_i^w \mathbf{p}_t^w$  equals  $p_{j,t}^w$  if wind bus  $j$  is located at bus  $i$  and zero otherwise. The injected power at a bus is defined as the sum of all power flows over the lines connected to that bus, and is a quadratic function of the voltage vector. The wind power is considered as real power only, based on [41].

3. **Bus voltage limits.** To prevent component failure, the voltage magnitude for every bus is constrained by the engineering limits of the network. The squared bus voltage magnitudes are also quadratic functions of the voltage vector. The bus voltages are bounded  $\forall k \in \mathcal{N}, \forall t \in \mathcal{T}$ :

$$|\underline{v}_k|^2 \leq \mathbf{x}_t^\top M_k \mathbf{x}_t \leq |\overline{v}_k|^2, \quad (3-1f)$$

where  $|\underline{\mathbf{v}}|, |\overline{\mathbf{v}}| \in \mathbb{R}^{N_b}$  are the lower and upper voltage magnitude limits, respectively.

4. **Line limits.** To prevent sagging and congestion of lines, the magnitude of the apparent power flow over a line cannot exceed  $|\overline{s_{lm}}|$ . The squared apparent power is a squared sum of two quadratic terms of  $\mathbf{x}_t$ , such that we have  $\forall(l, m) \in \mathcal{L}, \forall t \in \mathcal{T}$ :

$$(\mathbf{x}_t^\top Y_{lm} \mathbf{x}_t)^2 + (\mathbf{x}_t^\top Y_{lm}^* \mathbf{x}_t)^2 \leq |\overline{s_{lm}}|^2,$$

which can be reformulated using the Schur-complement [25, §A.5.5] to form a linear matrix inequality. The fourth order dependence on the voltage vector is now reduced to quadratic terms:

$$\begin{bmatrix} -|\overline{s_{lm}}|^2 & \mathbf{x}_t^\top Y_{lm} \mathbf{x}_t & \mathbf{x}_t^\top Y_{lm}^* \mathbf{x}_t \\ \mathbf{x}_t^\top Y_{lm} \mathbf{x}_t & -1 & 0 \\ \mathbf{x}_t^\top Y_{lm}^* \mathbf{x}_t & 0 & -1 \end{bmatrix} \preceq 0. \quad (3-1g)$$

5. **Reference bus constraint.** All voltage angles are relative to the voltage angle of the reference bus. The voltage angle of the reference bus is fixed at zero  $\forall t \in \mathcal{T}$ :

$$\mathbf{x}_t^\top E_{\text{ref}} \mathbf{x}_t = 0, \quad (3-1h)$$

where  $E_{\text{ref}}$  is a diagonal matrix from the standard basis vector  $e_{N_b+i_{\text{ref}}}$ , and  $i_{\text{ref}}$  is the index of the reference bus.

**Remark 3.1.** The power balance constraints (3-1d) and (3-1e) can be used to reformulate the generator dispatch in terms of the voltage vector as follows  $\forall k \in \mathcal{N}, \forall t \in \mathcal{T}$ :

$$C_k^G \mathbf{p}_t^G = \mathbf{x}_t^\top Y_k \mathbf{x}_t + p_{k,t}^D - C_k^w \mathbf{p}_t^w, \quad (3-2a)$$

$$C_k^G \mathbf{q}_t^G = \mathbf{x}_t^\top Y_k^* \mathbf{x}_t + q_{k,t}^D. \quad (3-2b)$$

Using this definition, one can substitute for  $C_k^G \mathbf{p}_t^G$  and  $C_k^G \mathbf{q}_t^G$  in the generation limits, thus combining (3-1b) and (3-1c) with (3-2) to form the following box constraints  $\forall k \in \mathcal{N}, \forall t \in \mathcal{T}$ :

$$\underline{p}_k^G \leq \mathbf{x}_t^\top Y_k \mathbf{x}_t + p_{k,t}^D - C_k^w \mathbf{p}_t^w \leq \overline{p}_k^G, \quad (3-3a)$$

$$\underline{q}_k^G \leq \mathbf{x}_t^\top Y_k^* \mathbf{x}_t + q_{k,t}^D \leq \overline{q}_k^G, \quad (3-3b)$$

where the lower and upper generation limits have also been extended to  $\mathcal{N}$  using  $\underline{p}_k^G = \overline{p}_k^G = q_k^G = \overline{q}_k^G = 0 \forall k \in \{\mathcal{N} \setminus \mathcal{G}\}$ .

**Remark 3.2.** Following Remark 3.1 and Equation (3-1a), one can reformulate the cost per hour using only the voltage vector  $\mathbf{x}_t$ :

$$f_G^x(\mathbf{x}_t, \mathbf{p}_t^w, \mathbf{p}_t^D) := \sum_{k \in \mathcal{G}} C_k^G \mathbf{c}^{li} (\mathbf{x}_t^\top Y_k \mathbf{x}_t + p_{k,t}^D - C_k^w \mathbf{p}_t^w) + C_k^G \mathbf{c}^{qu} \left( (\mathbf{x}_t^\top Y_k \mathbf{x}_t + p_{k,t}^D - C_k^w \mathbf{p}_t^w) \right)^2. \quad (3-4)$$

It is important to note that this function is of order four with respect to  $\mathbf{x}$ , it can be made quadratic<sup>2</sup>. To streamline the presentation, these steps are skipped.

<sup>2</sup>The cost function can be made linear with the use of the epigraph notation (see also [25, §4.1.3]). The resulting inequality constraint can be converted to a linear matrix inequality using the Schur complement (see also [25, §A.5.5]), which yields a quadratic function of  $\mathbf{x}_t$ .

Following Remarks 3.1 and 3.2, the decision variables  $\tilde{\mathbf{p}}^G$  and  $\tilde{\mathbf{q}}^G$  can be removed. We can then reformulate Problem (3-1) in a more compact form. Since it is a function of the wind trajectory, it will be denoted by  $\text{OPF}(\tilde{\mathbf{p}}^w)$ :

$$\begin{aligned} & \underset{\tilde{\mathbf{x}}}{\text{minimize}} && \sum_{t \in \mathcal{T}} f_G^x(\mathbf{x}_t, \mathbf{p}_t^w, \mathbf{p}_t^D) \\ & \text{subject to} && \text{power balance constraints} && (3-3), \\ & && \text{bus voltage constraints} && (3-1f), \\ & && \text{line flow constraints} && (3-1g), \\ & && \text{reference bus constraint} && (3-1h). \end{aligned}$$

### 3-1-2 Computational complexity of the OPF problem

After removing the dependency on the generator dispatch,  $\text{OPF}(\tilde{\mathbf{p}}^w)$  is a quadratically constrained quadratic program (QCQP) in  $\tilde{\mathbf{x}}$  only. The data matrices  $Y_k, Y_k^*, Y_{lm}, Y_{lm}^*$  are indefinite, which makes the QCQP non-convex [9, 42]. Non-convex QCQPs form a problem class that in general is very hard to solve. Many problems from this class are NP-hard. In fact, the OPF problem is proven to be NP-hard [43]. This implies that the OPF problem in this formulation may not be solvable in polynomial time. Therefore, a formulation that can approximate the optimal solution of the OPF problem with less computational effort is presented next.

## 3-2 Convexification of OPF problem

Historically, Newton-Raphson solvers and other heuristic non-linear solving methods, such as genetic algorithms, have been used to solve the OPF problem directly [19, 44, 45]. An alternative to this approach is to convexify the problem to a program which is solvable in polynomial time with the help of efficient convex solvers. The resulting solution may be identical to the optimal solution of the non-convex program. A convexification method that has received increasing attention in the past years is the Semidefinite Relaxation (SDR) [46]. The application of the SDR to OPF problems has been proposed by [47], and its validity has been justified in [9] by examination of the duality gap for certain types of problems. For a large class of networks, the SDR has proven to be ‘tight’, i.e. the optimal solution of the SDR is equal to the optimal solution of the original non-convex OPF problem.

In Section 3-2-1,  $\text{OPF}(\tilde{\mathbf{p}}^w)$ , which is a non-convex QCQP, is convexified and formulated as an SDP using the semidefinite relaxation technique. After this, we will discuss the computational complexity of the resulting convexified problem in Section 3-2-2.

### 3-2-1 Semidefinite relaxation of OPF problem

The semidefinite relaxation is based on the insight that the objective and constraints are all quadratic functions of  $\mathbf{x}_t$ , and hence linear functions of the outer product of  $\mathbf{x}_t$ . This can be shown with the help of the trace-operator:  $\mathbf{x}^T A \mathbf{x} = \text{Tr}(A^T(\mathbf{x}\mathbf{x}^T))$ . Recognizing this allows us to reformulate  $\text{OPF}(\tilde{\mathbf{p}}^w)$  as an equivalent problem in a matrix variable  $W_t := \mathbf{x}_t \mathbf{x}_t^T \in \mathbb{S}^{2N_b}$ .

Similar to  $\mathbf{x}_t$ ,  $W_t$  represents the operating state of the network, and is therefore called the state matrix. We define  $\mathcal{W}(\mathbf{p}^w, \mathbf{s}^D) \subset \mathbb{S}^{2N_b}$  as the set of feasible network states, such that  $W_t \in \mathcal{W}$  indicates a feasible network state. This set is constructed by substituting every quadratic term of  $\mathbf{x}_t$  by its linear counterpart in the set of constraints defining  $\text{OPF}(\tilde{\mathbf{p}}^w)$ , and has the following characteristics:

$$\begin{aligned} \mathcal{W}(\mathbf{p}^w, \mathbf{s}^D) := \left\{ W \in \mathbb{S}^{2N_b} \mid \begin{aligned} & \underline{p}_k^G \leq \text{Tr}(Y_k W) + p_k^D - C_k^w \mathbf{p}^w \leq \overline{p}_k^G, & \forall k \in \mathcal{N}, \\ & \underline{q}_k^G \leq \text{Tr}(Y_k^* W) + q_k^D \leq \overline{q}_k^G, & \forall k \in \mathcal{N}, \\ & |v_k|^2 \leq \text{Tr}(M_k W) \leq |\overline{v}_k|^2, & \forall k \in \mathcal{N}, \\ & \begin{bmatrix} -|\overline{s}_{lm}|^2 & \text{Tr}(Y_{lm} W) & \text{Tr}(Y_{lm}^* W) \\ \text{Tr}(Y_{lm} W) & -1 & 0 \\ \text{Tr}(Y_{lm}^* W) & 0 & -1 \end{bmatrix} \preceq 0, & \forall (l, m) \in \mathcal{L}, \\ & \text{Tr}(E_{\text{ref}} W) = 0 \end{aligned} \right\}, \end{aligned}$$

where  $\mathbf{p}^w$  is the wind power, and  $\mathbf{s}^D = \mathbf{p}^D + i\mathbf{q}^D$  is the demanded power. Consider now the following formulation as an equivalent optimization problem to  $\text{OPF}(\tilde{\mathbf{p}}^w)$ :

$$\underset{\tilde{W}}{\text{minimize}} \quad \sum_{t \in \mathcal{T}} f_G(W_t, \mathbf{p}_t^w, \mathbf{p}_t^D) \quad (3-5a)$$

$$\text{subject to} \quad W_t \in \mathcal{W}(\mathbf{p}_t^w, \mathbf{s}_t^D), \quad \forall t \in \mathcal{T}, \quad (3-5b)$$

$$W_t \succeq 0, \quad \forall t \in \mathcal{T}, \quad (3-5c)$$

$$\text{rank}(W_t) = 1, \quad \forall t \in \mathcal{T}, \quad (3-5d)$$

where  $f_G$  is defined as in Equation (3-4), but with every occurrence of  $\mathbf{x}_t^T Y_k \mathbf{x}_t$  replaced by  $\text{Tr}(Y_k W_t)$ . Constraints (3-5c) and (3-5d) have been introduced to guarantee the exactness of the SDR and consequently, the equivalence of  $\text{OPF}(\tilde{\mathbf{p}}^w)$  and Problem (3-5).

Problem (3-5) is non-convex, due to the presence of the rank-one constraint (3-5d). Removing (3-5d) relaxes the problem to an SDP. It has been shown in [9] and later in [48] that the rank-one constraint can be dropped without affecting the solution for most power networks. In [10, Proposition 1], the authors showed that when the convex relaxation of the AC OPF problem has solutions with rank at most two, then, forcing any arbitrary selected entry of the diagonal of the matrix  $W_t$  to be zero results in a rank-one solution. This condition is practically motivated since the voltage angle of one of the buses (the reference bus) is often fixed at zero in practice. Moreover, the corresponding value of the objective function is identical to that of the original AC OPF problem.

Based on these results, we drop the rank constraint from the formulation. We denote by  $\text{C-OPF}(\tilde{\mathbf{p}}^w)$  the convexified version of  $\text{OPF}(\tilde{\mathbf{p}}^w)$  in  $\tilde{W}$ , i.e. Problem (3-5) with the rank-one constraints (3-5d) removed. The computational complexity of this problem will be discussed next.

### 3-2-2 Computational complexity of the convexified OPF problem

We now examine the computational complexity of the SDP  $\text{C-OPF}(\tilde{\mathbf{p}}^w)$  by means of a worst-case computational complexity analysis (see also Section 2-3 for a brief explanation). The

dimension of the decision variable for one hour of C-OPF( $\tilde{\mathbf{p}}^w$ ) is  $2N_b$ . This decision variable is constrained to be a member of the set of feasible states for that hour  $\mathcal{W}(\mathbf{p}_t^w, \mathbf{s}_t^D)$ , which is defined by  $4N_b$  power injection limits,  $2N_b$  bus voltage limits,  $N_L$  line flow limits and 1 reference bus constraint. If we extend this to the full horizon, the problem consists of  $T$  instances of these matrices and constraint sets. Therefore,  $n = 2N_b T$ ,  $m = (6N_b + N_L + 1)T$ . We can then substitute for  $n$  and  $m$  in the expression for the computational complexity given in Equation (2-2), and expand the result. The highest order term will determine the order of the worst-case complexity:

$$\begin{aligned} & \mathcal{O}([m^2 n^2 + mn^3 + m^3]n^{1/2} \log(1/\alpha)) \\ &= \mathcal{O}\left(\left[ ((6N_b + N_L + 1)T)^2 (2N_b T)^2 + ((6N_b + N_L + 1)T)(2N_b T)^3 \right. \right. \\ & \quad \left. \left. + ((6N_b + N_L + 1)T)^3 \right] (2N_b T)^{1/2} \log(1/\alpha)\right), \\ &= \mathcal{O}(T^{9/2} N_b^{9/2} \log(1/\alpha)), \end{aligned}$$

from which we can conclude that the computational complexity for the C-OPF( $\tilde{\mathbf{p}}^w$ ) scales polynomially in the number of buses  $N_b$  and prediction horizon  $T$  with order 4.5 and logarithmically in the desired accuracy of the solution.

### 3-3 Extending OPF problem to reserve scheduling (OPF-RS)

Next, C-OPF( $\tilde{\mathbf{p}}^w$ ) is extended to include uncertain wind power. In Section 3-3-1, we formulate a program that finds a feasible operating state of the network for the uncertain wind power. The mismatch that arises due to this uncertainty is balanced using reserve power. This is defined and incorporated in the formulation in Section 3-3-2 to form the OPF-RS problem. We then examine different strategies to reformulate the uncertain program in Section 3-3-3.

#### 3-3-1 Including uncertain wind power in convexified OPF problem

Our proposed formulation C-OPF( $\tilde{\mathbf{p}}^w$ ) solves an OPF problem, taking the actual wind power trajectory  $\tilde{\mathbf{p}}^w$  into account. However, this information is not available to the TSO in the day-ahead scheduling problem. The only information available at the time of decision making is the *forecast* wind power trajectory, denoted by  $\tilde{\mathbf{p}}^{w,f}$ . We here define the difference between a generic actual wind power realization and the forecast wind power, as the wind power mismatch at each time step, e.g.  $\mathbf{p}_t^m = \mathbf{p}_t^w - \mathbf{p}_t^{w,f}$ . Due to the fact that  $\tilde{\mathbf{p}}^m$  is a random variable, the following technical assumption is necessarily in order to proceed to the next steps.

**Assumption 1.**  $\tilde{\mathbf{p}}^m$  are defined on some probability space  $(\mathcal{P}, \mathfrak{B}(\mathcal{P}), \mathbb{P})$ , where  $\mathcal{P} \subseteq \mathbb{R}^{N_w \times N_t}$ ,  $\mathfrak{B}(\cdot)$  denotes a Borel  $\sigma$ -algebra, and  $\mathbb{P}$  is a probability measure defined over  $\mathcal{P}$ .

Besides this assumption, no further assumptions are made on  $\mathcal{P}$ , and it can thus be considered as an unbounded and unknown set. We now define a problem that finds the optimal generator

dispatch for the forecast scenario, and finds feasible operating states for a generic wind power trajectory:

$$\underset{\tilde{W}^f, \tilde{W}}{\text{minimize}} \quad \sum_{t \in \mathcal{T}} f_G(W_t^f, \mathbf{p}_t^{w,f}, \mathbf{p}_t^D) \quad (3-6a)$$

$$\text{subject to} \quad W_t^f \in \mathcal{W}(\mathbf{p}_t^{w,f}, \mathbf{s}_t^D), \quad \forall t \in \mathcal{T}, \quad (3-6b)$$

$$W_t \in \mathcal{W}(\mathbf{p}_t^{w,f} + \mathbf{p}_t^m, \mathbf{s}_t^D), \quad \tilde{\mathbf{p}}^m \in \mathcal{P}, \forall t \in \mathcal{T}, \quad (3-6c)$$

$$W_t^f \succeq 0 \quad \forall t \in \mathcal{T}, \quad (3-6d)$$

$$W_t \succeq 0 \quad \forall t \in \mathcal{T}, \quad (3-6e)$$

where  $W_t^f$  is related to the state of the network in the case of forecast wind power, and  $W_t$  is a generic network state for a generic wind power trajectory at time step  $t \in \mathcal{T}$ . Constraints (3-6b) and (3-6c) ensure feasibility for every network state, while constraints (3-6e) enforce positive semidefiniteness of all network states. Note that constraints (3-6) are identical to the constraints of C-OPF( $\tilde{\mathbf{p}}^{w,f}$ ) and C-OPF( $\tilde{\mathbf{p}}^w$ ) combined.

### 3-3-2 Reserve power and reserve scheduling

To ensure demand satisfaction even in the presence of uncertain wind power generation, the TSO employs reserve power, to mitigate the mismatch between actual wind power and forecast wind power using the controllable generators [1]. Define  $\forall k \in \mathcal{G}, \forall t \in \mathcal{T}$ :

$$C_k^G \mathbf{r}_t := C_k^G \mathbf{p}_t^G - C_k^G \mathbf{p}_t^{G,f}$$

where  $\mathbf{r}_t \in \mathbb{R}^{N_G}$  denotes the amount of reserve power at time step  $t$  and  $\mathbf{p}_t^{G,f}$  is used to denote the generator power in the forecast case. Following Remark 3.1, we have  $\forall k \in \mathcal{G}, \forall t \in \mathcal{T}$  and for  $\tilde{\mathbf{p}}^m \in \mathcal{P}$ :

$$\begin{aligned} C_k^G \mathbf{p}_t^G &= \text{Tr}(Y_k W_t) + p_{k,t}^D - C_k^{rw}(\mathbf{p}_t^{w,f} + \mathbf{p}_t^m), \\ C_k^G \mathbf{p}_t^{G,f} &= \text{Tr}(Y_k W_t^f) + p_{k,t}^D - C_k^{rw} \mathbf{p}_t^{w,f}, \end{aligned}$$

and therefore, one can obtain the reserve power in terms of the network states  $W_t$  and  $W_t^f$ , such that  $\forall k \in \mathcal{G}, \forall t \in \mathcal{T}$ :

$$C_k^G \mathbf{r}_t := \text{Tr}(Y_k (W_t - W_t^f)), \quad (3-7)$$

where the term  $-C_k^{rw}(\mathbf{p}_t^m)$  is dropped since we assumed<sup>3</sup>  $\mathcal{F} \cap \mathcal{G} \in \emptyset$ , and thus every  $C_k^{rw}$  contains only zeros for every  $k \in \mathcal{G}$ .

The elements of  $\mathbf{r}_t$  can be positive and negative (the upspinning and downspinning reserve power, respectively) such that they are deployed for a power deficit and surplus to bring balance to the network and satisfy the demanded power [41]. Following the automatic generator regulation (AGR) mechanism [11], we also define two vectors  $\mathbf{d}_t^{\text{us}}, \mathbf{d}_t^{\text{ds}} \in \mathbb{R}^{N_G}$  to distribute the amount of up- or downspinning reserve power among the available generator for each time

<sup>3</sup>Please note that this assumption is done to streamline the presentation, and is not restrictive for any of the obtained results.

step  $t \in \mathcal{T}$ . To obtain the optimal control strategy for the AGR mechanism, we consider the following equality constraint  $\forall k \in \mathcal{G}, t \in \mathcal{T}$ :

$$\text{Tr} \left( Y_k(W_t - W_t^f) \right) = -C_k^G \mathbf{d}_t^{\text{us}} \min(\mathbf{1}^\top \mathbf{p}_t^m, 0) - C_k^G \mathbf{d}_t^{\text{ds}} \max(\mathbf{1}^\top \mathbf{p}_t^m, 0), \quad (3-8)$$

where  $\mathbf{1}$  is a vector of appropriate dimensions with all entries equal to one. In order to always negate the wind power mismatch using the reserve power and bring balance to the power network, we enforce the sum of the distribution vectors to be equal to one, using the following constraints  $\forall t \in \mathcal{T}$ :

$$\mathbf{1}^\top \mathbf{d}_t^{\text{us}} = 1, \quad \mathbf{1}^\top \mathbf{d}_t^{\text{ds}} = 1, \quad (3-9)$$

Define  $\mathbf{r}_t^{\text{ds}}, \mathbf{r}_t^{\text{us}} \in \mathbb{R}^{N_G}$  such that  $\forall k \in \mathcal{G}, \forall t \in \mathcal{T}$ :

$$-C_k^G \mathbf{r}_t^{\text{ds}} \leq \text{Tr} \left( Y_k(W_t - W_t^f) \right) \leq C_k^G \mathbf{r}_t^{\text{us}}, \quad (3-10a)$$

$$0 \leq \mathbf{r}_t^{\text{us}}, \quad 0 \leq \mathbf{r}_t^{\text{ds}}, \quad (3-10b)$$

such that all positive and negative elements in  $\mathbf{r}_t$  are upper and lower bounded by  $\mathbf{r}_t^{\text{us}}$  and  $-\mathbf{r}_t^{\text{ds}}$ , respectively. The corresponding linear up- and downspinning cost coefficients  $\mathbf{c}^{\text{us}}, \mathbf{c}^{\text{ds}} \in \mathbb{R}_+^{N_G}$  are used to define the cost of reserve  $\forall t \in \mathcal{T}$ :

$$f_R(\mathbf{r}_t^{\text{us}}, \mathbf{r}_t^{\text{ds}}) := (\mathbf{c}^{\text{us}})^\top \mathbf{r}_t^{\text{us}} + (\mathbf{c}^{\text{ds}})^\top \mathbf{r}_t^{\text{ds}}.$$

Using  $\Xi := \{\tilde{W}^f, \tilde{W}, \tilde{\mathbf{d}}^{\text{us}}, \tilde{\mathbf{d}}^{\text{ds}}, \tilde{\mathbf{r}}^{\text{us}}, \tilde{\mathbf{r}}^{\text{ds}}\}$  as the set of decision variables, and combining our previous discussions with the optimization Problem (3-6), we are now in the position to formulate a convexified OPF problem in combination with a RS problem in a more compact form. This problem will be denoted OPF-RS:

$$\begin{aligned} & \underset{\Xi}{\text{minimize}} && \sum_{t \in \mathcal{T}} \left( f_G(W_t^f, \mathbf{p}_t^{w,f}) + f_R(\mathbf{r}_t^{\text{us}}, \mathbf{r}_t^{\text{ds}}) \right) \\ & \text{subject to} && \text{feasible forecast state} && (3-6b), (3-6d), \\ & && \text{feasible generic state} && (3-6c), (3-6e), \\ & && \text{reserve distribution constraints} && (3-8), (3-9), \\ & && \text{reserve requirements constraints} && (3-10a), (3-10b). \end{aligned}$$

### 3-3-3 Formulating OPF-RS as a chance constrained program (CC-OPF-RS)

Using a more compact notation, we represent OPF-RS as follows:

$$\text{OPF-RS: } \begin{cases} \underset{\Xi \in \mathcal{X}}{\text{minimize}} & f(\Xi) \\ \text{subject to} & g(\Xi, \tilde{\mathbf{p}}^m) \leq 0, \text{ for } \tilde{\mathbf{p}}^m \in \mathcal{P}, \end{cases}$$

where  $f(\Xi)$  is the objective function,  $g(\Xi, \tilde{\mathbf{p}}^m) \leq 0$  represents all constraints that are functions of the uncertainty (i.e. constraints (3-6c) and (3-8)), and  $\mathcal{X}$  is the deterministic feasible set, formed by all the remaining constraints. Note that  $\mathcal{X}$  is a convex set, since all deterministic



constraints are linear in the elements of  $\Xi$ . OPF-RS is an uncertain semi-infinite SDP, due to the unknown and unbounded set  $\mathcal{P}$ . It is therefore computationally intractable and in general difficult to solve.

One can transform OPF-RS into a robust program by enforcing the uncertain constraints to be satisfied for all possible values of the uncertainty:

$$\begin{aligned} & \underset{\Xi \in \mathcal{X}}{\text{minimize}} && f(\Xi) \\ & \text{subject to} && g(\Xi, \tilde{\mathbf{p}}^m) \leq 0, \forall \tilde{\mathbf{p}}^m \in \mathcal{P}. \end{aligned}$$

This worst-case robust approach in the case of power systems optimization is undesirable for two reasons: first of all, the bounds of  $\mathcal{P}$  might not be available to the TSO, or they might be so excessive that a feasible solution does not exist. Secondly, the solution for this program would be very conservative, since no violations are allowed. This would lead to a degradation of the objective, i.e. very high generation and reserve power costs. Therefore, a more sophisticated approach is considered.

All operating limits are given as nominal values. One can argue that if the operating limit for a certain component is exceeded for a short time, that this would not directly lead the failure of this component. The TSO can thus accept a (very low) risk of violation, rather than allow no violation at all. Therefore, we use the concept of chance constraint programming, as introduced in [6] for DC OPF problems. In this formulation, we introduce a risk level  $\varepsilon \in (0, 1)$  which acts as a tuning parameter for the optimization. The selection of  $\varepsilon$  can be seen as the trade-off between feasibility and performance. The uncertain problem OPF-RS can thus be transformed to chance constrained program (CCP), as follows:

$$\text{CC-OPF-RS: } \begin{cases} \underset{\Xi \in \mathcal{X}}{\text{minimize}} & f(\Xi) \\ \text{subject to} & \mathbb{P}[\tilde{\mathbf{p}}^m \in \mathcal{P} : g(\Xi, \tilde{\mathbf{p}}^m) \leq 0] \geq 1 - \varepsilon. \end{cases}$$

Although this formulation is a much better fit for the type of problem at hand, it is still intractable due to the chance constraint. In the next section, we propose a technique to approximate  $\mathcal{P}$  such that it contains the probability mass distribution of  $\mathcal{P}$  almost surely with a high level of confidence, which allows us to reformulate CC-OPF-RS in a tractable way.

### 3-4 Conclusions

The optimal power flow problem is formulated as a non-convex QCQP, after which the SDR technique is applied to obtain a convex program, C-OPF. This program was defined for a given wind trajectory, but these are uncertain in the context of the day-ahead scheduling problems. The extension is made to the RS problem, resulting in an uncertain program OPF-RS. Instead of solving a robust program for all possible values of the uncertainty, we have formulated OPF-RS as a chance constrained program, CC-OPF-RS. The formulation as a CCP is used, since occasional violations can be allowed to better deal with the uncertainty. CC-OPF-RS is intractable due to the chance constraints. In the following chapter, tractable approximations are proposed in order to find a solution for CC-OPF-RS.



# Tractable Approximations for CC-OPF-RS Using the Scenario Approach

In the previous chapter, the optimal power flow problem with reserve scheduling is formulated as a chance constrained program CC-OPF-RS. This problem is computationally intractable, due to the chance constraints. As explained in Section 2-4, the scenario approach can be used to obtain tractable problems for which the optimal solution approximates the optimal solution of CCPs with a predefined confidence level. In this chapter, two different ways of applying the scenario approach to obtain a tractable approximation for CC-OPF-RS are described.

In Section 4-1, an approximation of the uncertainty set is formulated as a CCP and the scenario approach is used to define a tractable formulation of this approximation. Next, a robust OPF-RS problem is formulated for the approximated set. Since the scenario approach is not applied directly to CC-OPF-RS this approach is called the *indirect* scenario approach.

The *direct* application of the scenario approach to CC-OPF-RS is then presented in Section 4-2. The obtained program is intractable due to the large number of computationally expensive PSD constraints. A novel parametrization of the generic network state is proposed, for which the problem becomes tractable. Finally, some concluding remarks are given in Section 3-4.

### 4-1 Indirect scenario approach using vertex enumeration of uncertainty set

In this section, we apply the indirect scenario approach to CC-OPF-RS. First, we approximate the uncertainty set  $\mathcal{P}$  with a convex set  $\mathcal{H}$ . In Section 4-1-1, the method is explained and a theoretical connection between  $\mathcal{P}$  and  $\mathcal{H}$  regarding the level of approximation is made. Next, we formulate a robust OPF-RS for the approximated uncertainty set in Section 4-1-2, as a tractable approximation of CC-OPF-RS. Finally, we examine the computational complexity of the obtained formulation in Section 4-1-3.

#### 4-1-1 Approximation of the uncertainty

It is now of interest to characterize a set  $\mathcal{H}$  which approximates  $\mathcal{P}$ . We assume for simplicity that  $\mathcal{H}$  is an axis-aligned hyperrectangular set, such that  $\mathcal{H} := \times_{t \in \mathcal{T}} [\underline{\mathbf{h}}_t, \bar{\mathbf{h}}_t] \subset \mathbb{R}^{N_w \times N_t}$ . This is not a restrictive assumption and any convex set could have been chosen instead as described in [49]. Vectors  $\bar{\mathbf{h}}_t \in \mathbb{R}^{N_w}$  and  $\underline{\mathbf{h}}_t \in \mathbb{R}^{N_w}$  define the bounds of the hyperrectangular set for all wind buses at each time step  $t \in \mathcal{T}$ . To determine  $\mathcal{H}$  with minimal volume which approximates  $\mathcal{P}$  with probability  $1 - \varepsilon$ , the following CCP is formulated:

$$\underset{\bar{\mathbf{h}}, \underline{\mathbf{h}}}{\text{minimize}} \quad \sum_{t \in \mathcal{T}} \|\bar{\mathbf{h}}_t - \underline{\mathbf{h}}_t\|_1 \quad (4-1a)$$

$$\text{subject to} \quad \mathbb{P}[\tilde{\mathbf{p}}^m \in \mathcal{P} : \mathbf{p}_t^m \in [\underline{\mathbf{h}}_t, \bar{\mathbf{h}}_t], \forall t \in \mathcal{T}] \geq 1 - \varepsilon. \quad (4-1b)$$

Following [34], we use a randomization Problem (4-1) with confidence level  $1 - \beta$ :

$$\underset{\bar{\mathbf{h}}, \underline{\mathbf{h}}}{\text{minimize}} \quad \sum_{t \in \mathcal{T}} \|\bar{\mathbf{h}}_t - \underline{\mathbf{h}}_t\|_1 \quad (4-2a)$$

$$\text{subject to} \quad \mathbf{p}_t^m \in [\underline{\mathbf{h}}_t, \bar{\mathbf{h}}_t], \forall t \in \mathcal{T}, \forall \tilde{\mathbf{p}}^m \in \mathcal{S}, \quad (4-2b)$$

where  $\mathcal{S} = \{\tilde{\mathbf{p}}^{m,1}, \tilde{\mathbf{p}}^{m,2}, \dots, \tilde{\mathbf{p}}^{m,N_s}\} \in \mathcal{P}^{N_s}$  is a multi-extraction of i.i.d. samples from  $\mathcal{P}$ . Denote  $\mathcal{H}_{\mathcal{S}}^*$  as the optimal solution for Problem (4-2), where the subscript  $\mathcal{S}$  is used to denote the dependency on the multi-extraction. We next provide the following theorem that provides a theoretical connection between  $\mathcal{H}_{\mathcal{S}}^*$  and  $\mathcal{P}$  by means of the level of approximation.

**Theorem 1.** *Fix violation level  $\varepsilon \in (0, 1)$  and confidence level  $\beta \in (0, 1)$ , and let  $N_s$  be the smallest integer such that*

$$N_s \geq \frac{2}{\varepsilon} (2N_t N_w + \log \frac{1}{\beta}), \quad (4-3)$$

*and construct the set  $\mathcal{S} = \{\tilde{\mathbf{p}}^{m,1}, \tilde{\mathbf{p}}^{m,2}, \dots, \tilde{\mathbf{p}}^{m,N_s}\} \in \mathcal{P}^{N_s}$ , and let  $\mathcal{H}_{\mathcal{S}}^*$  be the optimal solution for Problem (4-2). Then,*

$$\mathbb{P}^{N_s}[\mathcal{S} \in \mathcal{P}^{N_s} : \mathbb{P}[\tilde{\mathbf{p}}^m \in \mathcal{P} : \tilde{\mathbf{p}}^m \in \mathcal{H}_{\mathcal{S}}^*] \geq 1 - \varepsilon] \geq 1 - \beta,$$

where  $\mathbb{P}^{N_s}$  denotes a  $N_s$ -fold product probability.

*Proof.* The proof is a direct result of [49, Th. 1].  $\square$

The interpretation of Theorem 1 is as follows. Given a generic sample  $\tilde{\mathbf{p}}^m \in \mathcal{P}$ , the probability of  $\tilde{\mathbf{p}}^m \in \mathcal{H}_{\mathcal{S}}^*$  is greater than  $1 - \varepsilon$  with confidence level  $1 - \beta$ . In the following, we omit the subscript  $\mathcal{S}$  from  $\mathcal{H}_{\mathcal{S}}^*$ , for the sake of readability. Following the approach of [3], we now formulate a robust OPF-RS for  $\mathcal{H}^*$ :

$$\underset{\Xi \in \mathcal{X}}{\text{minimize}} \quad f(\Xi) \quad (4-4a)$$

$$\text{subject to} \quad g(\Xi, \tilde{\mathbf{p}}^m) \leq 0, \forall \tilde{\mathbf{p}}^m \in \mathcal{H}^*. \quad (4-4b)$$

We now use Theorem 1 to make the following proposition:

**Proposition 1.** *The optimal solution to Problem (4-4) is a feasible solution of CC-OPF-RS with confidence  $1 - \beta$ .*

*Proof.* Following Theorem 1, the solution to Problem (4-4) will be feasible for all of  $\mathcal{H}^*$ , which encloses at least  $1 - \varepsilon$  of the probability mass distribution of  $\mathcal{P}$  with confidence of at least  $1 - \beta$ . The optimal solution to Problem (4-4) is therefore feasible with a probability greater than or equal to  $1 - \varepsilon$  for a generic sample  $\tilde{\mathbf{p}}^m \in \mathcal{P}$  with confidence  $1 - \beta$ .  $\square$

Using Proposition 1, Problem (4-4) is almost surely a valid approximation for CC-OPF-RS, i.e. the optimal solution of Problem (4-4) has the same probabilistic guarantees with high confidence. Problem (4-4) is now reformulated to increase tractability.

#### 4-1-2 Robust OPF-RS by means of vertex enumeration

All uncertain constraints are linear with respect to the uncertainty  $\tilde{\mathbf{p}}^m$ , with the exception of (3-8), which is non-linear due to the presence of the max and min operators and repeated here for completeness:

$$\text{Tr} \left( Y_k (W_t - W_t^f) \right) = -C_k^G \mathbf{d}_t^{\text{us}} \min(\mathbf{1}^\top \mathbf{p}_t^m, 0) - C_k^G \mathbf{d}_t^{\text{ds}} \max(\mathbf{1}^\top \mathbf{p}_t^m, 0). \quad (3-8)$$

In fact, these operators lead to hybrid operation since the two terms on the right-hand side cannot be non-zero simultaneously, since  $\forall \alpha \in \mathbb{R}, \min(\alpha, 0) \max(\alpha, 0) = 0$ . It is straightforward to show that (3-8) is equivalent to  $\forall k \in \mathcal{G}, \forall t \in \mathcal{T}$ :

$$\text{Tr} \left( Y_k (W_t - W_t^f) \right) = \begin{cases} -C_k^G \mathbf{d}_t^{\text{us}} (\mathbf{1}^\top \mathbf{p}_t^m) & \text{if } \mathbf{1}^\top \mathbf{p}_t^m < 0, \\ -C_k^G \mathbf{d}_t^{\text{ds}} (\mathbf{1}^\top \mathbf{p}_t^m) & \text{if } \mathbf{1}^\top \mathbf{p}_t^m > 0, \\ 0 & \text{otherwise.} \end{cases}$$

Following this observation, we first split  $\mathcal{H}^*$  into its time steps, such that  $\mathcal{H}_t^* \subseteq \mathbb{R}^{N_w}$  and  $\times_{t \in \mathcal{T}} \mathcal{H}_t^* = \mathcal{H}^*$ , since  $g(\Xi, \tilde{\mathbf{p}})$  is decomposable over all the time steps. We then split  $\mathcal{H}_t^*$  into two sets  $\forall t \in \mathcal{T}$ :

$$\begin{aligned} \underline{\mathcal{H}}_t^* &= \left\{ \mathbf{p}_t^m \in \mathcal{H}_t^* \mid \mathbf{1}^\top \mathbf{p}_t^m \leq 0 \right\}, \\ \overline{\mathcal{H}}_t^* &= \left\{ \mathbf{p}_t^m \in \mathcal{H}_t^* \mid \mathbf{1}^\top \mathbf{p}_t^m \geq 0 \right\}, \end{aligned}$$

such that  $\times_{t \in \mathcal{T}} (\underline{\mathcal{H}}_t^* \cup \overline{\mathcal{H}}_t^*) = \mathcal{H}^*$ . Graphically,  $\underline{\mathcal{H}}_t^*$  and  $\overline{\mathcal{H}}_t^*$  are created by separating the hyperrectangle  $\mathcal{H}_t^*$  with a hyperplane that has normal  $\mathbf{1}$ , resulting in two convex polyhedral sets, as shown in Figure 4-1. Note that both sets have overlap for the case  $\mathbf{1}^\top \mathbf{p}_t^m = 0$ . For this specific case, there is no hybrid behaviour because the right-hand-side of (3-8) is 0 for all  $k \in \mathcal{G}$ . Then, the following problem:

$$\underset{\Xi \in \mathcal{X}}{\text{minimize}} \quad f(\Xi) \quad (4-5a)$$

$$\text{subject to} \quad g(\Xi, \tilde{\mathbf{p}}^m) \leq 0, \forall \tilde{\mathbf{p}}^m \in \times_{t \in \mathcal{T}} \underline{\mathcal{H}}_t^*, \quad (4-5b)$$

$$g(\Xi, \tilde{\mathbf{p}}^m) \leq 0, \forall \tilde{\mathbf{p}}^m \in \times_{t \in \mathcal{T}} \overline{\mathcal{H}}_t^*, \quad (4-5c)$$

is equivalent to Problem (4-4), and by Proposition 1 it will be an approximation of the optimal solution for CC-OPF-RS with confidence  $1 - \beta$ .

**Remark 4.1.** Since there is no hybrid behaviour in  $\underline{\mathcal{H}}_t^*$  and  $\overline{\mathcal{H}}_t^*$ , constraint (3-8) can be written as two separate linear constraints  $\forall k \in \mathcal{G}, \forall t \in \mathcal{T}$ :

$$\begin{aligned} \text{Tr} \left( Y_k (W_t - W_t^f) \right) &= -C_k^G \mathbf{d}_t^{\text{us}} (\mathbf{1}^\top \mathbf{p}_t^m), & \forall \mathbf{p}_t^m \in \underline{\mathcal{H}}_t^*, \\ \text{Tr} \left( Y_k (W_t - W_t^f) \right) &= -C_k^G \mathbf{d}_t^{\text{ds}} (\mathbf{1}^\top \mathbf{p}_t^m), & \forall \mathbf{p}_t^m \in \overline{\mathcal{H}}_t^*. \end{aligned}$$

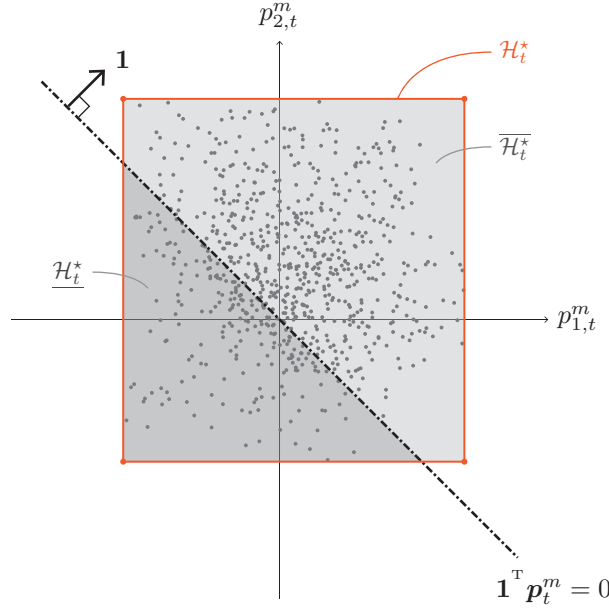


**Figure 4-1:** Illustration of approximation of the uncertainty for  $N_w = 2$ . The grey dots are the elements in  $\mathcal{S}$  at time step  $t$ . The red rectangle is  $\mathcal{H}_t^*$ , the smallest hyperrectangle that encloses those elements of  $\mathcal{S}$ .  $\underline{\mathcal{H}}_t^*$  and  $\overline{\mathcal{H}}_t^*$  are created by splitting  $\mathcal{H}_t^*$  in two at the hyperplane with normal  $\mathbf{1}$ , shown as the dashed line, such that the light shaded region is  $\overline{\mathcal{H}}_t^*$  and the dark shaded region corresponds to  $\underline{\mathcal{H}}_t^*$ . The red circles indicate all vertices of  $\underline{\mathcal{H}}_t^*$  and  $\overline{\mathcal{H}}_t^*$  that are not on the hyperplane. They coincide with the vertices of  $\mathcal{H}_t^*$ .

Using Remark 4.1, both constraint functions (4-5b) and (4-5c) are linear with respect to the uncertainty. Therefore, a robust solution for the whole set can be found by only considering the vertices. Define  $\text{vert}(\cdot)$  as a function that returns set of the vertices<sup>1</sup> of a set. Consider the vertices of  $\underline{\mathcal{H}}_t^*$  and  $\overline{\mathcal{H}}_t^*$ . Due to the definition, we have that

$$\mathbf{1}^\top \mathbf{p}_t^m = 0, \forall \mathbf{p}_t^m \in \{\text{vert}(\underline{\mathcal{H}}_t^*) \setminus \text{vert}(\overline{\mathcal{H}}_t^*)\}, \quad (4-6)$$

i.e. all vertices that coincide with hyperplane with normal  $\mathbf{1}$  correspond to zero total mismatch and thus to no hybrid behaviour. Therefore, we can characterize the upspinning behaviour with  $\text{vert}(\overline{\mathcal{H}}_t^*) \cap \text{vert}(\underline{\mathcal{H}}_t^*)$  and the downspinning behaviour with  $\text{vert}(\underline{\mathcal{H}}_t^*) \cap \text{vert}(\overline{\mathcal{H}}_t^*)$ . We number the vertices of  $\mathcal{H}_t^*$  with superscript  $i = 1, \dots, 2N_w$ , such that  $\mathbf{p}_t^{m,i}$  is the  $i$ -th vertex of  $\mathcal{H}_t^*$ . Collect all the indexes in  $\mathcal{I}$ , and let  $\underline{\mathcal{I}} \subset \mathcal{I}$  be defined as the set of indexes of  $\text{vert}(\overline{\mathcal{H}}_t^*) \cap \text{vert}(\underline{\mathcal{H}}_t^*)$ , and define  $\overline{\mathcal{I}} \subset \mathcal{I}$  in a similar fashion for  $\text{vert}(\underline{\mathcal{H}}_t^*) \cap \text{vert}(\overline{\mathcal{H}}_t^*)$ .

<sup>1</sup>For a hyperrectangle, this function is equal to every possible combination of the component wise minimum and maximum of all elements in the set, and can be found computationally efficient.

Problem (4-5) is now tractable by means of the worst-case (finite) SDP. Since we need to consider the network state for every vertex, the generic network state matrix is replaced by  $2N_w$  matrices for every time step  $t \in \mathcal{T}$ , such that  $\Xi_2 = \{\tilde{W}^f, \tilde{W}^1, \dots, \tilde{W}^{2N_w}, \tilde{\mathbf{d}}^{\text{us}}, \tilde{\mathbf{d}}^{\text{ds}}, \tilde{\mathbf{r}}^{\text{us}}, \tilde{\mathbf{r}}^{\text{ds}}\}$ . All the vertices of  $\mathcal{H}^*$  are used, and this approach is therefore called Vertex Enumeration (VE). We define the following problem as the vertex enumerated OPF-RS (VE-OPF-RS):

$$\underset{\Xi_2}{\text{minimize}} \quad \sum_{t \in \mathcal{T}} \left( f_G(W_t^f, \mathbf{p}_t^{w,f}) + f_R(\mathbf{r}_t^{\text{us}}, \mathbf{r}_t^{\text{ds}}) \right) \quad (4-7a)$$

$$\text{subject to} \quad W_t^f \in \mathcal{W}(\mathbf{p}_t^{w,f}, \mathbf{s}_t^D), \quad \forall t \in \mathcal{T}, \quad (4-7b)$$

$$W_t^f \succeq 0, \quad \forall t \in \mathcal{T}, \quad (4-7c)$$

$$W_t^i \in \mathcal{W}(\mathbf{p}_t^{w,f} + \mathbf{p}_t^{m,i}, \mathbf{s}_t^D), \quad \forall i \in \mathcal{I}, \forall t \in \mathcal{T}, \quad (4-7d)$$

$$W_t^i \succeq 0, \quad \forall i \in \mathcal{I}, \forall t \in \mathcal{T}, \quad (4-7e)$$

$$\text{Tr} \left( Y_k(W_t^i - W_t^f) \right) = -C_k^G \mathbf{d}_t^{\text{us}} (\mathbf{1}^T \mathbf{p}_t^{m,i}), \quad \forall i \in \underline{\mathcal{I}}, \forall k \in \mathcal{G}, \forall t \in \mathcal{T}, \quad (4-7f)$$

$$\text{Tr} \left( Y_k(W_t^i - W_t^f) \right) = -C_k^G \mathbf{d}_t^{\text{ds}} (\mathbf{1}^T \mathbf{p}_t^{m,i}), \quad \forall i \in \bar{\mathcal{I}}, \forall k \in \mathcal{G}, \forall t \in \mathcal{T}, \quad (4-7g)$$

$$-C_k^G \mathbf{r}_t^{\text{ds}} \leq \text{Tr} \left( Y_k(W_t^i - W_t^f) \right) \leq C_k^G \mathbf{r}_t^{\text{us}}, \quad \forall i \in \mathcal{I}, \forall k \in \mathcal{G}, \forall t \in \mathcal{T}, \quad (4-7h)$$

$$0 \leq \mathbf{r}_t^{\text{us}}, \quad 0 \leq \mathbf{r}_t^{\text{ds}}, \quad \forall t \in \mathcal{T}, \quad (4-7i)$$

$$\mathbf{1}^T \mathbf{d}_t^{\text{us}} = 1, \quad \mathbf{1}^T \mathbf{d}_t^{\text{ds}} = 1, \quad \forall t \in \mathcal{T}. \quad (4-7j)$$

By Proposition 1, the solution to this program is feasible for the CC-OPF-RS. The computational complexity of the solution is now examined.

### 4-1-3 Computational complexity of vertex enumerated OPF-RS

We will now examine the computational complexity of VE-OPF-RS as defined in Problem (4-7). If we compare VE-OPF-RS with C-OPF, it can be seen that the  $T$  matrix variables with their corresponding constraints have been replicated  $2N_w + 1$  times. Furthermore, we have added  $4T$  new vectors in  $\mathbb{R}^{N_G}$  to the decision space, and introduced  $4N_G$  constraints in for every matrix variable in constraints (4-7f) - (4-7h). Also,  $4N_G$  constraints are introduced for every vector in constraints (4-7i) - (4-7j). The addition of the vectors will not influence the order of the worst-case computational complexity, because the computational cost of finding a search direction for vector variables is of a lower order than for matrix variables [26]. Equation (2-2) can therefore be used to get an indication of the worst-case computational complexity of VE-OPF-RS. The dimension of the decision variable is  $n = 2N_b(2N_w + 1)T$ , and the number of constraints is  $m = (6N_b + 4N_G + N_L + 1)(2N_w + 1)T$ . Using a similar expansion as given in Section 3-2-2, this results in a total number of operations in  $\mathcal{O}(N_w^{9/2} T^{9/2} N_b^{9/2} \log(1/\epsilon))$ .

The computational complexity of VE-OPF-RS scales thus not only with a high order in the network size  $N_b$  and prediction horizon  $T$ , but also in the number of uncertain generators  $N_w$ . In modern day applications, there can be many uncertain power sources, for example due to the increasing use of residential photovoltaics. Moreover, the approximation of the uncertainty introduces extra conservatism, since an axis-aligned hyperrectangular box may not be the most compact approximation method. In the next Section, we present a novel way

to parametrize the network state such that the computational complexity of the resulting program is decoupled from the number of uncertain elements, and the scenario approach can be applied directly to CC-OPF-RS.

## 4-2 Direct scenario approach using conic parametrization of network state

In this section, we propose a parametrization of the generic network state to reduce the number of PSD constraints, such that the scenario approach can be applied directly to CC-OPF-RS. The approach is explained in Section 4-2-1, and arising tractability issues are described. To mitigate these issues, the principle of conic parametrization is introduced in Section 4-2-2, along with a simple example. The proposed parametrization is then applied to OPF-RS, as described in Section 4-2-3. In Section 4-2-4, the direct scenario approach is then applied to the parametrized problem and the computational complexity is discussed.

### 4-2-1 Direct scenario approach and tractability issues

Rather than approximating  $\mathcal{P}$  first, the scenario approach can also be applied directly to CC-OPF-RS. The required number of samples is based on an a-priori fixed violation level  $\varepsilon \in (0, 1)$  and confidence level  $\beta \in (0, 1)$  and the dimension of the control variable (see also Section 2-4 for a concise explanation of the scenario approach). As described in [12], the dimension of the control variable for OPF-RS problems is  $T(4N_G)$ : the real generator power, voltage magnitudes and the up- and downspinning vectors for every time step. Let  $N_s \in \mathbb{N}$  be the smallest integer such that

$$N_s \geq \frac{2}{\varepsilon}(4TN_G - 1 + \log 1/\beta). \quad (4-8)$$

Next, define  $\mathcal{S} = \{\tilde{\mathbf{p}}^{m,1}, \tilde{\mathbf{p}}^{m,2}, \dots, \tilde{\mathbf{p}}^{m,N_s}\} \in \mathcal{P}^{N_s}$  as a multi-extraction of samples from  $\mathcal{P}$ . Consider the following robust OPF-RS problem with respect to every sample in  $\mathcal{S}$ :

$$\underset{\Xi \in \mathcal{X}}{\text{minimize}} \quad f(\Xi) \quad (4-9a)$$

$$\text{subject to} \quad g(\Xi, \tilde{\mathbf{p}}^m) \leq 0, \forall \tilde{\mathbf{p}}^m \in \mathcal{S}, \quad (4-9b)$$

and let  $\Xi^{\text{opt}}$  be optimal solution to Problem (4-9). Based on [36, Th. 4],  $\Xi^{\text{opt}}$  has the following probabilistic guarantees:

$$\mathbb{P}^{N_s}[\mathcal{S} \in \mathcal{P}^{N_s} : \mathbb{P}[\tilde{\mathbf{p}}^m \in \mathcal{P} : g(\Xi^{\text{opt}}, \tilde{\mathbf{p}}^m) \leq 0] \geq 1 - \varepsilon] \geq 1 - \beta.$$

In other words: given a multi-extraction  $\mathcal{S}$  with cardinality  $N_s$  which satisfies (4-8), the optimal solution to Problem (4-9) is feasible for any generic sample  $\tilde{\mathbf{p}}^m \in \mathcal{P}$  with probability  $1 - \varepsilon$ , with confidence  $1 - \beta$ .

To implement Problem (4-9), one replaces the set of uncertain constraints for a generic wind trajectory with  $N_s$  sets of deterministic constraints for the samples of the uncertainty, called scenarios. Instead of a forecast and a generic network state, the decision variables now include



the forecast network state and  $N_s$  scenario network states for every time step. Each of the state matrices is subject to PSD constraints. The minimum number of samples  $N_s$  to guarantee reasonable violation and confidence levels  $\varepsilon, \beta$  is typically quite large. The resulting problem has therefore such a high number of computationally expensive PSD constraints, that it is computationally intractable.

To illustrate this, the worst-case computational complexity is determined. The dimension of the decision variables  $n = 2N_b(N_s + 1)T$ , and since every constraint set is repeated for every scenario state, the dimension of the constraints now increases to  $m = (6N_b + 4N_G + N_L + 1)(N_s + 1)T$ . Inspecting (4-8), it can be concluded that  $N_s \in \mathcal{O}(TN_G)$ . If one substitutes  $n$  and  $m$  in Equation (2-2) and keeps only keeping the highest order terms, one obtains a complexity that is in  $\mathcal{O}(T^9 N_G^{13/2} N_b^{9/2} \log(1/\alpha))$ . Due to the high order terms of  $T, N_G$  and  $N_b$ , the worst-case complexity grows very fast with increasing problem sizes. In the following, we therefore propose a parametrization of the scenario state, that aims to make the direct application of the scenario approach to CC-OPF-RS tractable.

#### 4-2-2 Tractability through conic parametrization of scenario state

Instead of introducing a new variable to represent every scenario state, a conic combination<sup>2</sup> of matrix variables, called coefficient matrices, is used to approximate the scenario state. The variable for these coefficient matrices corresponds to the uncertainty. We can then impose PSD-ness on the coefficient matrices, rather than on every scenario states separately. Since any conic combination of PSD matrices is a PSD matrix [25, §2.2.5], the approximated scenario state is guaranteed to be PSD.

To clarify the idea behind our proposed parametrization, a simple example is provided. Consider the following scenario program:

$$\underset{\{X_1, \dots, X_{N_s}\}}{\text{minimize}} \quad f(X_1, \dots, X_{N_s}) \quad (4-10a)$$

$$\text{subject to} \quad X_i \in \mathcal{X}(\delta_i), \quad \text{for } i = 1, \dots, N_s, \quad (4-10b)$$

$$X_i \succeq 0, \quad \text{for } i = 1, \dots, N_s. \quad (4-10c)$$

The decision variables are the scenario state, each corresponding to one scenario  $\delta_i \in \mathbb{R}$ . Every scenario has its corresponding decision variable  $X_i \in \mathbb{S}^d$ , which has to be PSD and in the feasible set  $\mathcal{X}(\delta_i) \subseteq \mathbb{S}^d$  for the corresponding uncertainty. A graphic representation of a very simple version of this problem is shown in Figure 4-2, where the feasible set is illustrated with the blue ellipse and the optimal solutions are indicated with red circles. Since  $d = 1$ , the PSDness of the matrix variable is here simply all non-negative values.

To solve this, we aim to parametrize  $X_i$  in  $\delta_i$  such that we implicitly satisfy every PSD constraint  $X_1 \succeq 0, \dots, X_{N_s} \succeq 0$ . We choose to define  $\hat{X}(\delta_i)$  as an affine function of  $\delta_i$ , such that the coefficients are the new decision variables. Since  $\delta_i$  can be negative, we apply a mapping  $P(\cdot) : \mathbb{R} \rightarrow \mathbb{R}_+$  that maps  $\delta_i$  to non-negative values, and define the approximated scenario state as follows:

$$\hat{X}(\delta_i) := A + BP(\delta_i), \quad \text{for } i = 1, \dots, N_s.$$

<sup>2</sup>A *conic combination* is a linear combination with only non-negative coefficients, see also [25, §2.1.5].

where  $A, B \in \mathbb{S}^d$  are introduced as the coefficient matrices. Since  $\hat{X}(\delta_i)$  is a conic combination of matrices,  $A, B \succeq 0 \implies \hat{X}_i \succeq 0$  for all scenarios. Therefore, we can replace constraints (4-10c) with  $A, B \succeq 0$ . The problem can now be stated in terms of the new parametrization of  $\hat{X}_i$ :

$$\underset{A, B \in \mathbb{S}^d}{\text{minimize}} \quad f(\hat{X}_1(\delta_1), \dots, \hat{X}_{N_s}(\delta_{N_s})) \quad (4-11a)$$

$$\text{subject to} \quad \hat{X}(\delta_i) \in \mathcal{X}(\delta_i), \quad \text{for } i = 1, \dots, N_s, \quad (4-11b)$$

$$A \succeq 0, B \succeq 0. \quad (4-11c)$$

Regardless of the number of scenarios  $N_s$ , Problem (4-11) has just two PSD constraints on  $A, B$ . The price for this increase in tractability is more restrictiveness. As illustrated in Figure 4-2, the solutions  $\hat{X}_i^{\text{opt}}$  must lie on the hyperplane  $A^{\text{opt}} + P(\delta_i)B^{\text{opt}}$ , rather than anywhere within the set  $\{X_i \in \mathcal{X}(\delta_i) \mid X_i \succeq 0\}$ . This means that the optimal objective for Problem (4-11) will provide an upper bound on the optimal objective of Problem (4-10), which is not necessarily tight. This is also the case for the simple example: it can be seen that the optimal value for  $X_2$  cannot be obtained using the parametrization.

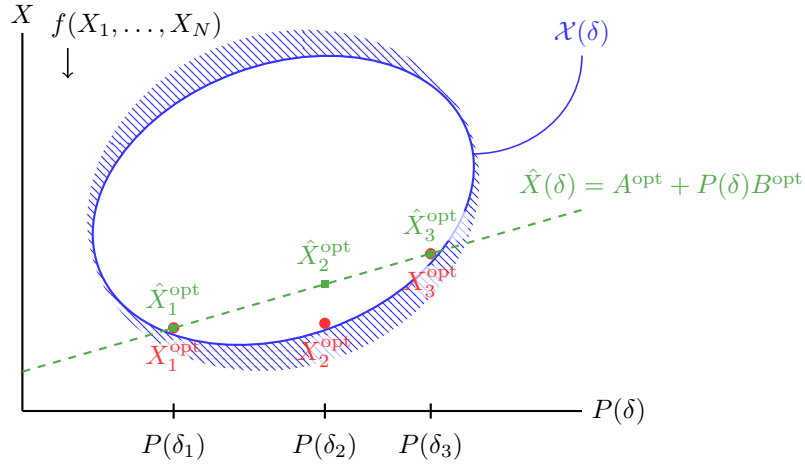


**Figure 4-2:**  $X, P(\delta)$  plot for a (parametrized) scenario program with  $d = 1, N_s = 3$ . The feasible set is the inside of the blue ellipse. Solutions are shown as red circles (green squares). The parametrized solution is more restrictive, since all solutions must lie on a hyperplane.

### 4-2-3 Conic parametrization of generic network state for OPF-RS

The parametrization approach is now applied to the OPF-RS problem. The scenario variables are the network states for a realization of the uncertainty for every time step.  $W_t^f$  and  $W_t^i$  are related through the reserve distribution equality constraints (3-8), such that the reserve power resulting from  $W_t^i$  has to be consistent with the distribution vectors. Motivated by this observation, we propose a novel parametrization of the generic network state that encodes this restriction implicitly. Let  $\hat{W}_t(\mathbf{p}_t^m) \in \mathbb{S}^{2N_b}$  be the parametrized generic network state  $\tilde{\mathbf{p}}^m \in \mathcal{P}, \forall t \in \mathcal{T}$ , defined as

$$\hat{W}_t(\mathbf{p}_t^m) := W_t^f + \max(-\mathbf{1}^\top \mathbf{p}_t^m, 0)W_t^{\text{us}} + \max(\mathbf{1}^\top \mathbf{p}_t^m, 0)W_t^{\text{ds}}, \quad (4-12)$$

where coefficient matrices  $W_t^{\text{us}}, W_t^{\text{ds}} \in \mathbb{S}^{2N_b}$  have been introduced for every  $t \in \mathcal{T}$ , and  $\hat{W}_t$  is a function of  $\mathbf{p}_t^m$ . The generic network state is decomposed in a deterministic component and two components which scale with the positive or negative uncertainty.

**Remark 4.2.** *Both  $\max(\mathbf{1}^\top \mathbf{p}_t^m, 0)$  and  $\max(-\mathbf{1}^\top \mathbf{p}_t^m, 0)$  are always non-negative and never non-zero simultaneously, such that the change in network state is determined by either  $W_t^{\text{ds}}$  or  $W_t^{\text{us}}$  in case of either a wind power surplus or deficit, respectively.*

Combining Remark 4.2 with the following constraints  $\forall t \in \mathcal{T}$

$$W_t^{\text{us}} \succeq 0, \quad W_t^{\text{ds}} \succeq 0, \quad (4-13)$$

implies that  $\hat{W}_t(\mathbf{p}_t^m) \succeq 0, \forall \mathbf{p}_t^m \in \mathbb{R}^{N_w}, \forall t \in \mathcal{T}$ , since  $\hat{W}_t(\mathbf{p}_t^m)$  is a conic combination of PSD matrices. To the best of our knowledge, the parametrization of the network state as a conic combination of PSD matrices is new, and it is one of the main contributions of this work.

In order to let parametrization (4-12) be a feasible and valid state of the network, we introduce the following constraints for  $\tilde{\mathbf{p}}^m \in \mathcal{P}, \forall t \in \mathcal{T}$ :

$$\hat{W}_t(\mathbf{p}_t^m) \in \mathcal{W}(\mathbf{p}_t^{w,f} + \mathbf{p}_t^m, \mathbf{s}_t^D). \quad (4-14)$$

We will now examine the definition of reserve power (3-7) expressed in the new parametrization  $\hat{W}_t(\mathbf{p}_t^m) \forall k \in \mathcal{G}, \forall t \in \mathcal{T}$ :

$$\begin{aligned} C_k^G \mathbf{r}_t &= C_k^G \mathbf{p}_t^G - C_k^G \mathbf{p}_t^{G,f} \\ &= \text{Tr} \left( Y_k (\hat{W}(\mathbf{p}_t^m) - W_t^f) \right) \\ &= \text{Tr} \left( Y_k (\max(-\mathbf{1}^\top \mathbf{p}_t^m, 0) W_t^{\text{us}} + \max(\mathbf{1}^\top \mathbf{p}_t^m, 0) W_t^{\text{ds}}) \right) \\ &= -\text{Tr}(Y_k W_t^{\text{us}}) \min(\mathbf{1}^\top \mathbf{p}_t^m, 0) + \text{Tr}(Y_k W_t^{\text{ds}}) \max(\mathbf{1}^\top \mathbf{p}_t^m, 0), \end{aligned} \quad (4-15)$$

where we have used  $\forall \alpha \in \mathbb{R}, \max(-\alpha, 0) = -\min(\alpha, 0)$  and the linearity of the trace operator. To see how the distribution of reserve power (4-15) is encoded in the parametrized state, we show the distribution constraints as they are defined in OPF-RS again:

$$C_k^G \mathbf{r} = -C_k^G \mathbf{d}_t^{\text{us}} \min(\mathbf{1}^\top \mathbf{p}_t^m, 0) - C_k^G \mathbf{d}_t^{\text{ds}} \max(\mathbf{1}^\top \mathbf{p}_t^m, 0), \quad (3-8)$$

where the left-hand side of (3-8) has been substituted for the reserve power of bus  $k$  using the definition of reserve in OPF-RS, (3-7). Comparing (4-15) to (3-8), one can see that the terms  $\text{Tr}(Y_k W_t^{\text{us}})$  and  $\text{Tr}(Y_k W_t^{\text{ds}})$  are equivalent to  $C_k^G \mathbf{d}_t^{\text{us}}$  and  $-C_k^G \mathbf{d}_t^{\text{ds}}$  respectively, i.e. they define the distribution of the up- and downspinning reserve. In the OPF-RS notation, the choice of a network state for some wind trajectory  $\tilde{\mathbf{p}}^m$  is required to be within the set of feasible states and has to satisfy (3-8) for every  $k \in \mathcal{G}, \forall t \in \mathcal{T}$ . This restriction is incorporated in the definition of the parametrized network state. Constraints (3-8) are therefore redundant for the parametrized problem. To ensure that the reserve power will always be always the exact opposite of the mismatch, the following set of constraints is introduced<sup>3</sup>  $\forall t \in \mathcal{T}$ :

$$\sum_{k \in \mathcal{G}} \text{Tr}(Y_k W_t^{\text{us}}) = 1, \quad \sum_{k \in \mathcal{G}} \text{Tr}(Y_k W_t^{\text{ds}}) = -1, \quad (4-16)$$

which replace constraints (3-9). Summing (4-15) over all generators  $k \in \mathcal{G}$  yields  $\forall \tilde{\mathbf{p}} \in \mathcal{P}, \forall t \in \mathcal{T}$ :

$$\begin{aligned} \sum_{k \in \mathcal{G}} C_k^G \mathbf{r}_t &= - \overbrace{\sum_{k \in \mathcal{G}} \text{Tr}(Y_k W_t^{\text{us}})}^{=1} \min(\mathbf{1}^\top \mathbf{p}_t^m, 0) + \overbrace{\sum_{k \in \mathcal{G}} \text{Tr}(Y_k W_t^{\text{ds}})}^{=-1} \max(\mathbf{1}^\top \mathbf{p}_t^m, 0), \\ \mathbf{1}^\top \mathbf{r}_t &= - \min(\mathbf{1}^\top \mathbf{p}_t^m, 0) - \max(\mathbf{1}^\top \mathbf{p}_t^m, 0), \\ &= -\mathbf{1}^\top \mathbf{p}_t^m, \end{aligned}$$

such that the total reserve power always negates the total mismatch. Note that for the downspinning term, the absence of the minus in (4-15) is compensated in (4-16). Since  $Y_k$  is indefinite for all  $k \in \mathcal{G}$ , this is possible.

After finding a solution to this program, the distribution vectors can be extracted from  $\tilde{W}^{\text{us}}, \tilde{W}^{\text{ds}}$  through the following relation  $\forall k \in \mathcal{G}, \forall t \in \mathcal{T}$ :

$$C_k^G \mathbf{d}_t^{\text{us}} = \text{Tr}(Y_k W_t^{\text{us}}), \quad C_k^G \mathbf{d}_t^{\text{ds}} = -\text{Tr}(Y_k W_t^{\text{ds}}). \quad (4-17)$$

Since the reserve distribution vectors  $\tilde{\mathbf{d}}^{\text{us}}, \tilde{\mathbf{d}}^{\text{ds}}$  are encoded in  $\tilde{W}^{\text{us}}, \tilde{W}^{\text{ds}}$ , they can be removed from the decision variables, and extracted a-posteriori using (4-17). The set of decision variables for this problem now reduces to:  $\Xi_p := \{\tilde{W}^f, \tilde{W}^{\text{us}}, \tilde{W}^{\text{ds}}, \tilde{\mathbf{r}}^{\text{us}}, \tilde{\mathbf{r}}^{\text{ds}}\}$ , where the subscript  $p$  has been used to indicate that this is the parametrized formulation. We define the parametrized optimal power flow with reserve scheduling (P-OPF-RS) as the following program:

$$\begin{aligned} &\underset{\Xi_p}{\text{minimize}} && \sum_{t \in \mathcal{T}} f_G(W_t^f, \mathbf{p}_t^{w,f}, \mathbf{p}_t^D) + f_R(\mathbf{r}_t^{\text{us}}, \mathbf{r}_t^{\text{ds}}) \\ &\text{subject to} && \text{feasible forecast state} && (3-6b), (3-6d), \\ & && \text{feasible generic parametrized state} && (4-13), (4-14), \\ & && \text{reserve distribution constraints} && (4-16), \\ & && \text{reserve requirements constraints} && (3-10a), (3-10b), \end{aligned}$$

where  $\mathbf{r}_t$  is replaced with its new definition (4-15) in constraints (3-10a). Since we have not splitted the uncertainty in the time steps, we still optimize with respect to the original wind trajectories. Especially optimization problems that have intertemporal constraints (for example ramping constraints) benefit from this.

It is important to realize that P-OPF-RS is not equivalent to OPF-RS. It is an approximation, since a parametrization of the generic network state has been used. P-OPF-RS is still an uncertain program, but the PSD constraints are no longer on the uncertain generic network state, but on the deterministic forecast network state and two deterministic coefficient matrices. We can therefore apply the scenario approach directly to P-OPF-RS, as discussed in the following section.

---

<sup>3</sup> In the optimization, the introduction of these equality constraints causes numerical issues in the solver since it is too restrictive. Therefore, we implement these constraints by introducing slack variable  $u \in \mathbb{R}_+^2$  and rewriting each equality constraint  $f(a) = b$  to the form  $b - u_1 \leq f(x) \leq b + u_2$ . By adding  $\mathbf{1}^\top u$  to the objective function,  $u$  is minimized, essentially pushing  $f(a)$  to equal  $b$ . After optimization, the optimized value of the slack variables is checked and turns out to be sufficiently small.

#### 4-2-4 Scenario approach for parametrization and computational complexity

Since the PSD constraints are now on the coefficient matrices instead of the generic network state, the scenario approach can be applied directly to P-OPF-RS to obtain a problem that is computationally tractable. We first formulate P-OPF-RS as a CCP, similar to how OPF-RS is transformed to CC-OPF-RS,

$$\underset{\Xi_p \in \mathcal{X}_p}{\text{minimize}} \quad f(\Xi_p) \quad (4-18a)$$

$$\text{subject to} \quad \mathbb{P}[\tilde{\mathbf{p}}^m \in \mathcal{P} : g_p(\Xi_p, \tilde{\mathbf{p}}^m) \leq 0] \geq 1 - \varepsilon, \quad (4-18b)$$

where  $g_p$  are the uncertain constraint functions for P-OPF-RS, i.e. constraints (4-14), (3-10a), and all other constraints for P-OPF-RS are used to construct  $\mathcal{X}_p$ , the deterministic feasible set for the parametrized problem. We can then apply the scenario approach to Problem (4-18). The resulting problem is called the scenario parametrized OPF-RS (SP-OPF-RS) problem, and is given by:

$$\begin{aligned} & \underset{\Xi_p}{\text{minimize}} \quad \sum_{t \in \mathcal{T}} f_G(W_t^f, \mathbf{p}_t^{w,f}, \mathbf{p}_t^D) + f_R(\mathbf{r}_t^{\text{us}}, \mathbf{r}_t^{\text{ds}}) \\ & \text{subject to} \quad W_t^f \in \mathcal{W}(\mathbf{p}_t^{w,f}, \mathbf{s}_t^D), \quad \forall t \in \mathcal{T}, \\ & \quad \hat{W}_t(\mathbf{p}_t^m) \in \mathcal{W}(\mathbf{p}_t^{w,f} + \mathbf{p}_t^m, \mathbf{s}_t^D) \quad \forall \tilde{\mathbf{p}}^m \in \mathcal{S}, \forall t \in \mathcal{T}, \\ & \quad \sum_{k \in \mathcal{G}} \text{Tr}(Y_k W_t^{\text{us}}) = 1, \quad \forall t \in \mathcal{T}, \\ & \quad \sum_{k \in \mathcal{G}} \text{Tr}(Y_k W_t^{\text{ds}}) = -1, \quad \forall t \in \mathcal{T}, \\ & \quad -C_k^G \mathbf{r}_t^{\text{ds}} \leq \text{Tr}(Y_k (\hat{W}(\mathbf{p}_t^m) - W_t^f)) \leq C_k^G \mathbf{r}_t^{\text{us}}, \quad \forall \tilde{\mathbf{p}}^m \in \mathcal{S}, \forall k \in \mathcal{G}, \forall t \in \mathcal{T}, \\ & \quad 0 \leq \mathbf{r}_t^{\text{us}}, \quad 0 \leq \mathbf{r}_t^{\text{ds}}, \quad \forall t \in \mathcal{T}, \\ & \quad W_t^f \succeq 0, \quad W_t^{\text{us}} \succeq 0, \quad W_t^{\text{ds}} \succeq 0, \quad \forall t \in \mathcal{T}. \end{aligned}$$

Having defined SP-OPF-RS, the computational complexity of the problem is examined. Instead of  $T(N_s + 1)$  matrix variables, we have reduced the program to only  $3T$  matrix variables, so  $n = 6N_b T$ . Note that for  $N_w > 1$ , this results in a reduction of the number of matrix variables compared to the VE-OPF-RS approach. By parametrizing, we have made  $n$  independent from the number of scenarios. The number of constraints per scenario has decreased slightly, since we have dropped the reserve distribution constraints (3-8) from the problem, so  $m = (6N_b + 2N_G + N_L + 1)(N_s + 1)T$ . Since the direct approach is used, the number of scenario  $N_s$  is still in  $\mathcal{O}(N_G T)$ . The resulting computational complexity is again obtained by expanding all terms and only keeping the highest order terms, and results in  $\mathcal{O}(T^{13/2} N_b^{9/2} N_G^4 \log(1/\alpha))$ , which is of much lower order than the robust OPF-RS for all scenarios in  $\mathcal{S}$ .

The idea of parametrizing the scenario state in the uncertainty originates from [11]. Here, the authors define the scenario state as an affine function of the uncertain wind power. The authors justify their approach by the fact that the generators change their output in a linear fashion as a result of some mismatch, due to the AGR scheme. The scenario state is parametrized in the mismatch as  $\tilde{\mathbf{p}}^m \in \mathcal{P}, \forall t \in \mathcal{T}$ :

$$\hat{W}_t(\mathbf{p}_t^m) := A_t + \sum_{k \in \mathcal{F}} (C_k^w (\mathbf{p}_t^{w,f} + \mathbf{p}_t^m)) B_{k,t},$$

where  $A_t$  and  $B_{t,k}$  are coefficient matrices in  $\mathbb{S}^{2N_b}$ . The total problem using this parametrization requires  $(2 + N_w)T$  matrices, instead of  $T(N_s + 1)$ . However, PSDness is still imposed on the every instance of the parametrized  $\hat{W}_t(\mathbf{p}_t^m)$ , resulting in  $T(N_s + 1)$  PSD constraints. The computationally costly operation of finding a search direction has to be carried out for every PSD constraint. Therefore, the computational complexity of the program has not decreased. The authors have limited the freedom of selecting a feasible scenario state to an affine function, but do not gain much in terms of tractability.

In our approach however, we apply a parametrization of the scenario state that is generalizable through only  $3T$  PSD constraints. We re-use the forecast state as the deterministic component of the generic network state, whereas the authors of [11] let the deterministic component be a new decision variable. Moreover, our parametrization discerns between a power surplus and deficit, and thus between up- or downspinning behaviour of the network. Therefore, the coefficient matrices have physical meaning and implicitly encode the distribution of reserve power. The improvement in computational tractability comes at the prize of more conservatism.

### 4-3 Conclusions

We have provided two different ways of approximating CC-OPF-RS. A schematic overview of the approximations is shown in Figure 4-3. The chance constraints from CC-OPF-RS are transformed to deterministic constraints using the scenario approach. This results in a formulation of OPF-RS for all samples in the multi-extraction  $\mathcal{S}$ , as shown in Figure 4-3 (a). This formulation is computationally intractable, due to the large number of PSD constraints. In Figure 4-3 (b), the indirect scenario approach is shown. The same problem is formulated, but now for the vertices of an approximation of the uncertainty set. Because the number of vertices will be very small compared to the number of elements in  $\mathcal{S}$ , this is a tractable problem. In Figure 4-3 (c), the direct scenario approach with parametrization is shown. OPF-RS is first parametrized to P-OPF-RS, and a problem for  $\mathcal{S}$  is formulated, called SP-OPF-RS. Since the number of PSD constraints is fixed in P-OPF-RS, this problem is also tractable.

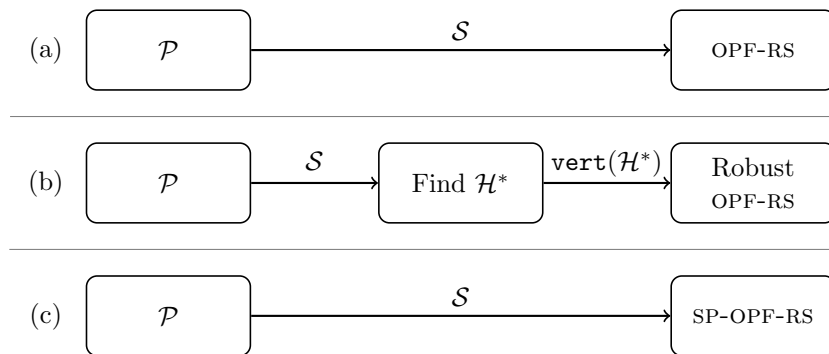


**Figure 4-3:** Schematic overview of different scenario approaches: (a) direct scenario approach for OPF-RS (intractable), (b) VE-OPF-RS (c) SP-OPF-RS

Both VE-OPF-RS and SP-OPF-RS are approximations for CC-OPF-RS, which both introduce some conservatism. VE-OPF-RS may overestimate the uncertainty by the approximation error

in finding  $\mathcal{H}^*$ , whereas in the parametrization approach every sample of the uncertainty is used directly. However, the conic parametrization of SP-OPF-RS introduces conservatism by limiting the choice of the network state to a conic combination of PSD matrices. The performance and probabilistic properties of solution for both formulations will be compared in Chapter 6.





# Decomposition of OPF-RS Problems

The non-convex OPF problem has been convexified to an SDP. It is then extended to an OPF-RS problem with uncertain WPG, and formulated as a CCP. We proposed two tractable approximations for the CCP, using the scenario approach. The computational complexity of the resulting problems VE-OPF-RS and SP-OPF-RS grows polynomial in the dimension of the network.

Although the approximations presented in previous chapters are tractable for reasonably sized systems, the dimension network state matrix is prohibitively large for real world applications, as realistic networks typically have multiple hundreds or even thousands of buses. In this chapter, two decomposition methods are discussed for power system optimization problems with a large matrix variable. This can be seen as an extension to the tractable approximations presented in Chapter 4, as with these techniques, day-ahead scheduling problems can be solved for larger networks.

In Section 5-1, the decomposition of the PSD constraints is discussed. The sparsity pattern of the data is used to decompose the computationally expensive PSD constraint on a large matrix variable, and an algorithm for the a-posteriori completion of the solution is presented.

Instead of only decomposing the PSD constraint, it is also possible to spatially decompose a power system optimization problem, using the concept of control areas. In Section 5-2, a multi-area problem is created by decomposing a large centralized problem into multiple sub-problems, which have overlapping constraints. An algorithmic approach is used to solve the resulting sub-problems in a distributed setting, and the application of this approach to OPF-RS problems is given. Finally, some concluding remarks are given in Section 5-3.

### 5-1 Sparsity decomposition for OPF-RS problems

In this section, we improve the tractability of OPF-RS problems for large networks by decomposing the computationally expensive PSD constraints on the state matrices with the use of the chordal theorem. The chordal theorem is first introduced in Section 5-1-1, and its use for

Clique	Buses
1	1, 2, 5,
2	2, 3, 4
3	2, 4, 5
4	4, 7, 9
5	6, 12, 13
6	4, 5, 9
7	5, 6, 9
8	9, 10, 11
9	6, 9, 11
10	6, 9, 13
11	9, 13, 14
12	7, 8

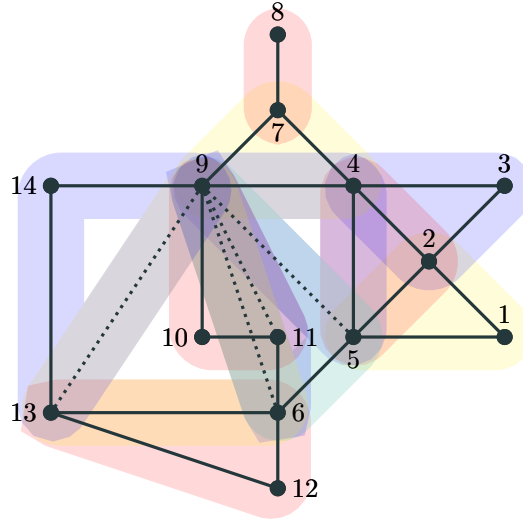


**Figure 5-1:** Illustration of the maximal cliques of the IEEE 14-bus network. The solid lines are actual lines of the power system, the dotted lines are added to make the network graph chordal. All maximal cliques are shown as shaded polygons.

the decomposition of PSD matrices is explained. The application of this approach is given for the SDP C-OPF in Section 5-1-2. Due to the decomposition, the solution is a partially filled matrix. We present an algorithm to complete the matrix using the properties of the state matrix and compare its performance in Section 5-1-3.

### 5-1-1 The chordal theorem and matrix completion

SDPs are computationally complex due to the matrix variable, which is subject to a PSD constraint. One can reduce the size of the computationally expensive PSD constraint by selecting certain sub-matrices of the original matrix variable and only impose PSD-ness on those matrices. The solution is a partially filled matrix, with only those entries filled that correspond to at least one of the sub-matrices. All other entries are undetermined. Various algorithms are available for *matrix completion*, the a-posteriori filling of the undetermined entries. In [50], Grone et al. provide the *chordal theorem*, that guarantees the completed matrix is PSD if and only if specific sub-matrices are PSD. To explain the chordal theorem, two definitions are first introduced:

**Definition 1.** [51, §3.1] *A graph is chordal if every cycle of length greater than three has a chord (an edge between non-consecutive nodes in the cycle).*

**Definition 2.** [51, §2.1] *A clique is a subset of nodes that together form a complete graph, i.e. the number of edges between any two nodes in a clique is equal to one. A clique is maximal if it is not a subset of any other cliques in the graph.*

Consider a symmetric PSD matrix  $X \in \mathbb{S}_+^d$ , and let  $G$  be a graph with nodes  $\{1, \dots, d\}$ . The chordal theorem states that one can reconstruct  $X$  using only the entries of  $X$  that correspond to the nodes in the maximal cliques of  $G$ , if and only if  $G$  is chordal. The chordal theorem has originally been defined for Hermitian matrices, but since a symmetric matrix

is a Hermitian matrix with all its imaginary values equal to zero, i.e.  $\mathcal{S} \subset \mathbb{H}$ , the chordal theorem also holds for symmetric matrices. The chordal theorem can thus be used to prove the equivalence between the PSDness of a matrix and the PSDness of its sub-matrices, thereby reducing the size of the PSD constraints and overall computational complexity. Based on this idea, various solving methods for decomposing SDPs with sparse problem data have been developed [51, 52].

### 5-1-2 Sparsity decomposition method applied to OPF problem

We now demonstrate how the chordal theorem can be used to decompose the PSD constraints of the C-OPF problem. Consider a graph  $G$  over all the buses of the power network.  $G$  has an edge between node  $i$  and  $j$  if the  $(i, j)$ -th entry of at least one of the data-matrices  $Y_k, Y_k^*, Y_{lm}, Y_{lm}^*, M_k$  is non-zero, such that the adjacency matrix of  $G$  is equal to the *aggregate sparsity pattern*. Due to the definition of the nodal admittance matrix, the aggregate sparsity pattern is identical to the network topology, and is usually very sparse. If  $G$  is not chordal, its chordal extension can be found by adding edges until the resulting graph is chordal. Using a greedy decomposition algorithm as proposed by Madani et al. in [16], we decompose  $G$  in  $K$  subsets of vertices, corresponding to the maximal cliques of the (extended) chordal graph. This decomposition algorithm has the advantage that it returns maximal cliques of a low order, i.e. the number of buses in a maximal clique is low. In Figure 5-1, an illustration of the IEEE 14-bus network with the resulting maximal cliques is shown.

Denote every maximal clique of  $G$  with  $\mathcal{C}_k \subset \mathcal{N}$ , and collect all cliques in  $\mathcal{C} = \{\mathcal{C}_1, \dots, \mathcal{C}_K\}$ . Every subset  $\mathcal{C}_k$  induces a sub-matrix from the original matrix by selecting the columns and rows corresponding to the buses in it. We now decompose the PSD constraints (3-5c) on the matrix variable in C-OPF  $\forall t \in \mathcal{T}$  using the following constraints:

$$W_t(\mathcal{C}_k, \mathcal{C}_k) \succeq 0, \quad \forall \mathcal{C}_k \in \mathcal{C}$$

For every  $t \in \mathcal{T}$ , the single PSD constraint on  $W_t$  is now transformed to  $K$  separate PSD constraints on sub-matrices of  $W_t$ . We call the resulting formulation decomposed optimal power flow, D-OPF.

**Proposition 2.** *The optimal objective value of D-OPF is equivalent to the optimal objective value of C-OPF.*

*Proof.* This is a direct result of [16, Theorem 1]. □

Using Proposition 2, the solution to a decomposed network has the same optimal objective as the original problem. Therefore, the decomposition can be used to make very large SDPs tractable, since the dimension of the largest maximal clique depends only on network topology. Let  $N_C$  be the number of buses in the largest maximal clique, i.e.  $N_C := \max_k |\mathcal{C}_k|$ . It is shown that for realistic networks,  $N_C$  is still of reasonable dimensions. For example, the Polish test system has over 3000 buses, but can be decomposed in cliques such that  $N_C = 27$  (see also [16] for a list of large power systems and their corresponding ‘treewidth’, the cardinality of the largest maximal cliques minus one). D-OPF has  $K$  matrix variables of dimension  $N_C$  at most, and the worst-case overall dimension of the matrix variable is therefore  $KN_C T$ . The number of constraints is unchanged, i.e.  $m = (6N_b + N_L + 4N_G + 1)T$ .

If we substitute  $n$  and  $m$  in Equation (2-2), we find that the total complexity for D-OPF is in  $\mathcal{O}(T^{9/2}K^{5/2}N_C^{5/2}N_b^2\log(1/\alpha))$ . Comparing this complexity with the original program,  $\mathcal{O}(T^{9/2}N_b^{9/2}\log(1/\alpha))$ , and considering that  $N_C \ll N_b$ , one can clearly see the impact of decomposition on the computational complexity.

The obtained solution from D-OPF is a partially filled matrix, which is denoted by  $W'$ . From this matrix, we aim to reconstruct a PSD matrix which is an optimal solution for C-OPF. The reconstructed matrix has to be rank-one to be a valid solution to C-OPF. Although the chordal theorem proves the possibility of completing a PSD matrix, it does not provide any guarantees on the rank of the completed result. We therefore provide a matrix recovery algorithm such that the resulting solution is a rank-one PSD matrix.

### 5-1-3 Rank-one matrix completion algorithm

Inspired by the voltage vector recovery algorithm in [16], we propose a matrix recovery algorithm which completes a partially filled state matrix to a rank-one PSD matrix. We modify the voltage recovery algorithm for the rectangular voltage notation, and extract a complex voltage vector from the partially filled solution. We then recover the full state matrix from the complex voltage vector. Algorithm 1 summarizes our proposed recovery procedure.

---

#### Algorithm 1 Matrix completion for rectangular voltage notation

---

- 1: Given: partially filled state matrix  $W' \in \mathbb{S}^{2N_b}$
  - 2: Initialize:  $\mathbf{v} \in \mathbb{C}^{N_b}$
  - 3: **for**  $k \in \mathcal{N}$  **do**
  - 4:    $|v_k| \leftarrow \sqrt{W'(k, k) + W'(k + N_b, k + N_b)}$
  - 5: **end for**
  - 6: **for**  $(l, m) \in \mathcal{L}$  **do**
  - 7:    $\angle W'_{lm} := \tan^{-1} \left( \frac{W'(l+N_b, m) - W'(l, m+N_b)}{W'(l, m) + W'(l+N_b, m+N_b)} \right)$
  - 8: **end for**
  - 9:  $\angle \mathbf{v} \leftarrow \arg \min_{-\pi \leq \angle \mathbf{v} \leq \pi} \sum_{(l, m) \in \mathcal{L}} |\angle W'_{lm} - \angle v_l + \angle v_m|$
  - 10:  $\mathbf{x} \leftarrow \left[ (|\mathbf{v}| \cos \angle \mathbf{v})^T, (|\mathbf{v}| \sin \angle \mathbf{v})^T \right]^T$
  - 11: Output:  $W \leftarrow \mathbf{x}\mathbf{x}^T$
- 

From  $W'$ , we first extract a complex voltage vector  $\mathbf{v}$ . The magnitude of the entries of  $\mathbf{v}$  is determined by summing the entries on the diagonal that correspond to the real and imaginary part of the same bus, and taking the square root. After this, the angle difference between buses is calculated based on the filled entries in  $W'$ . Since the sparsity pattern coincides with the network topology, the filled entries will correspond to the lines of the network, i.e. all entries of  $W'$  used in Line 7 are filled. The convex program in Line 9 extracts the globally optimal voltage vector such that corresponding angle differences are as close to those suggested by the matrix  $W'$ . The solution is used to build  $\mathbf{x}$ , which is then used to form the completed  $W$ .  $W$  is constructed from the outer product of a vector, and is therefore PSD and rank-one by definition.

The authors of [16] first use another completion algorithm based on the chordal theorem to complete  $W'$  and extract the optimal voltage vector from this completed matrix. Recognizing that the entries necessary for the latter extraction are already available in  $W'$ , we skip the matrix completion and extract a voltage vector from  $\tilde{W}$  directly, and use this vector to reconstruct a completely filled state matrix.

As a proof of concept, we solve C-OPF and D-OPF for one hour with the same fixed wind trajectory. The first observation is that the objective functions evaluated at either the first or second solution yield the same value, i.e. Proposition 2 holds. We complete the result of the second optimization using Algorithm 1. The extracted voltage vectors are compared in Figure 5-2. The two results are almost entirely identical, except for some small differences in the voltage angle. This can be attributed to the numerical error in solver.

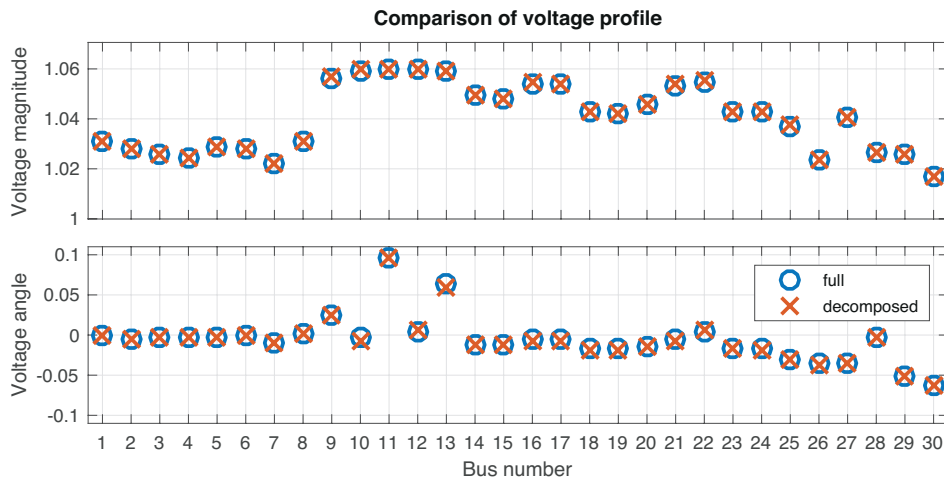


**Figure 5-2:** Comparison of obtained voltage profile from state matrix using a PSD constraint on the full matrix (blue circles) and on sub-matrices only (red crosses).

Since every formulation is essentially a replication of the C-OPF problem (only for more different time-steps and wind realizations, see Chapters 3 and 4), the decomposition technique can be applied to every formulation to decompose the PSD constraints. Note that the cliques only need to be determined once a-priori, and can be used to decompose all PSD constraints. The resulting problems will be called ‘decomposed’, such that DVE-OPF-RS and DSP-OPF-RS represent decomposed variants of VE-OPF-RS and SP-OPF-RS with every PSD constraint decomposed based on the sparsity pattern, respectively.

## 5-2 Multi-area decomposition of OPF-RS problems

Rather than solving a single OPF-RS problem for an isolated power system, we now consider multiple interconnected regions, called control areas. With the arrival of local energy production and storage, for example through the higher penetration of residential solar power and electric cars, the multi-area OPF problem has gained much relevance [53]. The collection of all control areas and interconnections can be lumped together to form a large network, which can be optimized centrally. However, there are several drawbacks to a centralized approach.

The operation of the larger network is usually not carried out by a single TSO, but by multiple TSOs, each responsible for the optimal and safe control of their local control area. Also, the centralized approach has computational drawbacks. As we have seen in Section 2-3, the worst-case computational complexity scales polynomially in the network size. It is therefore hard to find an accurate solution in reasonable time for larger systems. In practice, this is the main reason for the use of DC approximations to solve multi-area problems.

Several decomposition techniques are available for large semidefinite programs. We aim to use these to decompose a centralized OPF-RS problem into several local problems, based on the control areas. These local problems have to work together towards a solution for the global problem. Distributed solving methods have already been applied to power systems optimization, for example in [54], where an OPF problem is decomposed based on the sparsity pattern of the data, and then solved in a distributed setting using the Alternating Direction Method of Multipliers (ADMM). We use a similar approach, and formulate a decomposed problem which is then optimized using the ADMM. We decompose the original problem based on control areas, and not solely on the sparsity pattern of the data. This decomposition has been applied for the SDR of power system problems in [55], but then for the state-estimation problem instead of the OPF-RS problem.

In Section 5-2-1, we show how a network is decomposed into smaller interconnected systems, and how a single time step OPF problem with multiple control areas can be formulated as a general consensus problem. After this, the ADMM algorithm is used to solve this problem, as is explained in Section 5-2-2. This approach is then extended to full horizon OPF-RS problems in Section 5-2-3. Some concluding remarks are given in Section 5-3.

### 5-2-1 Formulating multi-area OPF problem

The decomposition of OPF problems in the local control areas is described in this section. To keep the notation light, the decomposition is explained with the following problem:

$$\underset{W \in \mathbb{S}^{2N_b}}{\text{minimize}} \quad f_G(W, \mathbf{p}^w, \mathbf{p}^D) \quad (5-1a)$$

$$\text{subject to} \quad W \in \mathcal{W}(\mathbf{p}^w, \mathbf{s}^D), \quad (5-1b)$$

$$W \succeq 0, \quad (5-1c)$$

where  $f_G$  and  $\mathcal{W}$  have been defined as described in Section 3-2-1. Note that Problem (5-1) is an instance of C-OPF with given wind trajectory and  $T = 1$ . The extension to reserve scheduling problems with longer prediction horizons will be given in later sections.

First, we will describe the division of the network in sub-networks corresponding to the control areas. After this, we will try to decompose Problem (5-1) in local problems, corresponding to these control areas. The single PSD constraint needs to be decomposed as well, as will be explained afterwards. We then obtain the decomposition of Problem (5-1) based on areas.

#### Dividing the network in control areas

Let the network be divided into several control areas, whose indices are collected in  $\mathcal{A} := \{1, \dots, N_a\}$ . Let  $\mathcal{N}_a \subset \mathcal{N}$  be defined as the subset of buses corresponding to a control

area  $a \in \mathcal{A}$ . Every bus belongs to exactly one control area, such that  $\mathcal{N}_a \cap \mathcal{N}_b = \emptyset$  for all  $a, b \in \mathcal{A}, a \neq b$ , and  $\bigcup_{a \in \mathcal{A}} \mathcal{N}_a = \mathcal{N}$ . Define  $\mathcal{B}_a$  as the set of areas that are connected to area  $a$ , such that  $\forall a \in \mathcal{A}$

$$\mathcal{B}_a := \{b \in \mathcal{A} \mid \exists i \in \mathcal{N}_a, \exists j \in \mathcal{N}_b, (i, j) \in \mathcal{L}\}.$$

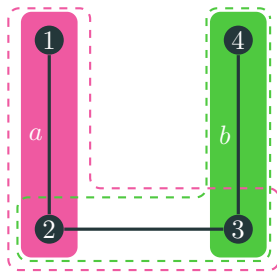
The lines that interconnect the areas are called tie-lines. These are collected  $\forall a \in \mathcal{A}$  in tie-line set  $\mathcal{T}_a \subset \mathcal{L}$ :

$$\mathcal{T}_a := \{(i, j) \in \mathcal{L} \mid i \in \mathcal{N}_a, j \notin \mathcal{N}_a\}.$$

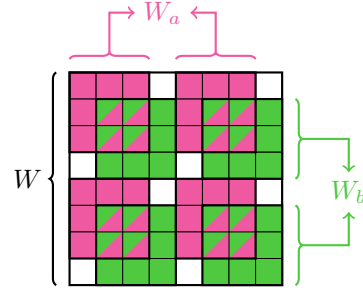
Problem (5-1) cannot be decomposed, since the feasible set and all constraints are defined for a single matrix variable  $W$ , which comprises the whole network. To decompose this variable for the different areas, we need to expand the bus sets corresponding to the areas to include the endpoints of the tie-lines connected to that area. The extended bus set  $\mathcal{N}_a^+$  is defined for every  $a \in \mathcal{A}$  as

$$\mathcal{N}_a^+ := \mathcal{N}_a \cup \{j \in \mathcal{N} \mid \exists i \in \mathcal{N}_a, (i, j) \in \mathcal{T}_a\}.$$

To clarify the above notations, an illustrative example for a multi-area 4-bus network is shown in Figure 5-3a. There are two areas defined in this network, identified in  $\mathcal{A} = \{a, b\}$ . Their respective bus sets are given by  $\mathcal{N}_a = \{1, 2\}, \mathcal{N}_b = \{3, 4\}$ , shown by the shaded regions in the figure. They are connected through a single tie-line  $(2, 3)$ , so  $\mathcal{T}_a = (2, 3), \mathcal{T}_b = (3, 2)$ . This means that the extended areas are  $\mathcal{N}_a^+ = \{1, 2, 3\}, \mathcal{N}_b^+ = \{2, 3, 4\}$ , shown with the dashed lassos. The definition of neighbouring areas is then:  $\mathcal{B}_a = \{b\}, \mathcal{B}_b = \{a\}$ .



(a) Layout of 4-bus network partitioned in two areas, where dashed lassos indicate the extended areas.



(b) Matrix variable and sub-matrices. The entries that overlap ( $[W_a]_{ab} = [W_b]_{ba}$ ) are half-shaded

**Figure 5-3:** Simple example of a multi-area network: a 4-bus network with two areas

### Decomposing matrix variable, objective and feasible set

We are now able to decompose  $W$  into sub-matrices corresponding to the extended areas. We define the network state of area  $a$  (with all its tie-lines included) as  $W_a \in \mathbb{S}^{2|\mathcal{N}_a^+|}$ , which is constructed by extracting a sub-matrix from  $W$  using only the rows and columns that correspond to the buses in  $\mathcal{N}_a^+$ . For every neighbouring area  $b \in \mathcal{B}_a$ , let the set  $\mathcal{E}_{ab}$  denote

the intersection of the extended bus sets:  $\mathcal{E}_{ab} := \mathcal{N}_a^+ \cap \mathcal{N}_b^+$ . We then define  $[W_a]_{ab}$  as the sub-matrix extracted from  $W_a$ , with its rows and columns corresponding to the buses in  $\mathcal{E}_{ab}$ , and likewise  $[W_b]_{ab}$  the extraction from  $W_b$  that correspond to the same buses. Note that the order of the subscript does not change the shared bus set between extended areas  $a$  and  $b$ , and therefore  $[W_a]_{ab}$  and  $[W_a]_{ba}$  refer to the same extraction from  $W_a$ .

An illustration of the different sub-matrices for a 4-bus network is shown in Figure 5-3b. It can be seen that the original state matrix is a  $8 \times 8$  matrix. The sub-matrices corresponding to the areas are two  $6 \times 6$  matrices, shown by the magenta and green shaded and half-shaded entries. The sub-matrices have overlap on 16 entries, which are half-shaded. These entries correspond to the buses that are the endpoints of tie-lines (e.g. bus 2 and 3).

Following [55], the data-matrices for the constraints are converted in the same fashion as the decision variables, i.e. by extracting the columns and rows corresponding to the buses in  $\mathcal{N}_a^+$ . These partitions of the data-matrices are denoted with  $[\cdot]_a$ . We can now define the feasible set for every sub-matrix, i.e. the local feasibility set denoted with  $\mathcal{W}_a(\mathbf{p}^w, \mathbf{s}^D)$ :

$$\mathcal{W}_a(\mathbf{p}^w, \mathbf{s}^D) := \left\{ W_a \in \mathbb{S}^{2|\mathcal{N}_a^+|} \mid \begin{aligned} \underline{p}_k^G &\leq \text{Tr}([Y_k]_a W_a) + p_k^D - C_k^w \mathbf{p}_k^w \leq \overline{p}_k^G, & \forall k \in \mathcal{N}_a, \forall a \in \mathcal{A}, \end{aligned} \right. \quad (5-2a)$$

$$\underline{q}_k^G \leq \text{Tr}([Y_k^*]_a W_a) + q_k^D \leq \overline{q}_k^G, \quad \forall k \in \mathcal{N}_a, \forall a \in \mathcal{A}, \quad (5-2b)$$

$$|v_k|^2 \leq \text{Tr}([M_k]_a W_a) \leq |\overline{v}_k|^2, \quad \forall k \in \mathcal{N}_a^+, \forall a \in \mathcal{A}, \quad (5-2c)$$

$$\begin{bmatrix} -|\overline{s}_{lm}|^2 & \text{Tr}([Y_{lm}]_a W_a) & \text{Tr}([Y_{lm}^*]_a W_a) \\ \text{Tr}([Y_{lm}]_a W_a) & -1 & 0 \\ \text{Tr}([Y_{lm}^*]_a W_a) & 0 & -1 \end{bmatrix} \preceq 0, \quad \forall (l, m) \in (\mathcal{N}_a^+ \times \mathcal{N}_a^+) \cap \mathcal{L}, \quad \forall a \in \mathcal{A}, \quad (5-2d)$$

$$\text{Tr}([E_{\text{ref}}]_a W_a) = 0 \}. \quad (5-2e)$$

Note that the power injection limits (5-2a) and (5-2b) are only enforced on the buses in the control area itself, and not on the extended area. The injection limits cannot be enforced on the neighbouring buses in  $\{\mathcal{N}_a^+ \setminus \mathcal{N}_a\}$ , because power injection at a bus is defined as the sum of all power flows over lines connected to a bus. The neighbouring buses have lines that connect to buses in  $\mathcal{N}_a$ , the tie-line(s) in  $\mathcal{T}_a$ , but they also have lines to buses in  $\mathcal{N}_b$ . The latter make it impossible to define the injected power in the neighbouring bus using the state matrix of area  $a$ . From an areas perspective, there is no limit on the power injection at the other end of a tie-line, allowing power to flow from and to the neighbouring areas. The line flow limits (5-2d) are defined for the intersection of buses in the extended area and the set of all lines, which is equivalent to the set of lines in an area including the tie-lines.

Consider the following local cost function  $f_G^a(W_a, \mathbf{p}^w, \mathbf{p}^D)$ :

$$f_G^a(W_a, \mathbf{p}^w, \mathbf{p}^D) := \sum_{k \in \mathcal{G}_a} c_k^{\text{li}} (\text{Tr}([Y_k]_a W_a) + p_k^D - p_k^w) + c_k^{\text{qu}} \left( (\text{Tr}([Y_k]_a W_a) + p_k^D - p_k^w) \right)^2,$$

where  $\mathcal{G}_a := \mathcal{G} \cap \mathcal{N}_a$  is defined as the generator buses that are part of the control area  $a$ , excluding the neighbouring buses, to avoid double inclusion of generator at the endpoints of tie-lines



in both local cost functions. The following problem is then equivalent to Problem (5-1):

$$\underset{\{W_a\}_{a \in \mathcal{A}}}{\text{minimize}} \quad \sum_{a \in \mathcal{A}} f_G^a(W_a, \mathbf{p}^w, \mathbf{p}^D) \quad (5-3a)$$

$$\text{subject to} \quad W_a \in \mathcal{W}_a(\mathbf{p}^w, \mathbf{s}^D), \quad \forall a \in \mathcal{A}, \quad (5-3b)$$

$$[W_a]_{ab} = [W_b]_{ba} \quad \forall a \in \mathcal{A}, \forall b \in \mathcal{B}_a, \quad (5-3c)$$

$$W \succeq 0. \quad (5-3d)$$

We have now defined Problem (5-1) as a set of  $|\mathcal{A}|$  problems, each with a local objective and feasible set. They are coupled through overlapping constraints (5-3c), to make sure that the sub-matrices are consistent, and (5-3d), the PSD constraint. The only constraint that still requires the full state matrix  $W$  is (5-3d). We will now explain how we decompose the dependency on  $W$  to allow a distributed solving of the problem.

### Decomposing PSD constraint

To decompose the centralized PSD constraint (5-3d), we make use of the chordal theorem [50], as explained in Section 5-1. We consider a graph  $G$  over  $\mathcal{N}$ , with its edges corresponding to the set of extended buses for all areas  $\{\mathcal{N}_a^+\}$ , meaning every bus in  $\mathcal{N}_a^+$  is connected to all other buses in  $\mathcal{N}_a^+$  with a single edge, for every area. This amounts to all the buses within every subset  $\mathcal{N}_a^+$  forming a maximal clique. Proposition 1 from [55] then states that this graph is chordal and all maximal cliques of  $G$  are captured by the subsets  $\{\mathcal{N}_a^+\}$ , under two assumptions:

**Assumption 2.** *The graph with the control areas as its nodes and the tie-lines between the areas as its edges is a tree, i.e. an acyclic connected graph.*

**Assumption 3.** *Every area has at least one bus that does not have overlap, i.e. does not have a tie-line connected to it.*

Assumption 2 is the most restrictive assumption, since this prevents multi-area networks that have cyclic interconnections between areas to be decomposed. However, distribution networks are usually spread out geographically and mostly not very intertwined. The typical number of tie-lines between networks tends to be very low. Assumption 3 will hold for almost every real-world power system, as there tend to be much more buses than tie-lines in multi-area systems.

If these two assumptions hold, the decomposition is valid, meaning that by restricting the sub-matrices corresponding to the extended areas to be PSD, the original matrix is also PSD, and can be completed from the local results using Algorithm 1. This enables one to split the single PSD constraint (5-3d) on  $W$  into  $|\mathcal{A}|$  smaller PSD constraints, and Problem (5-3) can be formulated in terms of the separate sub-matrix for every area.

### Multi-area OPF problem formulation

Furthermore, we decompose the equality constraints using auxiliary variables. Matrix  $\bar{W}_{ab} \in \mathbb{S}^{2|\mathcal{E}_{ab}|}$  is introduced for every pair of neighbouring areas  $a$  and  $b$ . For the sake of notational

brevity,  $\bar{W}_{ab}$  and  $\bar{W}_{ba}$  are used interchangeably to represent the same matrix. Problem (5-3) can now be rewritten as:

$$\begin{aligned} & \underset{\substack{\{W_a\}_{a \in \mathcal{A}}, \\ \{\bar{W}_{ab}\}_{a \in \mathcal{A}, b \in \mathcal{B}_a}}}{\text{minimize}} && \sum_{a \in \mathcal{A}} f_G^a(W_a, \mathbf{p}^w, \mathbf{p}^D) && (5-4a) \end{aligned}$$

$$\text{subject to } W_a \in \mathcal{W}_a(\mathbf{p}^w, \mathbf{s}^D), \quad \forall a \in \mathcal{A}, \quad (5-4b)$$

$$[W_a]_{ab} = \bar{W}_{ab} \quad \forall a \in \mathcal{A}, \forall b \in \mathcal{B}_a, \quad (5-4c)$$

$$W_a \succeq 0 \quad \forall a \in \mathcal{A}. \quad (5-4d)$$

Problem (5-4) is now only coupled through the equality constraints (5-4c). Every single coupling constraint  $[W_a]_{ab} = [W_b]_{ba}$  has been reformulated as two equality constraints  $[W_a]_{ab} = \bar{W}_{ab}$  and  $[W_b]_{ba} = \bar{W}_{ba} = \bar{W}_{ab}$ . Following Proposition 2, the optimal objective of the decomposed Problem (5-4) is equal to the optimal objective of the centralized Problem (5-3). Note that the decomposition is now based on the spatial lay-out of the power system, rather than the sparsity in the data. In the latter, the smallest possible sub-matrices are found, whereas the sub-matrices used in this decomposition correspond to the bus sets of the extended control areas, and can be quite substantial.

### 5-2-2 Distributed solving of multi-area OPF problem with ADMM algorithm

Problem (5-4) is a general consensus problem. It has a set of local constraints and variables, which are separable between the areas, and shared variables between two areas, the auxiliary variables  $\bar{W}_{ab}, \forall a \in \mathcal{A}, b \in \mathcal{B}_a$ . The local variables are related to the shared variables through the coupling constraints (5-4c).

The global consensus problem has been studied extensively in literature (see for example [56] for an extensive survey), because it arises in many different optimization problems, such as sensor networks, model fitting, machine learning, etc. In [38], Boyd applies the Alternating Direction Method of Multipliers (ADMM) to solve a consensus problem in a distributed setting. It has been proven that ADMM for this type of problem converges linearly [57]. We follow a similar approach as used in [55] to solve the decomposed OPF problem in a distributed manner.

The augmented Lagrangian function is used. This is the normal Lagrangian, with an extra quadratic term. For Problem (5-4), the augmented Lagrangian is defined as follows:

$$\begin{aligned} L(\{W_a\}, \{\bar{W}_{ab}\}, \{\Lambda_{ab}\}) := & \sum_{a \in \mathcal{A}} \left( f_G^a(W_a, \mathbf{p}^w, \mathbf{p}^D) + I_{W_a}(W_a) \right. \\ & \left. + \sum_{b \in \mathcal{B}_a} \left( \frac{\mu}{2} \|[W_a]_{ab} - \bar{W}_{ab} + \frac{\Lambda_{ab}}{\mu}\|_F^2 + \frac{1}{2\mu} \|\Lambda_{ab}\|_F^2 \right) \right) \end{aligned}$$

where  $I_{W_a}(W_a) : \mathbb{S}^{2|\mathcal{N}_a^+|} \rightarrow \{0, +\infty\}$  is the convex indicator function for constraints (5-4b) and (5-4d) that maps to infinity if one of the constraints is violated, and to zero otherwise, and step size  $\mu$  is a fixed constant, and multipliers  $\Lambda_{ab} \in \mathbb{S}^{2|\mathcal{E}_{ab}|}$  are introduced for every coupling constraint. Note that unlike  $\bar{W}_{ab}$  and  $\bar{W}_{ba}$ ,  $\Lambda_{ab}$  and  $\Lambda_{ba}$  cannot be used interchangeably,

since they correspond to different constraints. The indicator function makes sure all constraints (5-4b) and (5-4d) are satisfied and the squared norm forces constraint (5-4c) to be satisfied.

The augmented Lagrangian is optimized using a Gauss-Siedel pass on the primal variables and the auxiliary variables, after which the multipliers are updated [38]. Since either the primal or the auxiliary variables are fixed in the Gauss-Siedel steps, the problem can be decomposed for all the areas. The steps of the ADMM algorithm are now briefly described.

### Update primal variables

The multipliers and auxiliary variables are fixed at the value of the previous iteration. Since the minimization is only in  $W_a$ , all terms of  $\Lambda_{ab}$  only drop out. This results in  $|\mathcal{A}|$  separate SDPs:

$$W_a^{(k+1)} = \arg \min_{W_a} f_G^a(W_a, \mathbf{p}^w, \mathbf{p}^D) + I_{W_a}(W_a) + \sum_{b \in \mathcal{B}_a} \left( \frac{\mu}{2} \left\| [W_a]_{ab} - \bar{W}_{ab}^{(k)} + \frac{\Lambda_{ab}^{(k)}}{\mu} \right\|_F^2 \right) \quad \forall a \in \mathcal{A} \quad (5-5)$$

### Update auxiliary variables

The resulting sub-matrices  $\{W_a\}$  are used to update the auxiliary variables. The multipliers again are fixed at their previous value. Note that to update the auxiliary variables, each area only needs to communicate the part of its local state matrix that has overlap with its neighbouring area. If the multipliers  $\Lambda_{ab}$  are initialized with zero  $\forall a \in \mathcal{A}, \forall b \in \mathcal{B}_a$ , the update of the auxiliary variable simplifies to taking the average (see [38, §7.1]):

$$\bar{W}_{ab}^{(k+1)} = \frac{1}{2} \left( [W_a^{(k+1)}]_{ab} + [W_b^{(k+1)}]_{ba} \right) \quad \forall a \in \mathcal{A}, \forall b \in \mathcal{B}_a \quad (5-6)$$

### Update multipliers

For the multiplier update, no information needs to be exchanged, since the parts of the state matrix of neighbouring areas have already been communicated in the update of the auxiliary variables. The multipliers are updated as follows:

$$\begin{aligned} \Lambda_{ab}^{(k+1)} &= \Lambda_{ab}^{(k)} + \mu \left( [W_a^{(k+1)}]_{ab} - \bar{W}_{ab}^{(k+1)} \right) & \forall a \in \mathcal{A}, \forall b \in \mathcal{B}_a \\ &= \Lambda_{ab}^{(k)} + \frac{\mu}{2} \left( [W_a^{(k+1)}]_{ab} - [W_b^{(k+1)}]_{ba} \right) & \forall a \in \mathcal{A}, \forall b \in \mathcal{B}_a \end{aligned} \quad (5-7)$$

Using this algorithm, it is possible to solve the multi-area OPF problem in a distributed setting. If we assign a separate computing unit, ‘agent’, to each area, the communication graph would be identical to the graph that has the areas as nodes and the tie-lines as edges. To further illustrate the calculation and communication steps per agent, the ADMM algorithm is given from the agents perspective in Algorithm 2.

**Algorithm 2** Multi-area OPF for agent  $a$ 

- 
- 1: Initialize:  $k = 0, \Lambda_{ab}^{(0)} = 0, \bar{W}_{ab}^{(0)} = 0 \quad \forall b \in \mathcal{B}_a$
  - 2: **while** not converged **do**
  - 3:   Update  $W_a^{(k+1)}$  using (5-5)
  - 4:   Broadcast  $[W_a^{(k+1)}]_{ab}$  to all  $b \in \mathcal{B}_a$
  - 5:   Receive  $[W_b^{(k+1)}]_{ba}$  from all  $b \in \mathcal{B}_a$
  - 6:   Update  $\bar{W}_{ab}^{(k+1)}$  using (5-6) for all  $b \in \mathcal{B}_a$
  - 7:   Update  $\Lambda_{ab}^{(k+1)}$  using (5-7) for all  $b \in \mathcal{B}_a$
  - 8:    $k = k + 1$
  - 9: **end while**
- 

It can be seen that for each iteration, an agent needs to solve an SDP in Line 3. This is the step in the algorithm that has the highest computational cost. After this, only the parts of the local state matrix that have overlap with the neighbours are shared in Lines 4 and 5, using only simple operations (matrix addition, subtraction and scaling). The agents are able to reach consensus by exchanging only the relevant part of the local state matrix with neighbouring agents.

The convergence of the algorithm can be checked by looking at the residue sequence of the ADMM algorithm:

$$\eta^{(k)} = \sum_{a \in \mathcal{A}} \sum_{b \in \mathcal{B}_a} \|[W_a^{(k)}]_{ab} - \bar{W}_{ab}^{(k)}\|_F^2$$

If  $\eta$  is sufficiently small, all agents have reached consensus on the shared variables  $\{\bar{W}_{ab}\}$ .

The main advantage to decomposing large OPF-RS problems is the ability of every agent to independently find local solutions based on information received in the previous iteration. The calculations necessary for this step could therefore be carried out in parallel. Although an actual parallel implementation is outside the scope of this thesis, it is important to mention that the algorithms put forward by this result do allow such an implementation. Therefore, this approach is regarded as distributed solving of a large OPF problem.

In a sequential implementation, a computationally expensive SDP is solved by every agent at every iteration. Compared to the centralized problem, this SDP is considerably smaller, since the number of buses in the local problems is lower. ADMM algorithms typically need a large number of iterations to converge, so the local problems need to be solved many times before finding a good enough solution. Therefore, the ADMM approach without parallelization might not be the quickest method to solve an OPF-RS problem. However, when the global problem is too big to be handled by a single computing agent, for example due to memory limitations or computational constraints, the decomposition technique and ADMM algorithm as described above can provide a good way to decentralize the optimization.

### 5-2-3 Extension to multi-area OPF-RS problems

The method presented in previous sections is now extended to include the full prediction horizon, i.e. problems with  $T > 1$ . Every time step has its own corresponding state matrix,

for which the decomposition is identical to Problem (5-4). All local sub-matrices  $W_{a,t}$  are required to be feasible  $\forall a \in \mathcal{A}, \forall t \in \mathcal{T}$ . All the coupling constraints with the corresponding auxiliary variables and multipliers are also repeated  $T$  times, and Algorithm 2 can be used to find the optimal local sub-matrix for all time steps.

It is now of interest to include uncertain wind power in the multi-area OPF Problem (5-4), i.e. extend the deterministic OPF problem to an OPF-RS problem. We assume that the set of wind trajectories (both forecast and scenarios) is available to all local agents. One can either use the vertex enumeration or conic parametrization approach. For every matrix variable, auxiliary variables and multipliers are needed, creating extra computational overhead. The conic parametrization approach is preferred over the vertex enumeration approach, since the number of matrix variables in this approach is fixed (three times the number of time steps), whereas in the vertex enumeration approach the number of matrix variables depends on the number of wind buses.

Let  $\mathcal{S}$  be the multi-extraction set as defined in Section 4-2-1. One can decompose the parametrized scenario state according to the same process as described in Section 5-2-1 to obtain the following definition of the local parametrized scenario state  $\forall a \in \mathcal{A}, \forall \tilde{\mathbf{p}}^m \in \mathcal{S}, \forall t \in \mathcal{T}$ :

$$\hat{W}_{a,t}(\mathbf{p}_t^m) := W_{a,t}^f + \max(-\mathbf{1}^T \mathbf{p}_t^m, 0) W_{a,t}^{\text{us}} + \max(\mathbf{1}^T \mathbf{p}_t^m, 0) W_{a,t}^{\text{ds}},$$

where  $W_{a,t}^f, W_{a,t}^{\text{us}}, W_{a,t}^{\text{ds}} \in \mathbb{S}^{2|\mathcal{N}_a^+|}$  are defined as the sub-matrices from  $W_t^f, W_t^{\text{us}}, W_t^{\text{ds}}$  using only the rows and columns corresponding to the buses in  $\mathcal{N}_a^+$ .

Define the following constraints to ensure that every forecast and parametrized scenario sub-matrix is locally feasible and PSD  $\forall a \in \mathcal{A}, \forall t \in \mathcal{T}$

$$W_{a,t}^f \in \mathcal{W}_a(\mathbf{p}_t^{w,f}, \mathbf{s}_t^D), \quad (5-8a)$$

$$\hat{W}_{a,t}(\mathbf{p}_t^m) \in \mathcal{W}_a(\mathbf{p}_t^{w,f} + \mathbf{p}_t^m, \mathbf{s}_t^D), \quad \forall \tilde{\mathbf{p}}^m \in \mathcal{S}, \quad (5-8b)$$

$$W_{a,t}^f \succeq 0, \quad W_{a,t}^{\text{us}} \succeq 0, \quad W_{a,t}^{\text{ds}} \succeq 0. \quad (5-8c)$$

To have overlap between connected areas, coupling constraints are introduced for every sub-matrix and  $\forall a \in \mathcal{A}, \forall t \in \mathcal{T}$

$$[W_{a,t}^f]_{ab} = \bar{W}_{ab,t}^f, \quad \forall b \in \mathcal{B}_a, \quad (5-9a)$$

$$[W_{a,t}^{\text{us}}]_{ab} = \bar{W}_{ab,t}^{\text{us}}, \quad \forall b \in \mathcal{B}_a, \quad (5-9b)$$

$$[W_{a,t}^{\text{ds}}]_{ab} = \bar{W}_{ab,t}^{\text{ds}}, \quad \forall b \in \mathcal{B}_a, \quad (5-9c)$$

where auxiliary variables  $\bar{W}_{ab,t}^f, \bar{W}_{ab,t}^{\text{us}}, \bar{W}_{ab,t}^{\text{ds}} \in \mathbb{S}^{2|\mathcal{E}_{ab}|}$  are introduced for every other  $a \in \mathcal{A}, \forall b \in \mathcal{B}_a$ , such that  $\bar{W}_{ab,t}^f$  and  $\bar{W}_{ba,t}^f$  refer to the same auxiliary variable, and likewise for  $\bar{W}_{ab,t}^{\text{us}}, \bar{W}_{ab,t}^{\text{ds}}$  and  $\bar{W}_{ba,t}^{\text{us}}, \bar{W}_{ba,t}^{\text{ds}}$ . Using the local parametrization, we can define the local reserve requirements constraints  $\forall a \in \mathcal{A}, \forall \tilde{\mathbf{p}}^m \in \mathcal{S}, \forall t \in \mathcal{T}$ :

$$-C_k^G \mathbf{r}_t^{\text{ds}} \leq \text{Tr} \left( [Y_k]_a (\hat{W}_{a,t}(\mathbf{p}_t^m) - W_{a,t}^f) \right) \leq C_k^G \mathbf{r}_t^{\text{us}}, \quad \forall k \in \mathcal{G}_a, \quad (5-10a)$$

$$0 \leq \mathbf{r}_t^{\text{us}}, \quad 0 \leq \mathbf{r}_t^{\text{ds}}. \quad (5-10b)$$

Note that these constraints are only defined for generators in the control area, i.e.  $\forall k \in \mathcal{G}_a$ , since the local network state does not have information about any other generators. Therefore, the reserve costs per time-step are decomposed  $\forall a \in \mathcal{A}$ :

$$f_R^a(\mathbf{r}_t^{\text{us}}, \mathbf{r}_t^{\text{ds}}) := \sum_{k \in \mathcal{G}_a} C_k^G \mathbf{e}^{\text{us}} C_k^G \mathbf{r}_t^{\text{us}} + \mathbf{e}^{\text{ds}} C_k^G \mathbf{r}_t^{\text{ds}},$$

such that local reserve cost is simply the contribution of the local generators to the global reserve cost, i.e.  $\sum_{a \in \mathcal{A}} f_R^a(\cdot) = f_R(\cdot)$ . In every local area, there are only constraints on the entries of  $\tilde{\mathbf{r}}^{\text{us}}$  and  $\tilde{\mathbf{r}}^{\text{ds}}$  that correspond to the local generators in  $\mathcal{G}_a$ . These are also the only entries that are included in the local objective. This means that every agent only makes a decision on its own part of  $\tilde{\mathbf{r}}^{\text{us}}$  and  $\tilde{\mathbf{r}}^{\text{ds}}$ , and therefore a decomposition is unnecessary.

In SP-OPF-RS, the mismatch is balanced through equality constraints (4-16). We now formulate (4-16) in terms of the local sub-matrices  $\forall t \in \mathcal{T}$ :

$$\sum_{a \in \mathcal{A}} \sum_{k \in \mathcal{G}_a} \text{Tr} \left( [Y_k]_a W_{a,t}^{\text{us}} \right) = 1, \quad \sum_{a \in \mathcal{A}} \sum_{k \in \mathcal{G}_a} \text{Tr} \left( [Y_k]_a W_{a,t}^{\text{ds}} \right) = -1.$$

These equality constraints cannot be decomposed for all areas. Therefore, we introduce for every  $t \in \mathcal{T}$  local reserve distribution vectors  $\mathbf{d}_{a,t}^{\text{us}}, \mathbf{d}_{a,t}^{\text{ds}} \in \mathbb{R}^{N_G}$  and auxiliary variables  $\bar{\mathbf{d}}_t^{\text{us}}, \bar{\mathbf{d}}_t^{\text{ds}} \in \mathbb{R}^{N_G}$  such that the global equality constraints can be reformulated to the following local constraints  $\forall a \in \mathcal{A}, \forall t \in \mathcal{T}$ :

$$\text{Tr} \left( [Y_k]_a W_{a,t}^{\text{us}} \right) = C_k^G \mathbf{d}_{a,t}^{\text{us}}, \quad \text{Tr} \left( [Y_k]_a W_{a,t}^{\text{ds}} \right) = C_k^G \mathbf{d}_{a,t}^{\text{ds}}, \quad \forall k \in \mathcal{G}_a, \quad (5-11a)$$

$$\mathbf{1}^T \mathbf{d}_{a,t}^{\text{us}} = 1, \quad \mathbf{1}^T \mathbf{d}_{a,t}^{\text{ds}} = -1, \quad (5-11b)$$

$$\mathbf{d}_{a,t}^{\text{us}} = \bar{\mathbf{d}}_t^{\text{us}}, \quad \mathbf{d}_{a,t}^{\text{ds}} = \bar{\mathbf{d}}_t^{\text{ds}}. \quad (5-11c)$$

Constraints (5-11a) and (5-11b) can be decomposed for every area, whereas constraints (5-11c) are consensus constraints, very similar to (5-9), and can thus be decomposed with the use of a consensus algorithm.

Let  $\Xi_{\text{ma}} := \{\{\tilde{W}_a^f, \tilde{W}_a^{\text{us}}, \tilde{W}_a^{\text{ds}}\}_{a \in \mathcal{A}}, \tilde{\mathbf{r}}^{\text{us}}, \tilde{\mathbf{r}}^{\text{ds}}, \tilde{\mathbf{d}}^{\text{us}}, \tilde{\mathbf{d}}^{\text{ds}}\}$  be the set of decision variables and define  $\Theta := \{\{\tilde{W}_{ab}^f, \tilde{W}_{ab}^{\text{us}}, \tilde{W}_{ab}^{\text{ds}}\}_{a \in \mathcal{A}, b \in \mathcal{B}_a}, \tilde{\mathbf{d}}^{\text{us}}, \tilde{\mathbf{d}}^{\text{ds}}\}$  as the set of auxiliary variables for the multi area scenario parametrized OPF-RS (MASP-OPF-RS) problem. We then have that optimal objective of the following problem:

$$\begin{aligned} & \underset{\Xi_{\text{ma}}, \Theta}{\text{minimize}} && \sum_{a \in \mathcal{A}} \sum_{t \in \mathcal{T}} f_G^a(W_{a,t}^f, \mathbf{p}_t^{w,f}) + f_R^a(\mathbf{r}_t^{\text{us}}, \mathbf{r}_t^{\text{ds}}) \\ & \text{subject to} && \text{local network state constraints} && (5-8), \\ & && \text{local reserve requirement constraints} && (5-10), \\ & && \text{local reserve distribution constraints} && (5-11a), (5-11b), \\ & && \text{overlapping constraints} && (5-9), (5-11c), \end{aligned}$$

is equal to the optimal objective of SP-OPF-RS, but this problem is separable in the areas for all time steps.

We can now use the ADMM algorithm to solve MASP-OPF-RS. Multipliers  $\Lambda_{ab,t}^f, \Lambda_{ab,t}^{\text{us}}, \Lambda_{ab}^{\text{ds}} \in \mathbb{S}^{2|\mathcal{E}_{ab}|}$  are introduced  $\forall a \in \mathcal{A}, \forall b \in \mathcal{B}_a, \forall t \in \mathcal{T}$  for the overlapping matrix constraints, and

$\lambda_{a,t}^{\text{us}}, \lambda_{a,t}^{\text{ds}} \in \mathbb{R}^{N_G}$  are introduced  $\forall a \in \mathcal{A}, \forall t \in \mathcal{T}$  for the reserve distribution overlapping constraints. All the multipliers are collected in  $\Gamma$ . The augmented Lagrangian of the problem is then given by

$$\begin{aligned}
L(\Xi_{\text{ma}}, \Theta, \Gamma) = & \sum_{a \in \mathcal{A}} \sum_{t \in \mathcal{T}} f_G^a(W_{a,t}^f, \mathbf{p}_t^{w,f}) + f_R^a(\mathbf{r}_t^{\text{us}}, \mathbf{r}_t^{\text{ds}}) + I_{W_a}(W_{a,t}^f, W_{a,t}^{\text{us}}, W_{a,t}^{\text{ds}}) \\
& + \frac{\mu}{2} \left\| \mathbf{d}_{a,t}^{\text{us}} - \bar{\mathbf{d}}_t^{\text{us}} + \frac{\lambda_{a,t}^{\text{us}}}{\mu} \right\|_2^2 + \frac{\mu}{2} \left\| \mathbf{d}_{a,t}^{\text{ds}} - \bar{\mathbf{d}}_t^{\text{ds}} + \frac{\lambda_{a,t}^{\text{ds}}}{\mu} \right\|_2^2 \\
& + \sum_{b \in \mathcal{B}_a} \frac{\mu}{2} \left\| [W_{a,t}^f]_{ab} - \bar{W}_{ab,t}^f + \frac{\Lambda_{ab,t}^f}{\mu} \right\|_F^2 + \frac{\mu}{2} \left\| [W_{a,t}^{\text{us}}]_{ab} - \bar{W}_{ab,t}^{\text{us}} + \frac{\Lambda_{ab,t}^{\text{us}}}{\mu} \right\|_F^2 \\
& + \frac{\mu}{2} \left\| [W_{a,t}^{\text{ds}}]_{ab} - \bar{W}_{ab,t}^{\text{ds}} + \frac{\Lambda_{ab,t}^{\text{ds}}}{\mu} \right\|_F^2 + f(\Gamma)
\end{aligned}$$

where  $I_{W_a}(W_{a,t}^f, W_{a,t}^{\text{us}}, W_{a,t}^{\text{ds}})$  is the convex indicator function for all constraints except the overlapping constraints, and  $f(\Gamma)$  indicates terms of  $\Gamma$  only, which drop out in the ADMM algorithm and are omitted for the sake of brevity. The steps of the ADMM algorithm are comparable with the steps described in Section 5-2-2, i.e. update primal, update auxiliary and update multipliers. The equations used to update all variables are shown on the next page.

$$\begin{aligned}
\Xi_{\text{ma}}^{(k+1)} = \arg \min_{\Xi_{\text{ma}}} & \sum_{a \in \mathcal{A}} \sum_{t \in \mathcal{T}} f_G^a(W_{a,t}^f, \mathbf{p}_t^{w,f}) + f_R^a(\mathbf{r}_t^{\text{us}}, \mathbf{r}_t^{\text{ds}}) + I_{W_a}(W_{a,t}^f, W_{a,t}^{\text{us}}, W_{a,t}^{\text{ds}}) \\
& + \frac{\mu}{2} \left\| \mathbf{d}_{a,t}^{\text{us}} - \bar{\mathbf{d}}_t^{\text{us},(k)} + \frac{\lambda_{a,t}^{\text{us},(k)}}{\mu} \right\|_2^2 + \frac{\mu}{2} \left\| \mathbf{d}_{a,t}^{\text{ds}} - \bar{\mathbf{d}}_t^{\text{ds},(k)} + \frac{\lambda_{a,t}^{\text{ds},(k)}}{\mu} \right\|_2^2 \\
& + \sum_{b \in \mathcal{B}_a} \frac{\mu}{2} \left\| [W_a^f]_{ab} - \bar{W}_{ab}^{f,(k)} + \frac{\Lambda_{ab}^{f,(k)}}{\mu} \right\|_F^2 \\
& + \frac{\mu}{2} \left\| [W_a^{\text{us}}]_{ab} - \bar{W}_{ab}^{\text{us},(k)} + \frac{\Lambda_{ab}^{\text{us},(k)}}{\mu} \right\|_F^2 \\
& + \frac{\mu}{2} \left\| [W_a^{\text{ds}}]_{ab} - \bar{W}_{ab}^{\text{ds},(k)} + \frac{\Lambda_{ab}^{\text{ds},(k)}}{\mu} \right\|_F^2,
\end{aligned}$$

$$\begin{aligned}
\bar{W}_{ab,t}^{f,(k+1)} &= \frac{1}{2} \left( [W_{a,t}^{f,(k+1)}]_{ab} + [W_{b,t}^{f,(k+1)}]_{ba} \right) \\
\bar{W}_{ab,t}^{\text{us},(k+1)} &= \frac{1}{2} \left( [W_{a,t}^{\text{us},(k+1)}]_{ab} + [W_{b,t}^{\text{us},(k+1)}]_{ba} \right) \\
\bar{W}_{ab,t}^{\text{ds},(k+1)} &= \frac{1}{2} \left( [W_{a,t}^{\text{ds},(k+1)}]_{ab} + [W_{b,t}^{\text{ds},(k+1)}]_{ba} \right) \\
\bar{\mathbf{d}}_t^{\text{us},(k+1)} &= \frac{1}{|\mathcal{A}|} \sum_{a \in \mathcal{A}} \mathbf{d}_{a,t}^{\text{us},(k+1)} \\
\bar{\mathbf{d}}_t^{\text{ds},(k+1)} &= \frac{1}{|\mathcal{A}|} \sum_{a \in \mathcal{A}} \mathbf{d}_{a,t}^{\text{ds},(k+1)} \\
\Lambda_{ab,t}^{f,(k+1)} &= \Lambda_{ab,t}^{f,(k)} + \mu \left( [W_{a,t}^{f,(k+1)}]_{ab} - \bar{W}_{ab,t}^{f,(k+1)} \right) \\
\Lambda_{ab,t}^{\text{us},(k+1)} &= \Lambda_{ab,t}^{\text{us},(k)} + \mu \left( [W_{a,t}^{\text{us},(k+1)}]_{ab} - \bar{W}_{ab,t}^{\text{us},(k+1)} \right) \\
\Lambda_{ab,t}^{\text{ds},(k+1)} &= \Lambda_{ab,t}^{\text{ds},(k)} + \mu \left( [W_{a,t}^{\text{ds},(k+1)}]_{ab} - \bar{W}_{ab,t}^{\text{ds},(k+1)} \right) \\
\lambda_{a,t}^{\text{us},(k+1)} &= \lambda_{a,t}^{\text{us},(k)} + \mu \left( \mathbf{d}_{a,t}^{\text{us},(k+1)} - \bar{\mathbf{d}}_t^{\text{us},(k+1)} \right) \\
\lambda_{a,t}^{\text{ds},(k+1)} &= \lambda_{a,t}^{\text{ds},(k)} + \mu \left( \mathbf{d}_{a,t}^{\text{ds},(k+1)} - \bar{\mathbf{d}}_t^{\text{ds},(k+1)} \right)
\end{aligned}$$

In every iteration of this algorithm, multiple instances of SP-OPF-RS with an adapted objective are solved. Note that these instances are of lower dimension than the overall system matrix for a centralized problem would be.

### 5-3 Conclusions

We have provided two ways to decompose OPF-RS type problems. First, the decomposition of the computationally expensive PSD constraints is explained based on the chordal theorem. Due to the sparsity in the data matrices, typical for power systems, the computational complexity is greatly reduced. A matrix completion algorithm is proposed for the guaranteed rank-one reconstruction of the matrix variable.

In the second approach, a decomposition method is given for multi-area systems. The matrix variable and all corresponding constraints and objective function are partitioned according



to the control areas, such that for every control area a separate problem is created which is coupled only with auxiliary variables. Again, the PSD constraint is decomposed with the help of the chordal theorem, but now based on the bus sets that correspond to an area rather than the sparsity pattern. The ADMM algorithm is then used to solve the resulting general consensus problem. Finally, the extension to full horizon problems with reserve scheduling is made.

In the following chapter, the decomposition methods described in above are validated on a realistic IEEE benchmark system and a discussion on the tractability of the resulting optimization problems by means of computational time analysis is presented.



# Simulation Study

In this chapter, we present the results of the simulation study for all proposed formulations. The violation levels of the solutions are checked using power flow simulations. We first introduce the simulation set up in Section 6-1. In Section 6-2, the solutions and violation levels of VE-OPF-RS and SP-OPF-RS are compared to the DC benchmarks. The equivalence between these problems and the sparsity decomposed variants is shown in Section 6-3. In Section 6-4 the spatial decomposition technique for multi-area systems is demonstrated. Finally, some concluding remarks are given in Section 6-5.

## 6-1 Simulation set up

The simulation set up is discussed in this section. In Section 6-1-1, the modelling for the uncertain wind power and power system model is discussed. Next, we explain the optimization and solution extraction process in Section 6-1-2. The obtained solutions are then used in Power Flow (PF) simulations, which is discussed in Section 6-1-3. The Direct Current (DC) model is used to obtain a benchmark approach, and its implementation is briefly discussed in Section 6-1-4.

### 6-1-1 Modelling wind power and power system

We model the wind power as a deterministic component (the forecast) with an additive uncertainty (the mismatch). We use a Markov chain-based model that produces trajectories of the mismatch, with the temporal correlation taken into account, following [58]. The model is trained on a data-set corresponding to the hourly aggregated wind power production (actual and forecast) of Germany over the period 2006-2011. The mismatch is discretized in 41 states, and the probability of transitioning from a given state to any other state is calculated. The model is initialized with the forecast and can be run to generate samples of the uncertainty that have a similar probabilistic distribution as the actual wind power. The advantage of this approach is that the modelling of the uncertainty is based purely on data, and no assumptions

are made on the probabilistic properties of the wind power. In Figure 6-1, a full day of wind power is shown. The thick red line shows the forecast wind power, and all thin green lines are samples of wind trajectories. See also [59, §2.5] for an overview of the wind model used and its properties. Note that all our results on stochastic optimization are independent of the method used to obtain trajectories of the mismatch.

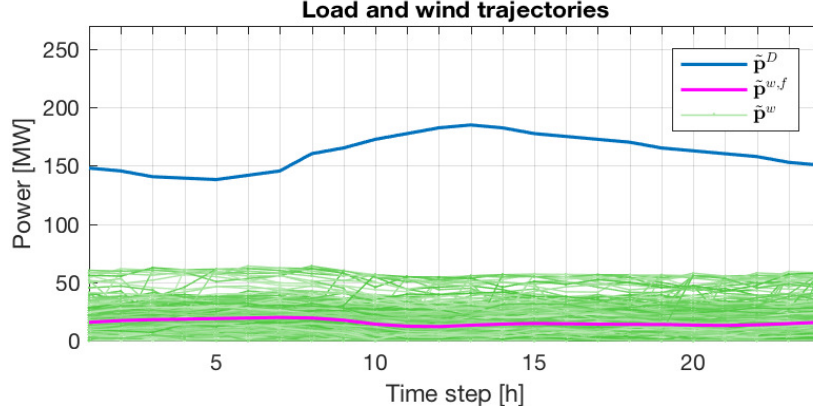


**Figure 6-1:** Load, wind forecast, and wind scenario trajectories as used in optimization.

Our methodology is applied to the 30-bus IEEE test case, a benchmark network commonly used in literature; its data can be retrieved from [60]. A schematic overview of the network is shown in Figure 6-2. We model the wind as a single in-feed of wind power at bus 10, because the wind model that has a single output. If we were to use multiple wind buses, we need to have a model that takes the joint probability into account. All proposed formulations are also valid for systems with multiple wind buses.

The load profile is assumed to be known in advance. The nominal load of each bus is multiplied with the load profile such that a time-varying load is available for every bus. The total load is shown as the blue line in Figure 6-1. Due to the high penetration of the wind power, congestion in the network is more likely, since an extra power source is introduced. We therefore increase the apparent power flow limits  $|\bar{s}|$  for all lines with 5%, to allow more deviations. This is justified by the fact that the IEEE test cases are quite old (specifically, the 30 bus test system is based on data from 1974), and most modern networks have been upgraded to handle more deviations due to the increased uncertainty from renewable energy sources. The reserve costs  $\forall k \in \mathcal{G}$  are derived from the test case as  $C_k^G e^{\text{us}} = (C_k^G e^{\text{qu}} \bar{p}_k^2 + C_k^G e^{\text{li}} \bar{p}_k) / \bar{p}_k$ , and the downspinning costs are defined as  $e^{\text{ds}} = 0.9e^{\text{us}}$ . All costs are shown in Table 6-1.

**Table 6-1:** Cost coefficients used in optimization

Generator	$e^{\text{li}}$	$e^{\text{qu}}$	$e^{\text{us}}$	$e^{\text{ds}}$
22	3	0.0625	6.125	5.513
1	3	0.02	4.6	4.14
2	3	0.0175	4.4	3.96
13	3	0.025	4	3.6
23	3	0.025	3.75	3.375
27	3	0.0083	3.4587	3.113

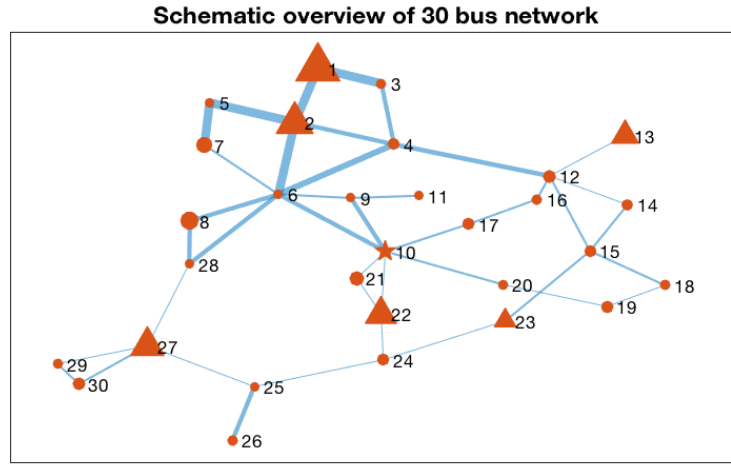


**Figure 6-2:** Schematic overview of the IEEE 30 bus test system. Circles indicate load buses, triangles generator buses and the star is the wind power in-feed. The size of each symbol corresponds to the respective demand or production capacity. The width of the lines corresponds to the line rating, such that a thick line corresponds to a high rating

### 6-1-2 Running optimization and extracting solutions

Having the network and wind model in place, we can run the optimization using the formulations as explained in the previous chapters. First, a set of scenarios is generated. To determine the number of samples needed for the scenarios, Equation (2-3) is used. Since the relation between  $N_s$  and  $\beta$  is inverse logarithmic (see Section 2-4-3), it is possible to select a high confidence level without impacting the sample complexity very much. We use  $\varepsilon = 0.05$  and  $\beta = 10^{-5}$ , corresponding to a 99.999% confidence on a maximum level of constraint violation of 5%. We implement all the algorithms using the MATLAB toolbox YALMIP [61] with the MOSEK [62] solver for SDPs, and the GUROBI [63] solver for linear programs. All simulations are run on a MacBook Pro Retina 13' with a 2,4 GHz Intel Core i5 processor and 8 GB of RAM.

In order to simulate the network to test the probabilistic properties of the obtained solution, we extract the generator settings, voltage magnitudes and reserve distribution vectors from the decision variables. The generator voltage magnitudes are related to the diagonal entries of  $\tilde{W}^f$ , using the following relation  $\forall k \in \mathcal{G}, \forall t \in \mathcal{T}$ :

$$|v_{k,t}| = \sqrt{\operatorname{Re}(v_k)^2 + \operatorname{Im}(v_k)^2} = \sqrt{W_t^f(k, k) + W_t^f(N_b + k, N_b + k)}. \quad (6-1a)$$

Using Remark 3.1, the optimal generator dispatch and voltage magnitude are extracted from  $\tilde{W}^f$ , such that we have  $\forall k \in \mathcal{G}, \forall t \in \mathcal{T}$ :

$$p_{k,t}^G = \operatorname{Tr}(Y_k W_t^f) + p_{k,t}^D - p_{k,t}^w. \quad (6-1b)$$

The reserve power is defined as  $\forall k \in \mathcal{G}, \forall t \in \mathcal{T}$

$$C_k^G \mathbf{r}_t = -C_k^G \mathbf{d}_t^{\text{us}} \min(\mathbf{1}^T \mathbf{p}_t^m, 0) - C_k^G \mathbf{d}_t^{\text{ds}} \max(\mathbf{1}^T \mathbf{p}_t^m, 0), \quad (6-2)$$

where  $\tilde{\mathbf{d}}^{\text{us}}, \tilde{\mathbf{d}}^{\text{ds}}$  are obtained either from the optimal solution directly in the case of VE-OPF-RS or extracted from the coefficient matrices using Equation (4-17) in the case of PC-OPF-RS. The resulting reserve power is then implemented in the simulations  $\forall k \in \mathcal{G}, \forall t \in \mathcal{T}$  as

$$p_{k,t}^G = \max(\min(p_{k,t}^{G,f} + C_k^G \mathbf{r}_t, \overline{p_k^G}), \underline{p_k^G}),$$

such that the generator dispatch is always within the limits. For the sparsity decomposed programs DVE-OPF-RS and DSP-OPF-RS, Algorithm 1 is first used to complete the state and coefficient matrices.

### 6-1-3 Testing solutions with power flow simulation

After retrieving a solution, the network is simulated using MATPOWER [64], commercial software for solving (optimal) power flow problems using successive quadratic programming. In the PF problem, the generator dispatch and loads are fixed. The resulting power flows over the network are then calculated without taking any other limits into account.

We generate a set of  $10^4$  scenarios, different from those used in optimization but using the same wind model. These scenarios will be used in Monte Carlo (MC) simulations.

The PF problem is simulated for the forecast case with the nominal generator dispatch, and for every scenario with the nominal generator dispatch plus the reserve power. The wind power is implemented as a negative load on the wind-bus. After simulating the network, the resulting power flows and voltage magnitudes are evaluated. All other quantities (i.e. the generator dispatch and loads) are fixed in the power flow simulations, and therefore it is only necessary to check the lineflows and voltage magnitudes. The percentage of scenarios which violate the constraints is an empiric measure for the probability of constraint violation for a generic sample  $\tilde{\mathbf{p}} \in \mathcal{P}$ . A schematic overview of the optimization and simulation process for all proposed formulations is given in Figure 6-4.

### 6-1-4 Benchmarking with direct current model

A comparison using a DC model of the power network is delivered as a benchmark approach, following [10]. A detailed description of the DC model can be obtained from [4, 5] and is also described in Appendix A.

The solution of the DC benchmark program is the real generator power and distribution vectors for every hour,  $\{\tilde{\mathbf{p}}^{G,\text{dc}}, \tilde{\mathbf{d}}^{\text{us,dc}}, \tilde{\mathbf{d}}^{\text{ds,dc}}\}$ . One also needs the generator voltage magnitudes in order to run the power flow simulations. In [10], the nominal voltage magnitude (1 p.u.) was used for all time steps and scenarios. This most likely results in larger violations, since the reactive power flows are not taken into account, and the voltage magnitudes are assumed constant at 1 p.u. when using the DC model.

We here develop a novel benchmark approach, namely converted DC (CDC), to have a more sophisticated comparison by solving the following program:

$$\underset{\tilde{W}}{\text{minimize}} \quad \sum_{t \in \mathcal{T}} \sum_{k \in \mathcal{G}} \left( p_{k,t}^{G,\text{dc}} - \left( \text{Tr}(Y_k W_t) + p_{k,t}^D - p_{k,t}^{w,f} \right) \right)^2 \quad (6-3a)$$

$$\text{subject to} \quad W_t \in \mathcal{W}(\mathbf{p}_t^{w,f}, \mathbf{s}_t^D), \quad \forall t \in \mathcal{T}, \quad (6-3b)$$

$$W_t \succeq 0, \quad \forall t \in \mathcal{T}. \quad (6-3c)$$

The solution to this program is a trajectory of feasible (AC) network states  $\tilde{W}$ , such that the generator dispatch is as close as possible to  $\tilde{p}^{G,dc}$ . The distribution vectors used in simulation will be equal to those obtained from the solution of the DC framework. A schematic overview of the optimization and simulation process to obtain and validate both the benchmark and proposed formulations is given in Figure 6-3.

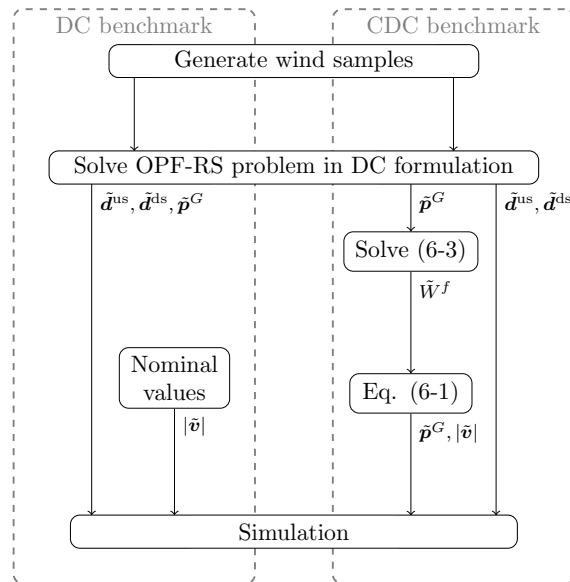


**Figure 6-3: ]**

Schematic overview of optimization and simulation process for the DC (left) and converted DC (right) benchmark approach

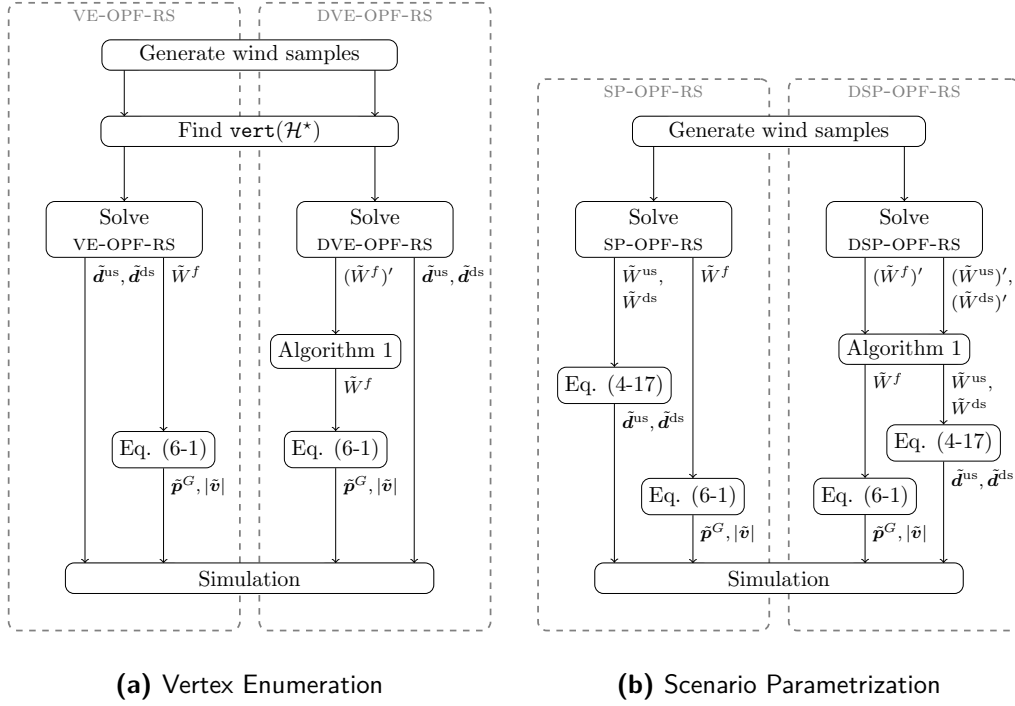


**Figure 6-4:** Schematic overview of optimization and simulation processes for the proposed approaches. In both figures, the proposed optimization is shown on the left, and the decomposed variant on the right.

## 6-2 Results for tractable approximations of CC-OPF-RS

In this section, the simulation results for all tractable approximations of CC-OPF-RS are discussed, i.e. VE-OPF-RS and SP-OPF-RS. In Section 6-2-1, the optimization results are shown, and the optimization times and the different objectives are given. After this, the optimal generator dispatch and distribution vectors for the different problems are compared in Section 6-2-2. Finally, the solutions are simulated to test their probabilistic properties. These results are shown in Section 6-2-3.

### 6-2-1 Optimization results for tractable approximations

VE-OPF-RS and SP-OPF-RS are solved using for the set-up described in Section 6-1. In all cases, the solver finds a feasible solution and exits without errors. We repeated the optimization with the same wind trajectories 10 times, and averaged the optimization time as an indication of the computational effort required for a solution. The resulting average optimization times and optimal objectives for the different formulations are shown in Table 6-2.

It can be seen that VE-OPF-RS has a slightly better performance in terms of the objective function. The optimal objective of SP-OPF-RS is about 3% higher than the optimal objective of VE-OPF-RS. Moreover, VE-OPF-RS finds a solution in a shorter amount of time. Since we only use one wind bus ( $N_w = 1$ ), the number of semidefinite matrix variables is identical



**Table 6-2:** Optimization times and optimal objectives for the 30-bus test case

	$f(\Theta^{\text{opt}})$	Average opt. time (s)
VE-OPF-RS	151.78	417.63
SP-OPF-RS	156.73	457.71

for both formulations ( $(2N_w + 1)T = 3T$ ). The increased overhead of having more scenarios makes SP-OPF-RS computationally more expensive, but this will diminish when more wind buses are used.

To demonstrate the computational advantage of SP-OPF-RS, we optimize the same network, but now with multiple wind buses. We again repeat the experiment 10 times to obtain the average optimization times shown in Figure 6-5. Based on the worst-case computational complexity analysis, one expects the actual computational complexity of VE-OPF-RS to increase with the number of wind buses, whereas one expects the actual complexity of SP-OPF-RS to stay roughly the same. We consider the average optimization times as an indication of the actual computational complexity of the problem. One can clearly observe in Figure 6-5 that the optimization time for VE-OPF-RS indeed grows with the number of buses, and that the time required for SP-OPF-RS is almost flat.

Note that the solutions obtained from this experiment have no guarantees, since the wind model used does not provide joint probabilities for multiple wind buses. This experiment is merely an illustration of the favourable computational cost of the SP-OPF-RS formulation for systems with multiple wind buses.

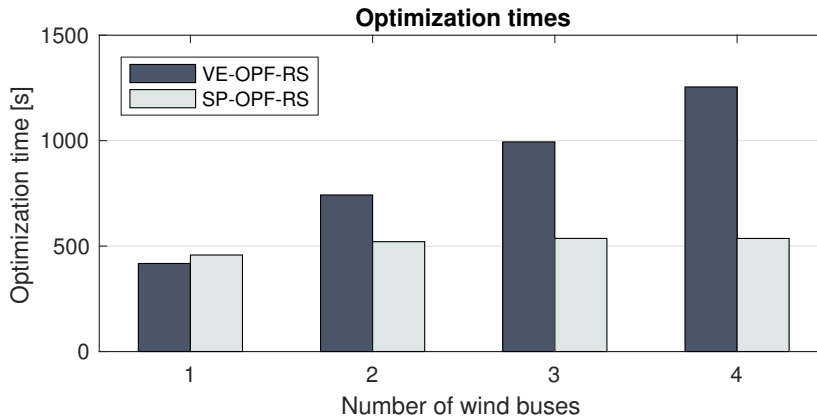


**Figure 6-5:** Average computational time for VE-OPF-RS and SP-OPF-RS systems with multiple wind buses. The optimization time for VE-OPF-RS increases with the number of wind buses, but stays almost flat for SP-OPF-RS.

Having obtained the optimal solutions for all the formulations, one can inspect the optimal generator dispatch and distribution vectors, as is presented in the following section.

### 6-2-2 Comparing generator dispatch and reserve distribution

After running the optimization, one obtains an optimal trajectory of feasible network states  $\tilde{W}^f$ . Using Equation (6-1a), the generator dispatch  $\tilde{p}^G$  is extracted from this trajectory. The resulting dispatch per time step is shown in Figure 6-6. The total height of each bar is equal to the total produced power. Each partition of the bar corresponds to the output of one generator, and the lowest part is the forecast wind power, indicated with ‘w’. The order of the generators corresponds to the relative production costs, e.g. the generator at bus 27 has the lowest cost and the generator at bus 22 the highest.

For VE-OPF-RS (Figure 6-6a), it can be seen that generator 27, which has the lowest production costs, is used to mitigate any variance in the forecast wind power. The output of the more expensive generators is decreased in the hours with less demand (3 to 7). In the peak hours (12 to 14), generator 23 is used to satisfy the extra load, while all other generators are more or less constant. The generator dispatch for SP-OPF-RS (Figure 6-6b)) is slightly different. There is less distinction between the dispatch for low and peak hours.

The shaded area behind the bars corresponds to the total demand per time step. The production exceeds the demand for every hour, for both formulations. This is expected, since any solution for which the load is not satisfied is infeasible, and all formulations yielded feasible solutions. The overproduction is due to the fact that load satisfaction is not enforced as an equality constraint, but rather as a lower bound on the power production, which is then pushed down by the objective. The amount of overproduction is below 2 MW for both formulation for every time step, which is deemed acceptable.

Next, the optimal distribution vectors  $\tilde{d}^{\text{us}}$ ,  $\tilde{d}^{\text{ds}}$  for both formulations are compared. These time varying vectors are shown as shaded squares in Figure 6-7, where a darker shade corresponds to more participation in the up- or downspinning reserve for a given generator and hour. Again, the order of the generators corresponds to the reserve cost vectors, such that the highest reserve cost corresponds to the first row and the lowest reserve cost to the last row.

For the reserve distribution of the VE-OPF-RS formulation (Figure 6-7a), all the upspinning reserve comes from generator 27 for all hours, which has the lowest cost. The downspinning reserve is distributed over 27 and 23 for certain hours, and only 27 for the other hours. To understand this behaviour, it is insightful to look at the generator dispatch in combination with the reserve power. In Figure 6-8, the relative production for every generator is shown, i.e. the actual production divided by the capacity of that generator. The width of the bars corresponds to the total capacity, i.e. a wide bar is a generator with a large capacity and a narrow bar is a generator with a small capacity. The generator dispatch is shown as the grey bars, and the up- and downspinning reserves are shown as green and red arrows, respectively. The reserve is calculated with Equation (6-2), using the worst case positive and negative mismatches from the wind samples used in optimization.

We now examine the generator output for  $t = 5$  where demand is low, and for  $t = 11$ , one of the peak hours. At time step 5 (Figure 6-8a), all upspinning reserve is provided by generator 27. It is however impossible for generator 27 to also provide all the downspinning reserve, as the dispatched output of that generator is lower than the required downspinning reserve. Therefore, a part of the downspinning reserve is distributed to the generator at bus 23. This is a clear example why having asymmetric reserve distribution, i.e. a separate up- and downspinning strategy, can improve performance: if a single reserve distribution

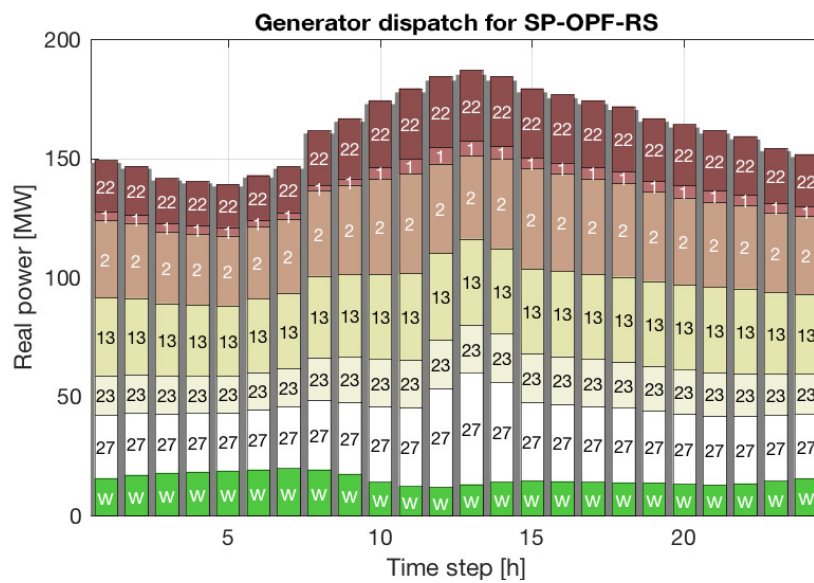
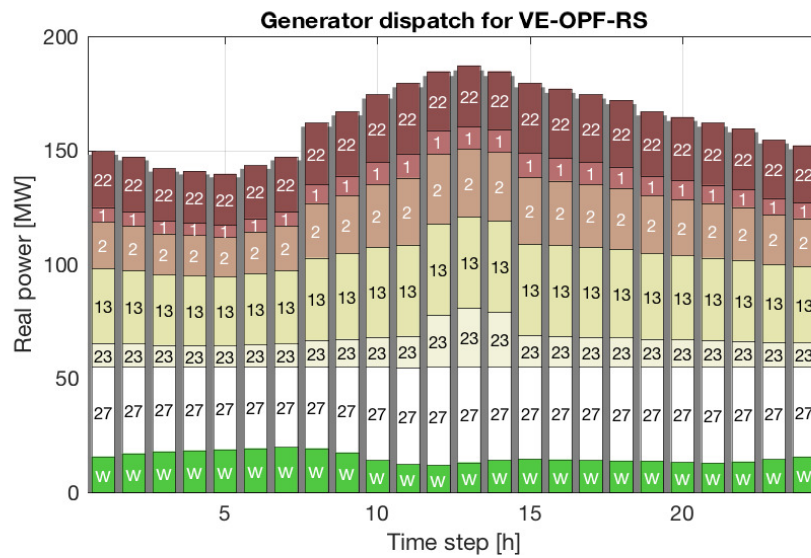
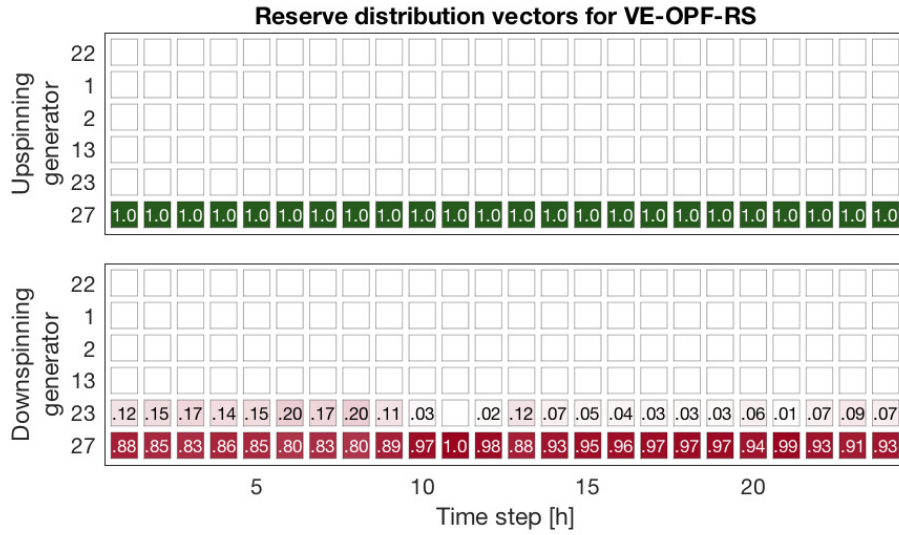
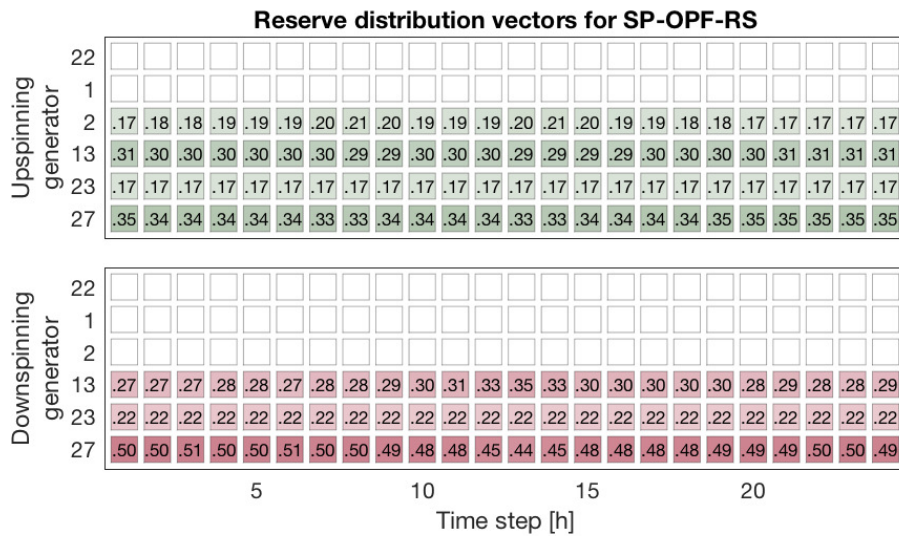


**Figure 6-6:** Generator dispatch per hour for different formulations for the 30-bus test case. The grey shaded area corresponds to the total demand per hour. The numbers correspond to the generator buses, and the lowest part of each bar (green) indicates the wind power per hour.



(a)



(b)

**Figure 6-7:** Up- and downspinning reserve distribution vectors per generator and hour for different formulations for the 30-bus test case. Darker cells correspond to higher contribution to the reserve power. The generators are ordered from high to low reserve costs.

vector were used, the upspinning reserve would have to be distributed in the same way as the downspinning reserve, causing generator 23 to provide upspinning reserve as well, which would have resulted in higher reserve costs. Comparing this situation with time step 11 (Figure 6-8b), it is clear to see that due to the higher demand, the output of all generators, including generator 27, has increased. Due to this increase, generator 27 is now able to satisfy not only the upspinning, but also the downspinning reserve requirements.

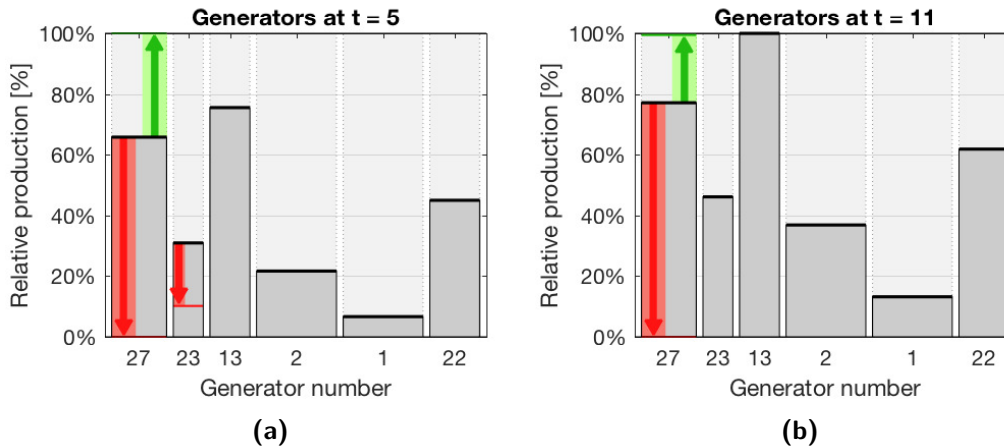


**Figure 6-8:** Generator dispatch and reserve power for VE-OPF-RS at different time steps for the 30-bus test case. The width and height of the bars corresponds to the capacity and relative production of a generator, respectively. The upward green arrow indicates upspinning reserve, the downward red arrow indicates downspinning reserve. At  $t = 5$ , the downspinning reserve is distributed over two generators.

Next, we examine the reserve distribution for SP-OPF-RS, shown in Figure 6-7b. The reserve is spread out more evenly, using the four generators with the lowest cost for upspinning and three generators with the lowest cost for downspinning. For the upspinning, the distribution along the four generators is very equal and constant throughout the entire prediction horizon. The downspinning reserve is distributed on the three generators with the lowest cost, with generator 27 providing the majority of the reserve for all hours. Inspecting the same time steps in Figure 6-9, one can see how the reserve is distributed for the low and peak time steps. At both hours, the reserve distribution is very similar. At  $t = 5$ , not a single generator is fully used, and at  $t = 11$  generator 13 is used fully when the maximum upspinning reserve is provided.

In VE-OPF-RS, the scenario state can be chosen freely, as long as the network is in balance. In the SP-OPF-RS formulation on the other hand, the scenario state is defined as a conic combination of coefficient matrices. Clearly, the latter does not allow for the strict use of only one generator, but requires multiple generators to be used. This is also the reason why the optimal objective for VE-OPF-RS is slightly below the optimal objective for SP-OPF-RS. We will now implement both solutions in power flow simulations and check whether the resulting violation levels, to see if the probabilistic guarantees hold.

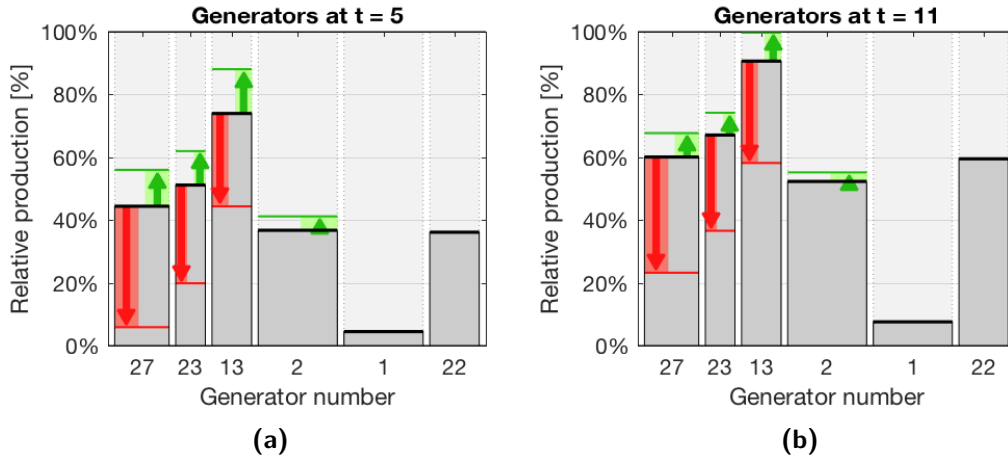


**Figure 6-9:** Generator dispatch and reserve power for SP-OPF-RS at different time steps for the 30-bus test case. The width of the bars corresponds to the capacity of a generator. The upward green arrow indicates upspinning reserve, the downward red arrow indicates downspinning reserve. For both time steps, the reserve is distributed over the multiple generators.

### 6-2-3 Violation levels based on power flow simulations

The probability of constraint violation for the obtained generator dispatches and reserve distributions for both formulations is examined with the use of Monte-Carlo simulations as described in Section 6-1-3. We simulate the network using the two solutions described in the previous section. To benchmark the probabilistic properties, the results are compared with the DC and CDC benchmark solutions.

The relative line loadings for all hours and samples are shown as box plots per line in Figure 6-10 for the (C)DC benchmarks, and VE-OPF-RS and SP-OPF-RS. The relative line loading is defined as the apparent power flow over a line divided by the line rating  $\forall(l, m) \in \mathcal{L}$

$$|s_{lm}^{\text{rel}}| := \frac{|s_{lm}|}{|s_{lm}^{\text{max}}|},$$

such that a loading higher than 100% corresponds to a violation of the lineflow limit. The DC benchmark (Figure 6-10a) result shows the biggest violations, followed by the CDC benchmark (Figure 6-10b). For both the benchmark results, line 10, 30, 31, and 35 are overloaded in a large share of all the line loadings. The VE-OPF-RS solution shows much less violation, as only line 10 is slightly overloaded, whereas the SP-OPF-RS solution shows almost no violations for all hours and scenarios. It appears that the distribution of the reserve power over multiple generators caused the power flows to be better divided over all the lines, resulting in less congestion.

The number of violating<sup>1</sup> network states is counted for each hour, and divided by the total number of samples. The resulting fraction is an empiric measure of the probability on constraint violation per hour. In Figure 6-11 the results are shown. As expected, the benchmark

<sup>1</sup>A network state is violating if at least one of the line limits is not satisfied.

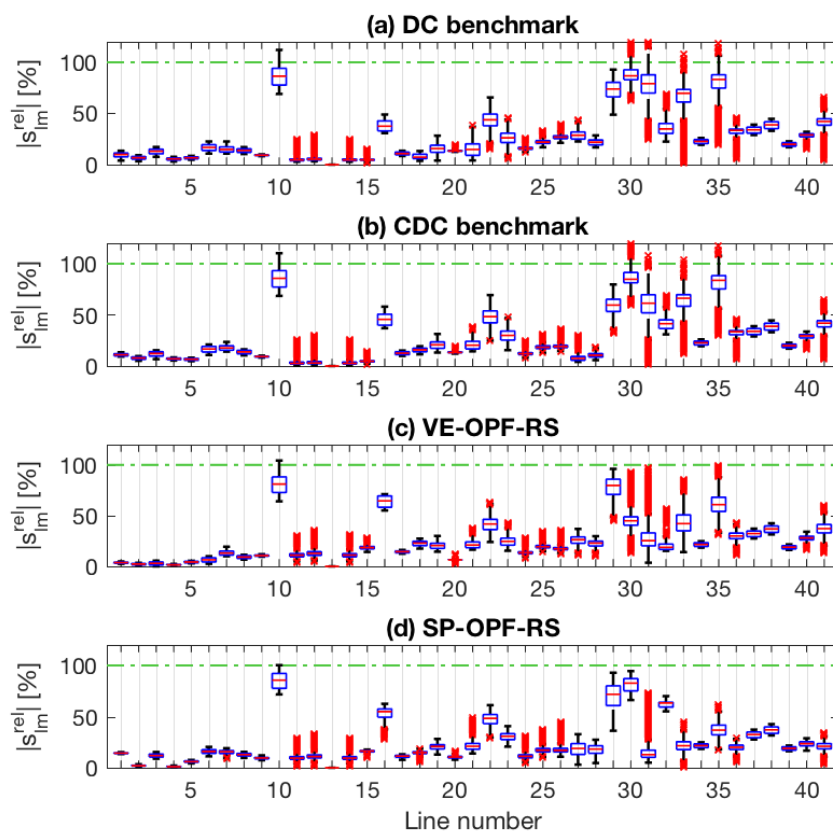


**Figure 6-10:** Relative line loading for all hours and scenarios per line for the 30-bus test case. The red line represents the median value, edges of each box correspond to the 25th and 75th percentiles, the whiskers extend to 99% coverage, and the red marks denote the data outliers. The green dashed line indicates the limit. The upper plots (a) and (b) show the DC benchmark results, and the lower plots (c) and (d) show the proposed approaches.

solutions show a very high level of violation during the peak hours. Although the CDC solution reduces the chance of lineflow limit violation, the theoretical limit is exceeded for every  $t \geq 8$ . This can be explained by the fact that in the DC framework, the bus voltages are assumed to be constant at nominal value and all reactive power flows are neglected. Therefore, the empirical chance of constraint violation is well above the theoretical limits once the benchmark solutions are implemented in the AC power flow simulations.

The empirical chance of constraint violation for the VE-OPF-RS results is well below the theoretical limit, at most 1.01% at  $t = 13$ . The line limit violations for SP-OPF-RS are omitted in Figure 6-11, since the violations are too small to be visible (at most 0.05% at  $t = 13$ ).

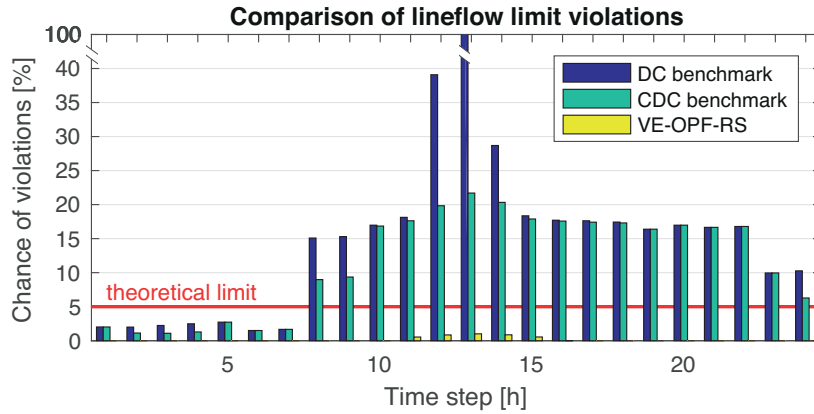


**Figure 6-11:** Empirical violation level of lineflow limit for different formulations for the 30-bus test case.

Next we examine the relative voltage magnitudes per bus for all hours and all samples in Figure 6-12). The relative voltage magnitudes are defined very similar to the line loadings  $\forall k \in \mathcal{N}$ ,

$$|v_k^{\text{rel}}| := \frac{|v_k| - \underline{|v_k|}}{\overline{|v_k|} - \underline{|v_k|}},$$

such that a relative voltage magnitude below 0% corresponds to a bus voltage which is below the lower limit, and a relative voltage magnitude greater than 100% indicates a violation of the upper limit. There is no violation of the voltage magnitude limits for any of the results, for all time steps and scenarios. The voltage magnitudes for the parametrization approach are lower compared to the other results.

Both VE-OPF-RS and SP-OPF-RS are now empirically proven to be feasible solutions for CC-OPF-RS. VE-OPF-RS is the most optimal, because there is more freedom, while SP-OPF-RS is very conservative. Both DC and CDC are infeasible for CC-OPF-RS. We will now continue to discuss the results for the sparsity decompositions, to reduce the computational complexity.



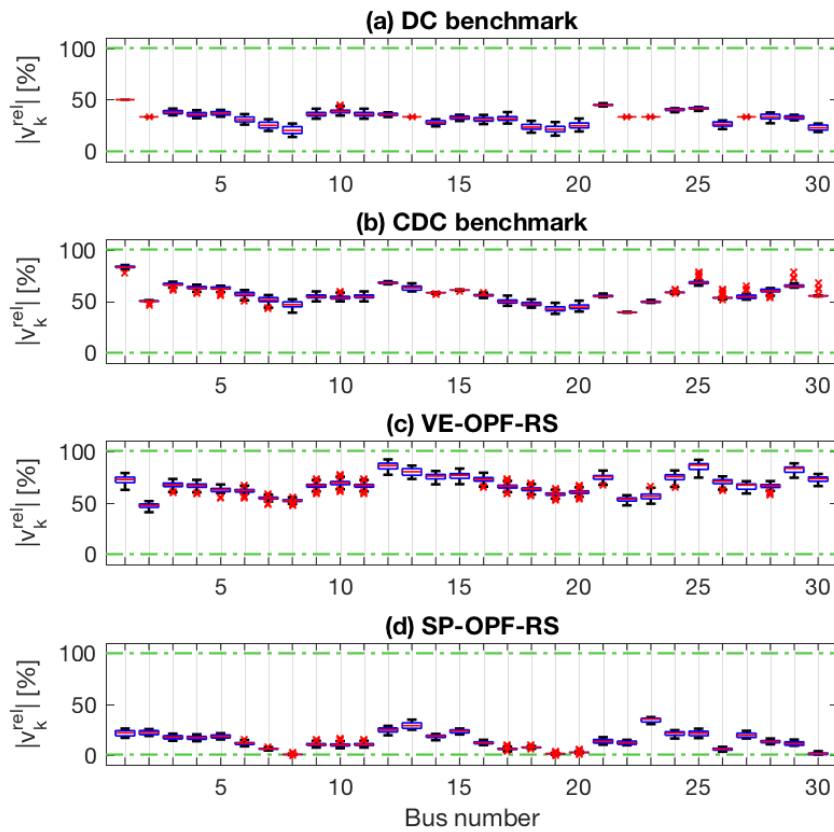


**Figure 6-12:** Relative bus voltages for all hours and scenarios per line for the 30-bus test case. The red line represents the median value, edges of each box correspond to the 25th and 75th percentiles, the whiskers extend to 99% coverage, and the red marks denote the data outliers. The green dashed lines indicate the limits. The upper plots (a) and (b) show the (C)DC benchmark results, and the lower plots (c) and (d) show the proposed approaches.

## 6-3 Results for sparsity decomposition method

The results for the proposed formulation with the sparsity decomposition are presented. The optimal objectives and optimization times are presented in Section 6-3-1. After this, the optimal solutions are shown and the violation levels are checked using power flow simulations in Section 6-3-2.

### 6-3-1 Optimal solutions for the sparsity decomposed formulations

The greedy tree decomposition algorithm proposed in [16] and implemented in [65] is used to decompose the network in cliques. Every PSD constraint from VE-OPF-RS and SP-OPF-RS is decomposed according to these cliques, resulting in DVE-OPF-RS and DSP-OPF-RS, respectively. The solution is obtained from these programs, and Algorithm 1 is used to complete the partially filled state matrices, after which Equation (6-1a) yields the generator dispatch and distribution vectors.

The optimization is run 10 times for both DVE-OPF-RS and DSP-OPF-RS, and the optimal objective and average optimization times are shown in Table 6-3 along with the original values from Table 6-2. Note that the optimal objective of the decomposed programs is equal to the optimal objective of the original programs, and thus Proposition 2 holds. Furthermore, there is a large decrease in optimization times, resulting in a speed-up of approximately 14 times for both formulations. The advantages in terms of computational cost for the sparsity decomposition are evident in this case. Note that since the 30 bus network is still relatively small, even bigger speed-ups are possible when larger networks are optimized.

**Table 6-3:** Optimization times and optimal objectives for the (decomposed) 30-bus test case

	$f(\Theta^{\text{opt}})$	Average opt. time (s)
VE-OPF-RS	151.78	417.63
DVE-OPF-RS	151.78	30.0 (13,92× faster)
SP-OPF-RS	156.73	457.71
DSP-OPF-RS	156.73	31.2 (14,67× faster)

The generator dispatches and distribution vectors are shown in Figure 6-13 and Figure 6-14. Comparing these figures with Figure 6-6 and Figure 6-7, it can be seen that the solutions from the decomposed programs are almost identical to the solutions of the original programs, and we refer the reader to Section 6-2-2 for a general discussion and comparison of these solutions.

Next, the empirical violation levels of the decomposed programs are compared with the violation levels of the original programs. Due to the similarity of the decomposed and original solutions, we expect to find very similar violation levels.

### 6-3-2 Violation levels for sparsity decomposed formulations

The obtained solutions are again implemented in power flow simulations using the same set of 10000 wind trajectories as used in Section 6-1-3. The resulting power flows and voltage

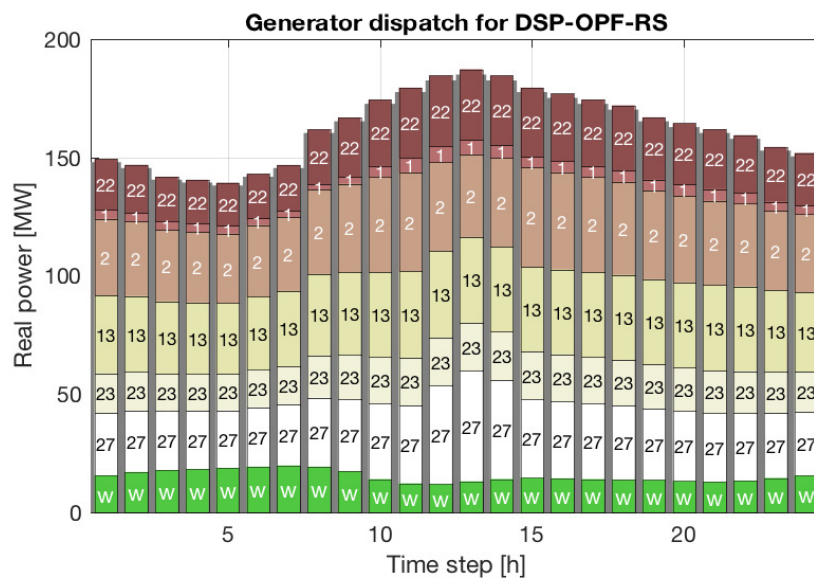
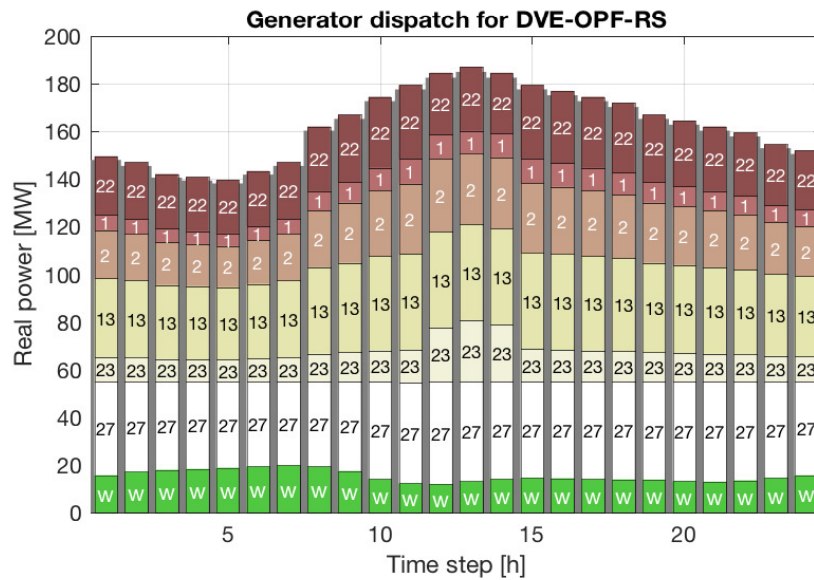
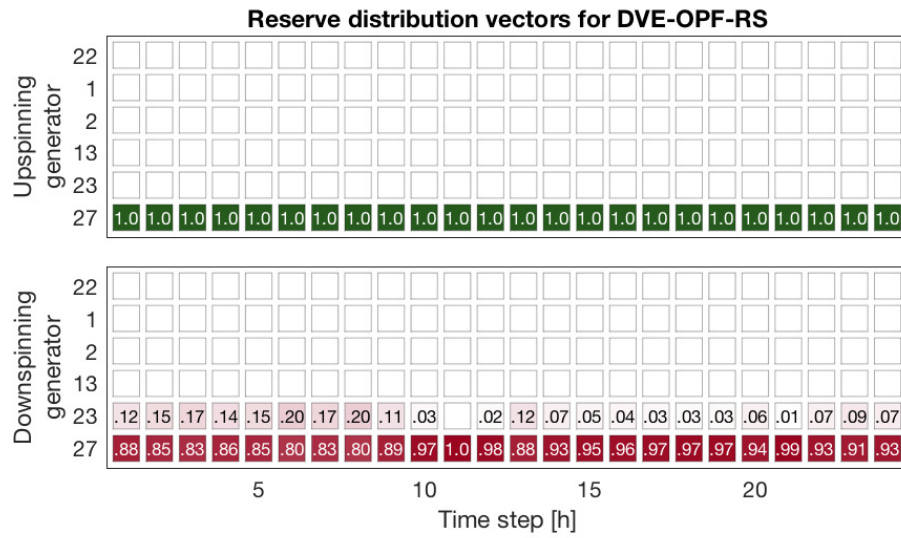
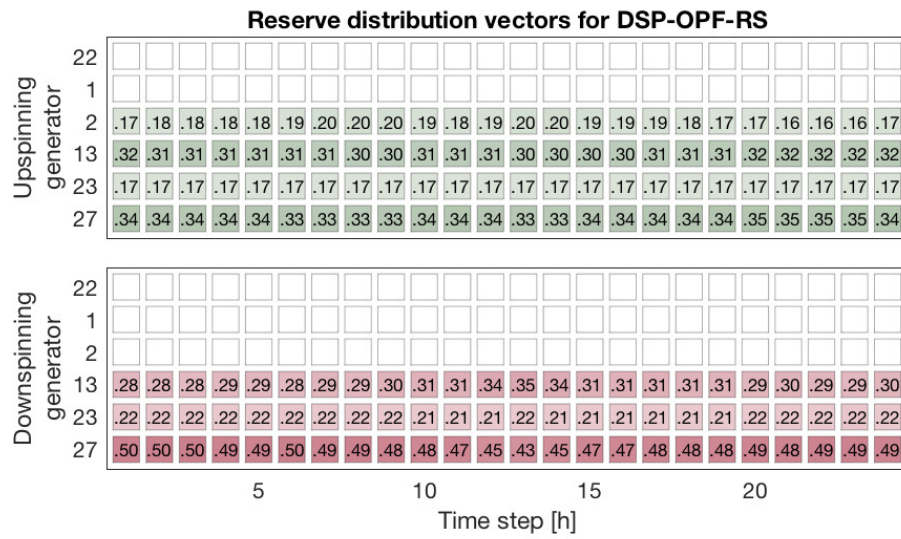


**Figure 6-13:** Generator dispatch per hour for different sparsity decomposed formulations for the 30-bus test case. The grey shaded area corresponds to the total demand per hour. The numbers correspond to the generator buses, and the lowest part of each bar (green) indicates the wind power per hour.



(a)



(b)

**Figure 6-14:** Graphical display of up- and downspinning reserve distribution vectors per generator and hour for different formulations for the 30-bus test case. Darker cells correspond to higher contribution to the reserve power.

magnitudes are checked for violations. We now compare the decomposed results with the original results of the proposed formulations, and leave out the DC benchmark, since both DC benchmark approaches resulted in solutions with excessive violation levels, and are therefore invalid.

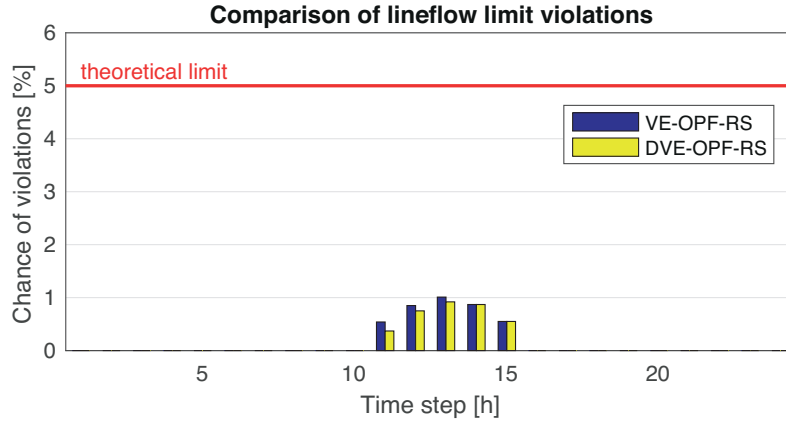


**Figure 6-15:** Empirical violation level of lineflow limit for different formulations for the 30-bus test case

As can be seen in Figure 6-15, the probability of line flow constraint violations is very similar for VE-OPF-RS and DVE-OPF-RS. SP-OPF-RS and DSP-OPF-RS are omitted in this figure, since their maximum violations levels are at 0.05% and 0.02%, respectively. The probability of voltage magnitude constraint violations is zero for all formulations at all hours and scenarios. We can therefore conclude that the sparsity decomposition of PSD constraints is a valid way to reduce computational complexity, without affecting the a-priori probabilistic guarantees. The sparsity decomposed programs DVE-OPF-RS and DSP-OPF-RS are therefore valid approximations for CC-OPF-RS.

## 6-4 Simulation results for multi-area networks

In this section, the results for multi-areas are given. First, the decomposed network is shown and the selection of the step size is discussed in Section 6-4-2. After this, the resulting solutions are shown and the violation levels are examined in Section 6-4-3.

### 6-4-1 Decomposition set-up

To create a realistic multi-area network, we use two identical IEEE 14-bus networks. We connect a tie-line between bus 5 of the first network and bus 10 of the second network, resulting in a 28-bus network with two areas. The multi-area decomposition framework as described in Section 5-2-1 is used. The extended areas are obtained by adding the endpoints of the tie-lines to the areas, such that the buses are grouped in two overlapping sets, as shown in Figure 6-16.

This decomposition is used to formulate a MASP-OPF-RS problem. Two agents are initialized and the ADMM algorithm is used to coordinate the local estimates towards convergence.

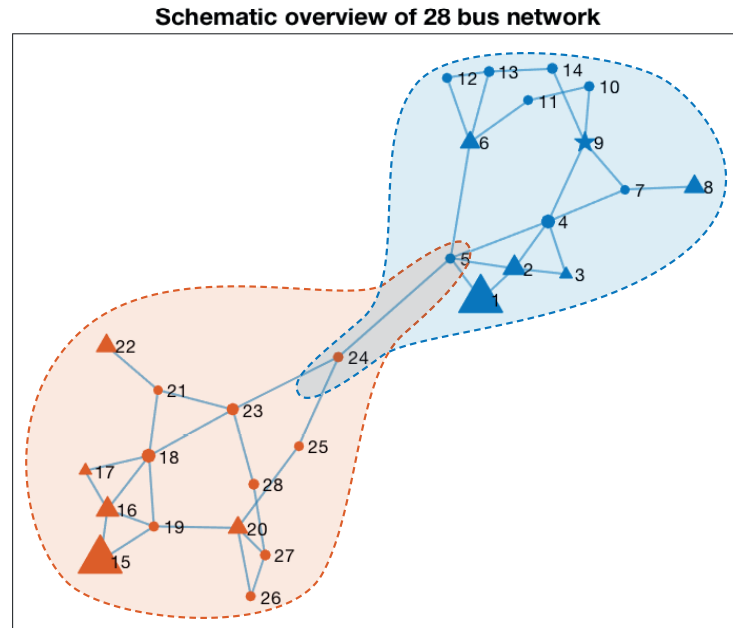


**Figure 6-16:** Schematic overview of the decomposed 28-bus test system. The different colors of the buses indicate the different control areas of the network, and the shaded lassos are the extended control areas.

After each iteration, the residual is checked. If the residual is sufficiently small, the algorithm is stopped and the current iterates are used as the solution. Before this algorithm can be implemented, a step size  $\mu$  has to be defined. In the following, the selection of this step size is explained.

#### 6-4-2 Selection of step-size for ADMM algorithm

Step-size coefficient  $\mu$  is an important tuning parameter for the ADMM algorithm. The step-size is the weight on the residuals in the objective. The residuals represent the level of disagreement the local estimates have with the average. If the step size is large, the iterates generally converge faster to a consensus, but since the weight on the original objective is relatively low, the consensus solution might be sub-optimal. If a smaller step size is selected, the iterates converge slower to consensus, but the performance of the solution in terms of the original objective function can be better. The selection of  $\mu$  is therefore a trade-off between the rate of convergence of the ADMM iterations and the performance of the solution.

The step size is selected using a heuristic approach. The ADMM algorithm is run for a fixed number of iterations, and the residual sequences  $\eta$  are shown in Figure 6-17. It is visible that the first steps of the algorithm are not very sensitive to the selection of  $\mu$ , and show similar behaviour for different values of  $\mu$ . Later, a higher  $\mu$  results in faster convergence. The performance of the final iterates is evaluated for every step size. It is observed that for  $\mu = 100$ , the performance is still acceptable, while the convergence is fast enough.

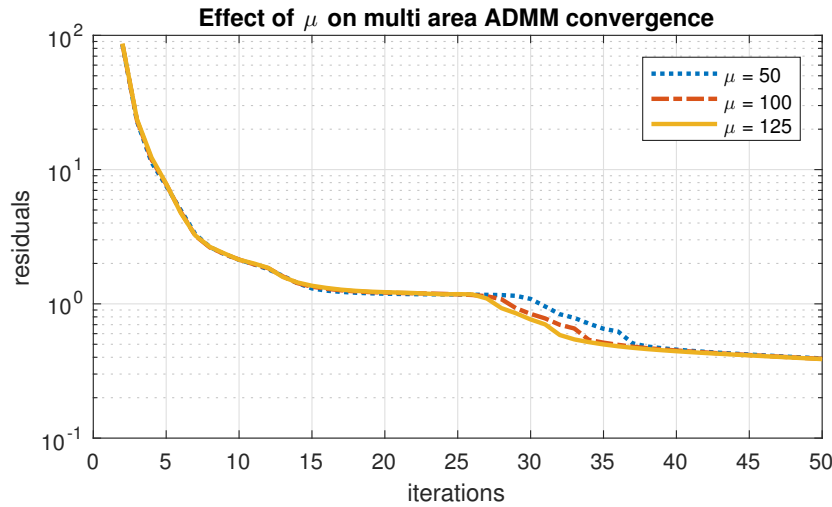


**Figure 6-17:** Effect of varying step-size  $\mu$  on the convergence of ADMM algorithm. The algorithm converges for large enough step-size, the convergence is very similar.

### 6-4-3 Simulation results for multi area problems

Having selected the appropriate step size  $\mu$ , the algorithm is run until the primal residual  $\eta$  is sufficiently small, i.e. below  $10^{-2}$  for each hour. This appears to be after 158 iterations. As a benchmark, we also solve the 28-bus network centrally using the SP-OPF-RS formulation. The resulting optimal objectives and optimization times are shown in Table 6-4.

**Table 6-4:** Optimization times and optimal objectives for the 28-bus test case

	$f(\Theta^{\text{opt}})$	Opt. time (s)
SP-OPF-RS	327.57	432.30
MASP-OPF-RS	335.24	5970.83

Since we use a sequential approach and multiple SDPs have to be solved at every iteration, the time needed to solve MASP-OPF-RS is much longer than the time needed for SP-OPF-RS. However, if the computation of the local solutions is done in parallel, the time per iterations would be reduced to half of the sequential time. The MASP-OPF-RS has a slightly higher objective. The objective for each agent of MASP-OPF-RS is not only to have an economic and secure dispatch of generation of their local generators, but also to be in agreement with neighbouring agents on the power flows between the two networks. Therefore, a sub-optimal solution is obtained.

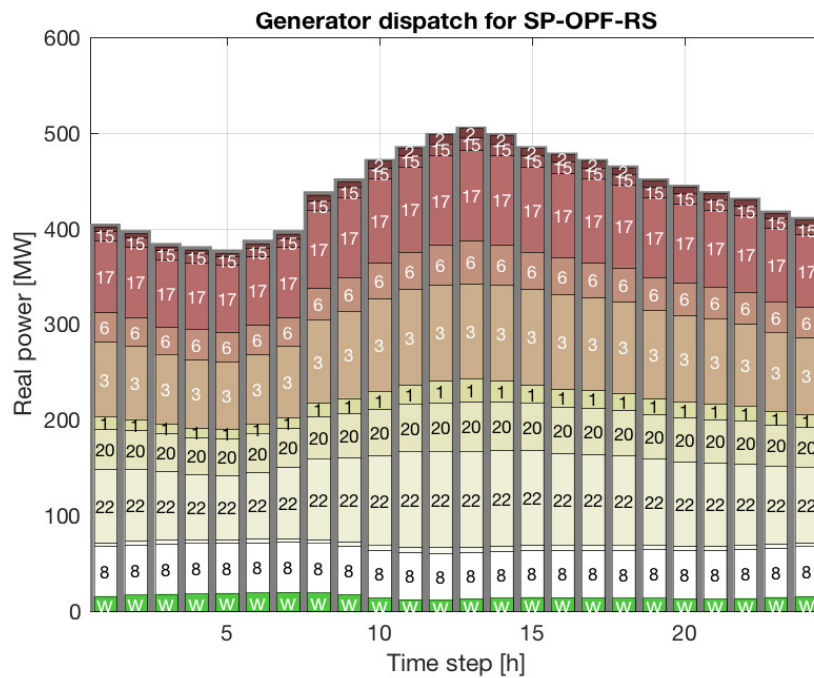
The resulting dispatch and distribution vectors are extracted from the final iterates. The generator dispatch is compared with the centralized solution in Figure 6-18. The distributed solution is very similar to the centralized solution.

The distribution vectors are displayed in Figure 6-19. It can be seen that the results are quite similar for the centralized and distributed result. The upspinning reserve is completely provided by the generator with the lowest cost, generator 8. The downspinning reserve is distributed over the first and second generator for the distributed solution, but in the

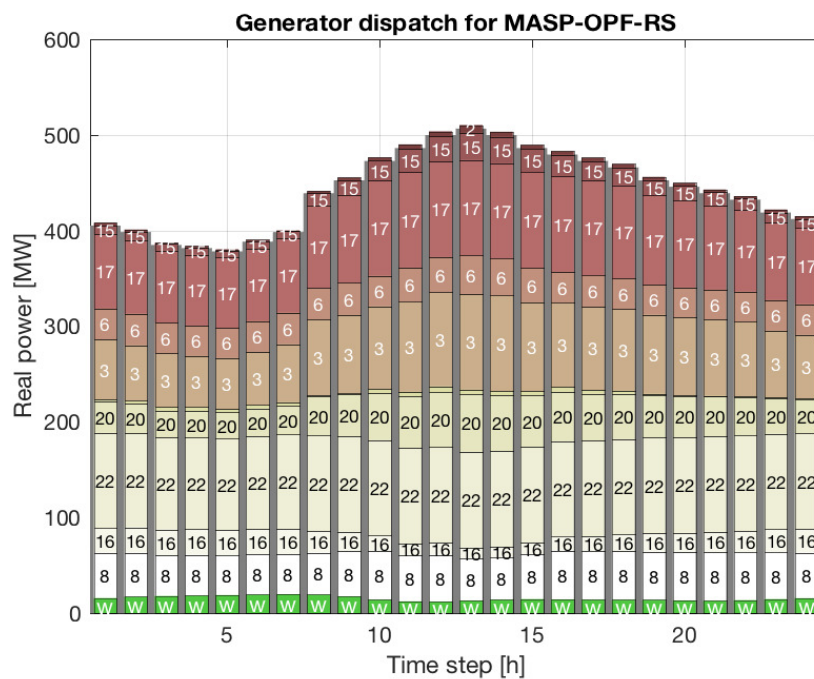
centralized approach it is mostly provided by generator 8. For both the centralized and distributed solutions, the reserve is distributed over more generators during the peak hours, because the dispatch of the generators is higher in those hours, so less reserve power is available per generator.

The resulting solutions are simulated with a new set of 10000 wind trajectories to compare the violation levels. The encountered violation levels resemble results from the 30 bus test case, and both the centralized and distributed solutions have a very low probability of line violations: at most 0.02% and 0.06% at the peak hours, respectively. We can therefore conclude that the probabilistic guarantees are still valid for the distributed solution.



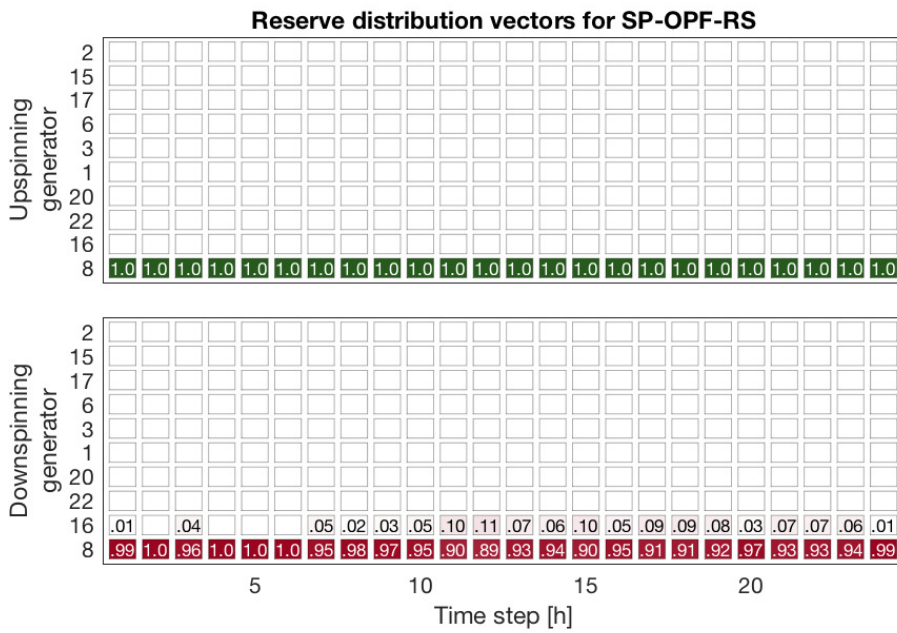


(a) centralized

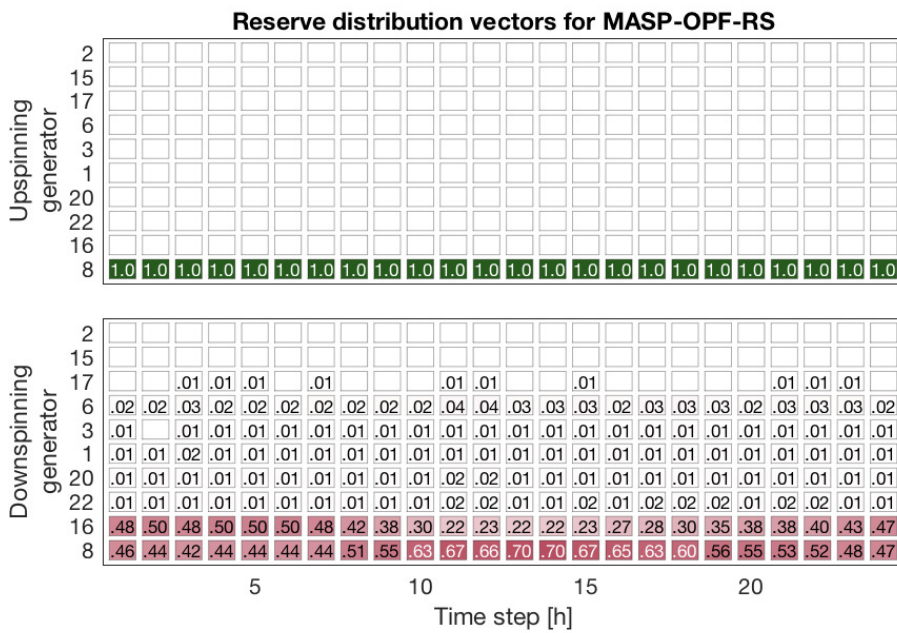


(b) distributed

**Figure 6-18:** Generator dispatch per hour for centralized and distributed solutions for the 28-bus test case. The grey shaded area corresponds to the total demand per hour. The numbers correspond to the generator buses, and the lowest part of each bar (green) indicates the wind power per hour.



(a) centralized



(b) distributed

**Figure 6-19:** Graphical display of up- and downspinning reserve distribution vectors per generator and hour for centralized and distributed solutions for the 28-bus test case. Darker cells correspond to higher contribution to the reserve power.

## 6-5 Conclusions

In this chapter, the set-up of the simulation is presented. The VE-OPF-RS and SP-OPF-RS formulations are used to solve a problem for a 30-bus test system. The resulting generator dispatch and distribution vectors are examined. The VE-OPF-RS approach has a slightly lower cost, since the reserve power is only provided by the generators with the lowest cost. For the SP-OPF-RS solution, the reserve power is more distributed.

The solutions are implemented in PF simulations. The violation level for line loadings and bus voltage magnitudes is compared with the DC benchmarks. The assumptions made in the DC modelling framework do not hold in the AC simulations, resulting in higher violation levels. The conversion from DC to CDC somewhat reduced the violation level, but for both the original DC and the CDC solutions, the violation level exceeds the theoretical limit for the majority of the time steps. For both VE-OPF-RS and SP-OPF-RS, the violation levels are well below the theoretical limit. The VE-OPF-RS solution is somewhat less conservative, whereas the SP-OPF-RS is more conservative with a very low violation level at the cost of a slight increase in the objective. For both the proposed approaches, the a-priori probabilistic guarantees hold. We have therefore showed that the solutions obtained from both formulations are feasible for CC-OPF-RS formulation.

Next, the decomposition methods are validated using the same test system. First, the decomposed variants of the proposed formulations are solved, and afterwards the partially filled matrices are completed with the help of our proposed algorithm. Almost the same solution is found in a considerable lower amount of time, with an average speed-up of approximately 14 times. The solutions have been validated with the same PF simulations, and the resulting violation levels are found to be similar to the original levels. The sparsity decomposition has therefore proven to be an effective way to reduce computational complexity while keeping the probabilistic guarantees of the solution intact.

Finally, the multi-area decomposition is applied to two interlinked 14-bus systems. The selection of the step size is justified using a heuristic approach. After this, the ADMM algorithm is used to find solutions to the OPF-RS problem in a distributed setting, and the result is compared to the centralized solution for the same network. The solutions obtained by the centralized and distributed approach are very similar, so we can conclude that the ADMM algorithm has converged. The violation levels for the decomposed and centralized solutions are checked using PF simulations. The theoretical limit is not exceeded in both cases, and both solutions are therefore feasible for CC-OPF-RS. Therefore, our proposed multi-area decomposition framework is a valid decomposition method which allows for distributed solving of OPF-RS type problems.



---

## Chapter 7

---

# Conclusions

In this thesis, we proposed a new optimization problem to address the problem of reserve scheduling under an AC power flow set-up, for systems with uncertain WPG. For the AC power flow formulation we used a modification of the relaxation presented in [9] and incorporated it in the stochastic reserve scheduling problem formulation. To deal with the uncertainty, the problem is formulated as a CCP, such that violations are allowed with a low probability.

Using a randomization technique (the scenario approach), a deterministic problem which approximates the CCP with a-priori feasibility guarantees is formulated. The resulting problem has a high number of matrix decision variables, leading to computational tractability issues for realistic networks. Therefore, two tractable approximations are proposed.

We first use the scenario approach to approximate a convex set which contains almost surely the probability mass distribution of the uncertain wind power trajectories. We rely on the special property of reserve scheduling problems which leads to linear constraint functions with respect to the uncertain parameters. We can therefore formulate a robust problem for only the vertices of the approximated set, VE-OPF-RS. Using the proposed approach, the number of scenarios is reduced significantly which is beneficial for the tractability. The second tractable approximation we propose is a novel RS formulation, SP-OPF-RS, in which the distribution of reserve is encoded directly in the network state as a non-linear parametrization of the uncertainty. By using a conic combination of matrices, the positive semidefiniteness of all network states is implied, using only three PSD constraints per time step. Unlike existing works in RS, our proposed parametrization has a practical meaning and is directly related to the distribution of reserve power.

Finally, we provide two ways to decompose large OPF-RS problems, based on the sparsity pattern and control areas. First, a sparsity decomposition method is presented. Based on the chordal theorem, we decompose computationally expensive PSD constraints for both the proposed formulations. Due to the sparsity in the data matrices, typical for power systems, the computational complexity is greatly reduced. A matrix completion algorithm is proposed for the guaranteed rank-one reconstruction of the matrix variable. Second, a decomposition

technique suitable for multi-area systems is presented. The matrix variable and all corresponding constraints and objective function are partitioned according to the control areas, such that for every control area a separate problem is created which is coupled only with auxiliary variables. With the help of the chordal theorem, the PSD constraint is again decomposed, but now based on the bus sets that correspond to an area rather than the sparsity pattern. The ADMM algorithm is then used to solve the resulting general consensus problem.

All formulations described above are validated on the IEEE 30-bus test system and compared to the DC benchmark solutions. With the use of Monte Carlo simulations of the power flows, the empirical level of constraint violation is checked. For both VE-OPF-RS and SP-OPF-RS, the violation levels are well below the theoretical limit, whereas the solutions from the DC benchmark lose their feasibility guarantees in the AC framework. The solutions obtained from both formulations are therefore feasible solutions for the CCP. The VE-OPF-RS solution is somewhat less conservative, whereas the SP-OPF-RS is more conservative with a very low violation level at the cost of a higher objective.

Next, the sparsity decomposition methods are validated using the same set-up. First, the decomposed variants of the proposed formulations are solved, and afterwards the partially filled matrices are completed with the help of our proposed algorithm. Almost the same solution is found in a considerable lower amount of time, with an average speed-up of approximately 14 times. The solutions have been validated with the same PF simulations, and the resulting violation levels are found to be similar to the original levels. The sparsity decomposition is therefore shown to be an effective way to reduce computational complexity while keeping the probabilistic guarantees of the solution intact.

Finally, the multi-area decomposition is applied to two interlinked 14-bus systems. The selection of the step size is justified using a heuristic approach. After this, the ADMM algorithm is used to find solutions to the OPF-RS problem in a distributed setting, and the result is compared to the centralized solution for the same network. The solutions obtained by the centralized and distributed approach are very similar. The violation levels for the decomposed and centralized solutions are checked using PF simulations. The theoretical limit is not exceeded in both cases, and both solutions are therefore feasible for CC-OPF-RS. Therefore, our proposed multi-area decomposition framework is a valid decomposition method which allows for distributed solving of OPF-RS type problems.

## Future Research Directions

In this section, several future research directions are proposed. First, we propose several ideas for future research on the new formulations VE-OPF-RS and SP-OPF-RS in Section 8-1. In Section 8-2, we continue to propose different applications for the sparsity decomposition. Finally, possible improvements to the multi-area decomposition framework are proposed in Section 8-3.

### 8-1 Extensive testing of tractable reformulations

#### 8-1-1 Testing with different wind models

The validity of the proposed approaches is proven theoretically for any uncertainty source, but only demonstrated for one specific wind model. A broad comparison using different models will help to show the robustness of the proposed approaches. Especially, wind models with multiple wind buses (i.e. that not only consider temporal, but also spatial correlation between wind buses, such that the trajectories per wind bus have a joint probability) could be an interesting follow-up on the current research.

The computational advantage of the SP-OPF-RS approach for problems with multiple wind buses has already been demonstrated in this work, but since there is no correlation between the trajectories, the results did not have any probabilistic guarantees. The scenario state is parametrized in the *sum* of all uncertain wind powers. It still remains to be researched whether the conic parametrization in the sum is too restrictive to find feasible scenarios states for systems with multiple uncertain wind powers.

If this appears to be the case, the conic parametrization can be extended, such that every uncertainty source has its own set of separate PSD coefficient matrices, similar to the parametrization proposed in [11], but then with the PSDness implied due to the conic combination. It is important to mention that in such a formulation, the number of PSD matrices would again be  $T(2N_w + 1)$ , which is identical to the number of PSD matrices for VE-OPF-RS,

and therefore any computational advantage would be lost. However, the comparison of violation levels for such problems between SP-OPF-RS and VE-OPF-RS would be very interesting. The theoretical results hold not only for the uncertain generation of wind power, but can also be applied to different forms of uncertainty, such as uncertain loads. More exotic adaptations to the models could include local power storage (see [66]) or the deration of wind power as downspinning reserve (see [67]).

### 8-1-2 Application of indirect scenario approach to different OPF-RS formulations

The current work focused on the SDR formulation of OPF-RS problems. The indirect scenario approach can also be extended to other convex relaxations. A good candidate would be the Feasible Point Pursuit-Successive Convex Approximation (FFP-SCA) algorithm proposed in [68] and applied to an OPF problem in [69]. The formulation in [69] is very similar to our OPF formulation before relaxation,  $\text{OPF}(\tilde{\mathbf{p}}^w)$ , such that one can leverage the linear dependency on the negative and positive total mismatch. One can then approximate the uncertainty set using the indirect scenario approach as described in Section 4-1, such that the resulting problem has a low number of scenarios, and the FFP-SCA algorithm can then be used to solve the (non-convex) problem.

Note that the SDR outperforms the FFP-SCA algorithm in terms of optimal objective value and computational burden, but FFP-SCA can identify constraints that make an OPF problem infeasible, and thus find solutions to problems that may be infeasible in the SDR. We assumed that a feasible solution to the OPF-RS problem existed, but the FFP-SCA algorithm can be of interest for OPF-RS problems where feasibility is not given. A good example of such a problem might be a network topology optimization: given a certain amount of uncertainty and demand, the FFP-SCA problem can identify the constraints which make the problem infeasible, such that the TSO can consider upgrading the corresponding components (such as congested lines).

### 8-1-3 Different approximations of uncertainty set to reduce conservatism

In our research, we have used an axis-aligned hyperrectangular set to approximate the uncertainty set for simplicity. Any convex set is however valid. To further clarify the conservatism introduced by the VE approach, different sets might be used to approximate the uncertainty set, such as an ellipsoidal set, for which the approximation might be less conservative.

## 8-2 Extending application of sparsity decomposition methods

### 8-2-1 Sparsity decomposition for large scale OPF-RS problems

The validity of the VE-OPF-RS and SP-OPF-RS approximations for CC-OPF-RS have been shown for the 30 bus system with a single uncertain wind bus. We have chosen the 30 bus network, because it is of such dimensions that OPF-RS problems can be solved as a whole in reasonable time. This allowed us to demonstrate the similarity between solutions from the sparsity decomposition and original formulation. Future research should focus on testing our proposed



formulations DVE-OPF-RS and DSP-OPF-RS for larger problems which cannot be solved as a whole, such as the Polish test system with over 3000 buses. Although the authors of [16] showed that the sparsity decomposition is valid for large scale OPF problems, the extension to RS problems has not yet been made.

### **8-2-2 Sparsity decomposition for local matrices of multi-area decomposition**

We have considered applying the sparsity decomposition as described in Section 5-1 for the local updates of the multi-area decomposition as described in Section 5-2, thus obtaining a tractable approximation for CC-OPF-RS that is first decomposed in the defined control areas and then each of these decomposed state matrices is again decomposed based on the sparsity pattern of the local data matrices. We have observed that for the 28-bus multi-area system, the addition of a sparsity decomposition to the optimization process introduced more overhead than it reduced the computational complexity, because the sub-networks were already of comprehensive size (two sub-networks with 15 buses each). To be able to exchange the information on overlapping nodes, it is necessary to run a matrix completion procedure, such as Algorithm 1, at every iteration. However, for large scale multi-area OPF-RS problems, the double decomposition (spatial and sparsity) would be a promising approach, due to the large speed-ups gained from sparsity decomposition.

It is however important to mention that the matrix completion procedure at every step could introduce approximation errors which might propagate through the sub-networks and deteriorate as the algorithm progresses, because the ADMM algorithm typically needs a large number of iterations to converge. Whether or not this problem occurs (either with our proposed algorithm in particular, or in general) is still an open question.

## **8-3 Distributed approaches for OPF-RS problems**

### **8-3-1 Distributed implementation of multi-area decomposition**

The multi-area decomposition framework as described in Section 5-2 allows for the solving in a distributed setting. Every agent has its own set of constraints and decision variables. By communicating its decisions and receiving averages of those decisions from all other agents, the agent can independently update its decisions variables. A distributed implementation would be an interesting follow-up on the presented framework, such that the computational time is more comparable to centralized approaches.

### **8-3-2 Varying wind samples between agents in multi-area decomposition**

Another direction which was pursued during this research was the decomposition of entire OPF-RS problems over scenarios, i.e. multiple instances of the whole network, each with a subset of the scenarios. This approach is motivated by the fact that in the direct scenario approach the high number of scenarios causes tractability issues due to the repetition of matrix variables. Different algorithmic approaches which allow for distributed settings were researched, such as active constraint consensus and proximal gradient methods. It appeared

that the extra computational burden introduced by solving an SDP at every iteration resulted in a large increase in computation time, while not improving the quality of the results. By solving the same problem multiple times, each time with different scenarios, the overall complexity increased instead of decreased, and this approach was therefore abandoned in favour of researching tractable ways of formulating OPF-RS problems and sparsity and multi-area decompositions.

In the current multi-area decomposition framework, we have assumed that all agents have the same set of scenarios, i.e. samples of trajectories available to them. It will be worth investigating whether dividing the scenarios between the agents will result in similar solutions. Since all agents have to reach consensus on their decisions, every agent implicitly has information of all the scenarios, but only explicitly knows its own subset of the scenarios. The resulting solutions could then be tested for their corresponding violation level using PF simulations, to see whether the probabilistic guarantees hold.

### **8-3-3 Different consensus algorithm for multi-area decomposition**

The proposed multi-area decomposition leads to a general consensus problem, for which any consensus algorithm can be used to coordinate the agents towards a global consensus. In the current work, the ADMM algorithm is used as a consensus algorithm for the decomposed problem. The computational time for this algorithm to converge was quite large compared to the centralized approaches, even in a hypothetical parallel implementation. A comparison of performance and computational effort for different consensus algorithms to solve the same multi-area OPF-RS problem was outside the scope of this thesis. An interesting direction for future research would be to use a different consensus algorithm which converges in a lower number of iterations, such that the computational effort and time to solve a multi-area OPF-RS problem in a distributed setting would be reduced.

---

# Appendix A

---

## Direct Current Modelling Framework

The Direct Current (DC) approximation of a power system will be derived and the classical DC OPF problem will be formulated in Section A-1. In the DC framework, all the system equations are linear, resulting in a problem formulation that is easy to solve. In Section A-2, Wind Power Generation (WPG) will be integrated in the DC framework to come up with a CCP formulation of the DC OPF with reserve scheduling.

### A-1 Classical direct current (DC) OPF

The non-linear relation of the complex voltage and currents through the admittance matrix ( $\mathbf{I} = \mathbf{Y}\mathbf{E}$ ) is simplified using the following assumptions, based on [17]:

**Assumption 4.** *The voltage at every bus of the network remains constant at 1 p.u.<sup>1</sup>*

**Assumption 5.** *The active power losses in the branches are neglected. In particular, the branch resistance and charging capacitance are negligible. The admittance of each branch will then reduce to  $\frac{1}{jx_s}$ .*

**Assumption 6.** *All voltage angles are small, so  $\sin \theta_{lm} \approx \theta_{lm}$ , where  $\theta_{lm}$  is the angle in radians across the branch connecting the buses  $l$  and  $m$ .*

Furthermore, no phase-shifting transformers are assumed to be present, so  $\theta_{lm,\text{shift}} = 0$  for all  $(l, m) \in \mathcal{L}$ . This assumption is made to streamline the presentation, but can be included in the DC OPF problem as described in [64].

The power flow over each line at time-step  $t$  can be calculated using the following *linear* equation:

$$P_t^f = B^f \Theta_t \quad (\text{A-1})$$

---

<sup>1</sup>p.u. stands for per unit, a normalized unit common in power system analysis. A baseline is chosen for the voltage, and all voltages are divided by this voltage. 1 p.u. means that all the bus voltages are nominal.

where  $P_t^f \in \mathbb{R}^{N_l}$  is the vector containing the power flows  $P_{lm,t}$  for each line  $(l, m) \in \mathcal{L}$  at time-step  $t$ ,  $\Theta_t \in \mathbb{R}^{N_b}$  is the vector of all the voltage angles at every bus  $\theta_{k,t}$  at time-step  $t$ , and  $B^f \in \mathbb{R}^{(N_l \times N_b)}$  is the imaginary part of the nodal admittance matrix. Only the imaginary part is used, because active power losses are neglected for lines (Assumption 5). The power flows can be expressed as a linear function of  $\Theta$  because the angles are assumed to be small (Assumption 6).

The power injected at each time-step  $t$  for all the buses is defined as:

$$P_t^{\text{inj}} = C^G P_t^G - P_t^D \quad (\text{A-2})$$

where  $P_t^{\text{inj}} \in \mathbb{R}^{N_b}$ ,  $P_t^G \in \mathbb{R}^{N_G}$  and  $P_t^D \in \mathbb{R}^{N_b}$  are the vectors containing the injected, generated and demanded power at time-step  $t$  respectively. The matrix  $C^G$  is the sparse connection matrix of appropriate dimension. The entry  $(i, j)$  equals one if bus  $i$  has generator  $j$  connected to it, and zero otherwise.

Through Kirchoffs current law, the active power injection at bus  $k$  can be defined as:

$$P_t^{\text{inj}} = B^{\text{bus}} \Theta_t \quad (\text{A-3})$$

where  $B_{\text{bus}} \in \mathbb{R}^{N_b \times N_b}$  is the nodal admittance matrix in the DC framework.

It is common practice for OPF calculations to define one of the buses as a reference<sup>2</sup> bus. The voltage angle of this bus will be fixed at 0, so all the other voltage angles are expressed as an offset to the reference bus. In the DC approximation the magnitude of the voltage is assumed to be constant (Assumption 4), so the only variable changing is the voltage angle.

Combining (A-1) and (A-3), it is possible to eliminate the voltage angle from the equations. It is necessary to invert  $B^{\text{bus}}$  for this, but since  $B^{\text{bus}}$  is singular by construction, this is not possible. Using the properties of the reference bus, this can be circumvented.

Following [17], the row and column corresponding to the reference bus are removed from  $B^{\text{bus}}$  to form  $\tilde{B}^{\text{bus}} \in \mathbb{R}^{(N_b-1) \times (N_b-1)}$ . The same is done for the power injection vector: the entry corresponding to the reference bus is removed to create  $\tilde{P}_t^{\text{inj}} \in \mathbb{R}^{(N_b-1)}$ . Reordering the buses to set the reference bus to the last position allows for the following expression of  $\Theta_t$  and the power flows  $P_t^f$ :

$$\Theta_t = \begin{bmatrix} (\tilde{B}^{\text{bus}})^{-1} \tilde{P}_t^{\text{inj}} \\ 0 \end{bmatrix} \quad \Rightarrow \quad P_t^f = B^f \begin{bmatrix} (\tilde{B}^{\text{bus}})^{-1} \tilde{P}_t^{\text{inj}} \\ 0 \end{bmatrix}$$

By doing so, the reference angle is forced to zero, and the power flows over all the lines have become a function of the power injection vector rather than the voltage angles. Since the demand profile is assumed to be known, the only variable is  $P_t^G$ . This allows the formulation

---

<sup>2</sup>The reference bus is in some power systems literature called the ‘slack bus’, but to avoid confusion with ‘slack variables’ as are commonly found in optimization literature, that term will not be used in this work.

of the classical DC OPF problem as a quadratic program (QP):

$$\underset{[P_t^G]_{t=1}^{N_t}}{\text{minimize}} \quad \sum_{t=1}^{N_t} \sum_{k \in \mathcal{G}} \left( c_k^{\text{qu}} (P_{k,t}^G)^2 + c_k^{\text{li}} P_{k,t}^G \right) \quad (\text{A-4a})$$

$$\text{subject to:} \quad \mathbf{1}^\top \tilde{P}_t^{\text{inj}} = 0, \quad (\text{A-4b})$$

$$P_k^{G,\text{min}} \leq P_{k,t}^G \leq P_k^{G,\text{max}}, \quad (\text{A-4c})$$

$$- Pf, \text{max} \leq B^f \begin{bmatrix} (\tilde{B}^{\text{bus}})^{-1} \tilde{P}_t^{\text{inj}} \\ 0 \end{bmatrix} \leq Pf, \text{max}, \quad (\text{A-4d})$$

$$\text{for } t = 1, \dots, N_t, \quad \forall k \in \mathcal{G}$$

The objective function considers the cost of the active power generation for each generator over the time horizon with quadratic cost vector  $c^{\text{qu}} \in \mathbb{R}_+^{N_G}$  and linear cost vector  $c^{\text{li}} \in \mathbb{R}_+^{N_G}$ . In some literature, for example [47], a fixed cost vector  $c^{\text{fi}}$  is also added to the cost function, but since this does not change the location of the optimal solution, it is omitted here.

The set of power balancing constraints (A-4b) enforces the sum of all the injected powers at each time step to equal zero, to let generation always meet demand. The vector  $\mathbf{1} \in \mathbb{R}^{N_b}$  has all entries equal to 1. The generator limits are encoded in the second set of constraints (A-4c), bounding the generated power for a given generator  $k$ . The last set of constraints (A-4d) are the line capacities. Each line  $(l, m)$  has a maximum line capacity  $P_{lm}^{\text{max}}$  that represents the rated amount of power it can transmit in both directions.  $Pf, \text{max} \in \mathbb{R}^{N_l}$  represents the capacities stacked over all the lines. By bounding power flows by the negative and positive maximum capacities, the safe transportation of energy is ensured.

The problem is separable in the time steps, since no coupling between the time-steps are present, such as ramping limits. Therefore, the problem can be reduced to 24 separate DC OPF problems, whose objective functions can be summed to retrieve the total problem as given above.

## A-2 Integrating wind power in DC OPF

Having defined the classical DC OPF problem as a deterministic QP, we can now introduce the uncertainty in the form of WPG. The uncertainty will enter the formulation in the form of chance constraints, resulting in a CCP formulation of the DC OPF with uncertain WPG.

The wind-power is modelled as active power injection on the buses  $i \in \mathcal{W}$ , following [4]. Since the wind power production is uncertain, it is a random variable. The variable is the wind power trajectory over the time horizon,  $[P_t^w]_{t=1}^{N_t} \in \Delta \subseteq \mathbb{R}^{(N_w \times N_t)}$ , and therefore a stochastic process. The forecast wind-power is denoted by  $[P_t^{w,f}]_{t=1}^{N_t} \in \mathbb{R}^{(N_w \times N_t)}$  and is deterministic.

Let  $P_t^m \in \mathbb{R}$  be the total wind power mismatch, or the difference between the summed forecast and the summed actual wind power. In some literature, this mismatch is called the prediction error, but it represents the same quantity.  $R_t \in \mathbb{R}^{N_G}$  is the reserve active power which is a function of the mismatch. The mismatch is distributed along the committed generators according to two distribution vectors  $d_t^{\text{us}}, d_t^{\text{ds}} \in \mathbb{R}^{N_G}$ , following the representation of reserves as discussed in [4], Section II B. If a generator  $k$  is not participating in the secondary frequency

control, its respective element in the distribution vectors will be 0.  $R_t$  is defined in such a way, that at time  $t$  a positive mismatch (surplus, requires down-spinning) is distributed according to  $d_t^{\text{ds}}$  and a negative mismatch (deficit, requires up-spinning) is distributed according to  $d_t^{\text{us}}$ .

$$\begin{aligned} P_t^m &= \sum_{h \in \mathcal{W}} P_{h,t}^w - P_{h,t}^{w,f} \\ R_t &= d_t^{\text{us}} \max(0, -P_t^m) - d_t^{\text{ds}} \max(0, P_t^m) \end{aligned} \quad (\text{A-5})$$

With this definition, two new power injection vectors can be composed. The first, denoted  $P_t^{\text{inj},f}$  represents the injected power for the deterministic case (i.e. the WPG in-feed is equal to its forecast value and no reserve are used), the second represents the probabilistic case (a scenario) and is denoted by  $P_t^{\text{inj},s}$ . Both have the same dimensions as the original  $P_t^{\text{inj}}$ .

$$\begin{aligned} P_t^{\text{inj},f} &= C^G P_t^G + C^w P_t^{w,f} - P_t^D \\ P_t^{\text{inj},s} &= C^G (P_t^G + R_t) + C^w P_t^w - P_t^D \end{aligned}$$

where  $C^w$  is the sparse connection matrix connecting the WPG in-feeds to the buses, constructed in the same way as  $C^G$ .

Because different costs are associated with either up- or downspinning for each generator, a different cost vector is used for each. The up- and downspinning costs are assumed to be linear and time invariant. Let  $c^{\text{us}}, c^{\text{ds}} \in \mathbb{R}_+^{N_G}$  be the costs for up- and downspinning each generator, respectively. This allows the up- and downspinning costs to be calculated separately. The DC OPF can now be extended to not only solve for the optimal generator dispatch, but also for the optimal reserve distribution vectors. Because  $[P_t^w]_{t=1}^{N_t}$  is an uncertain parameter, the

DC OPF will be formulated as a CCP (see Section 2-4 for more information about CCPs).

$$\begin{aligned} \text{minimize} \quad & \sum_{t=1}^{N_t} \left( \sum_{k \in \mathcal{G}} \left( c_k^{\text{qu}} (P_{k,t}^G)^2 + c_k^{\text{li}} P_{k,t}^G \right) + (c^{\text{us}})^\top R_t^{\text{us}} + (c^{\text{ds}})^\top R_t^{\text{ds}} \right) \quad (\text{A-6a}) \\ & \begin{bmatrix} P_t^G, d_t^{\text{us}}, \\ d_t^{\text{ds}}, R_t^{\text{us}}, \\ R_t^{\text{ds}} \end{bmatrix}_{t=1}^{N_t} \end{aligned}$$

$$\text{subject to} \quad \mathbf{1}^\top P_t^{\text{inj},f} = 0, \quad (\text{A-6b})$$

$$P_k^{G,\min} \leq P_{k,t}^G \leq P_k^{G,\max}, \quad (\text{A-6c})$$

$$-Pf,\max \leq B^f \begin{bmatrix} (\tilde{B}^{\text{bus}})^{-1} \tilde{P}_t^{\text{inj},f} \\ 0 \end{bmatrix} \leq Pf,\max, \quad (\text{A-6d})$$

$$\mathbb{P} \left\{ \begin{array}{l} [P_t^w]_{t=1}^{N_t} \in \Delta \\ \mathbf{1}^\top P_t^{\text{inj},s} = 0, \end{array} \right. \quad (\text{A-6e})$$

$$P_k^{G,\min} \leq P_{k,t}^G + R_{k,t} \leq P_k^{G,\max}, \quad (\text{A-6f})$$

$$-Pf,\max \leq B^f \begin{bmatrix} (\tilde{B}^{\text{bus}})^{-1} \tilde{P}_t^{\text{inj},s} \\ 0 \end{bmatrix} \leq Pf,\max, \quad (\text{A-6g})$$

$$-R_t^{\text{ds}} \leq d_t^{\text{us}} \max(0, -P_t^m) - d_t^{\text{ds}} \max(0, P_t^m) \leq R_t^{\text{us}} \quad (\text{A-6h})$$

$$R_t^{\text{us}} \geq 0, \quad (\text{A-6i})$$

$$R_t^{\text{ds}} \geq 0 \left. \vphantom{R_t^{\text{us}}} \right\} \geq 1 - \epsilon \quad (\text{A-6j})$$

$$\text{for } t = 1, \dots, N_t, \quad \forall k \in \mathcal{G}$$

with  $R_{k,t} = \mathbf{e}_k \left( d_t^{\text{us}} \max(0, -P_t^m) - d_t^{\text{ds}} \max(0, P_t^m) \right)$ , where  $\mathbf{e}_k$  represents a vector with only the  $k$ -th entry equal to 1 and the rest zero.  $R_t^{\text{us}}, R_t^{\text{ds}} \in \mathbb{R}^{N_G}$  are the maximum up- and downspinning reserves needed, or the reserve requirements at time  $t$ . They are included in the objective function, multiplied by the corresponding cost vectors and summed over all the timesteps. This makes the objective function not only a representation of the total incurred generation costs, but also reserve requirement costs. The deterministic constraints (A-6b)-(A-6d) are exactly the same as in the classical DC OPF, with the exception that the power injection vector now also contains the forecast wind-power ( $P_t^{\text{inj},f}$ ).

The probabilistic constraints (A-6e)-(A-6g) state that for a uncertain wind-power trajectory  $[P_t^w]_{t=1}^{N_t}$ , the chance of constraint satisfaction should be at least  $1 - \epsilon$ . Constraints (A-6h)-(A-6j) define the maximum up- and down-spinning in such a way, that  $R_t^{\text{ds}}$  will contain the absolute value of all the negative elements of  $R_t$ , and  $R_t^{\text{us}}$  will have all the positive elements.

The above CCP can be converted to a SCP. In this case, the set of soft chance constraints (A-6e)-(A-6j) will be substituted for  $N$  sets of hard constraints, where  $N$  is the number of scenarios as determined by Equation (2-3). For every set of constraints, another realization of  $[P_t^w]_{t=1}^{N_t}$  is used. Using this approach, the solution of the SCP will be an  $\epsilon$ -solution of the CCP with confidence  $1 - \beta$ .





---

# Glossary

## List of acronyms






AC	Alternating Current
ADMM	Alternating Direction Method of Multipliers
AGR	Automatic Generator Regulation
C-OPF	Convexified Optimal Power Flow
CC-OPF-RS	Chance-constrained Optimal Power Flow with Reserve Scheduling
CCP	Chance-constrained Program
CDC	Converted Direct Current
D-OPF	Decomposed Optimal Power Flow
DC	Direct Current
DSP-OPF-RS	Decomposed Scenario Parametrized Optimal Power Flow with Reserve Scheduling
DVE-OPF-RS	Decomposed Vertex Enumerated Optimal Power Flow with Reserve Scheduling
FPP-SCA	Feasible Point Pursuit-Successive Convex Approximation
HTG	Hydro Thermal Generation
IPM	Interior Point Method
MASP-OPF-RS	Multi-area Scenario Parametrized Optimal Power Flow with Reserve Scheduling
OPF-RS	Optimal Power Flow with Reserve Scheduling
OPF	Optimal Power Flow
PF	Power Flow
PSD	Positive Semidefinite
QCQP	Quadratically Constrained Quadratic Program
RCP	Robust Convex Program
RS	Reserve Scheduling
SCP	Scenario Convex Program
SDP	Semidefinite Program
SDR	Semidefinite Relaxation
SP-OPF-RS	Scenario Parametrized Optimal Power Flow with Reserve Scheduling
TSO	Transmission System Operator
VE-OPF-RS	Vertex Enumerated Optimal Power Flow with Reserve Scheduling
WPG	Wind Power Generation

## List of symbols

$\alpha$	accuracy for solution	$m$	number of constraints
$\beta$	confidence level	$M_k$	voltage magnitude data matrix
$\delta$	uncertain parameter	$n$	dimension of decision variable
$\Delta$	uncertainty set	$N_b$	number of buses
$\varepsilon$	violation level	$N_G$	number of generators
$\Gamma$	set of multipliers	$N_L$	number of lines
$\Lambda, \lambda$	multipliers	$N_s$	number of scenario
$\mathcal{A}$	set of areas	$N_t$	length of prediction horizon
$\mathcal{B}_a$	set of neighbouring areas to area $a$	$N_w$	number of wind buses
$\mathcal{E}_{ab}$	overlapping buses between $a$ and $b$	$p$	real power
$\mathcal{F}$	set of wind buses	$\mathbf{p}^{w,f}$	forecast wind power
$\mathcal{G}$	set of generator buses	$\mathbf{p}^D, \mathbf{q}^D$	real/reactive demanded power
$\mathcal{H}$	approximation of uncertainty set	$\mathbf{p}^G, \mathbf{q}^G$	real/reactive generator power
$\mathcal{L}$	set of lines	$\mathbf{p}^m$	wind mismatch
$\mathcal{N}$	set of buses	$\mathbf{p}^w$	wind power
$\mathcal{P}$	uncertainty set for wind mismatch	$q$	reactive power
$\mathcal{T}$	set of time steps	$\mathbf{r}$	reserve power
$\mathcal{T}_a$	set of tie-lines for area $a$	$\mathbf{r}^{\text{us}}, \mathbf{r}^{\text{ds}}$	up/downspinning requirements
$\mathcal{W}$	set of feasible states	$s$	apparent power
$\mu$	step size	$t$	time step
$\Theta$	set of auxiliary variables	$\mathbf{v}$	complex voltage
$\underline{\mathbf{h}}, \bar{\mathbf{h}}$	upper and lower bounds for $\mathcal{H}$	$W$	network state
$\Xi$	set of decision variables	$W^f$	network state for forecast
$a, b$	area index	$W^{\text{us}}$	upspinning coefficient matrix
$\mathbf{c}^{\text{li}}$	linear cost coefficients	$W^{\text{ds}}$	downspinning coefficient matrix
$\mathbf{c}^{\text{qu}}$	quadratic cost coefficients	$\hat{W}$	parametrized network state
$\mathbf{c}^{\text{us}}, \mathbf{c}^{\text{ds}}$	up/downspinning cost coefficients	$\mathbf{x}$	rectangular voltage
$C^G, C^w$	generator/wind connection matrix	$Y_{lm}$	real powerflow data matrix
$\mathbf{d}^{\text{us}}, \mathbf{d}^{\text{ds}}$	up/downspinning distribution	$Y_{lm}^*$	reactive powerflow data matrix
$E_{\text{ref}}$	reference bus data matrix	$Y_k$	real power injection data matrix
$k$	bus index	$Y_k^*$	reactive power injection data matrix

---

## Bibliography

- [1] A. Papavasiliou, S. S. Oren, and R. P. O'Neill, "Reserve Requirements for Wind Power Integration: A Scenario-Based Stochastic Programming Framework," *IEEE Trans. Power Syst.*, vol. 26, no. 4, pp. 2197–2206, nov 2011. [Online]. Available: <http://ieeexplore.ieee.org/document/5739566/> 
- [2] J. Warrington, P. J. Goulart, S. Mariethoz, and M. Morari, "Robust reserve operation in power systems using affine policies," in *2012 IEEE 51st IEEE Conf. Decis. Control*. Maui, Hawaii USA: IEEE, dec 2012, pp. 1111–1117. [Online]. Available: <http://ieeexplore.ieee.org/document/6425913/> 
- [3] K. Margellos, V. Rostampour, M. Vrakopoulou, M. Prandini, G. Andersson, and J. Lygeros, "Stochastic unit commitment and reserve scheduling: A tractable formulation with probabilistic certificates," in *Eur. Control Conf.*, Zurich, Switzerland, 2013, pp. 2513–2518. [Online]. Available: <http://ieeexplore.ieee.org/document/6669532/> 
- [4] M. Vrakopoulou, K. Margellos, J. Lygeros, and G. Andersson, "A Probabilistic Framework for Reserve Scheduling and N-1 Security Assessment of Systems With High Wind Power Penetration," *IEEE Trans. Power Syst.*, vol. 28, no. 4, pp. 3885–3896, nov 2013. [Online]. Available: <http://ieeexplore.ieee.org/document/6570751/> 
- [5] V. Rostampour, "Tractable Reserve Scheduling Formulations for Power Systems with Uncertain Generation," MSc Thesis, Politecnico di Milano, 2012.
- [6] D. Bienstock, M. Chertkov, and S. Harnett, "Chance-Constrained Optimal Power Flow: Risk-Aware Network Control under Uncertainty," *SIAM Rev.*, vol. 56, no. 3, pp. 461–495, jan 2014. [Online]. Available: <http://epubs.siam.org/doi/10.1137/130910312> 
- [7] G. Andersson, *Electric power systems*, 2010.
- [8] B. Stott, J. Jardim, and O. Alsac, "DC Power Flow Revisited," *IEEE Trans. Power Syst.*, vol. 24, no. 3, pp. 1290–1300, aug 2009. [Online]. Available: <http://ieeexplore.ieee.org/document/4956966/> 



- [9] J. Lavaei and S. H. Low, “Zero Duality Gap in Optimal Power Flow Problem,” *IEEE Trans. Power Syst.*, vol. 27, no. 1, pp. 92–107, feb 2012. [Online]. Available: <http://ieeexplore.ieee.org/document/5971792/>



- [10] V. Rostampour, K. Margellos, M. Vrakopoulou, M. Prandini, G. Andersson, and J. Lygeros, “Reserve requirements in AC power systems with uncertain generation,” in *IEEE PES ISGT Eur. 2013*. Copenhagen, Denmark: IEEE, oct 2013, pp. 1–5. [Online]. Available: <http://ieeexplore.ieee.org/document/6695354/>



- [11] M. Vrakopoulou, M. Katsampani, K. Margellos, J. Lygeros, and G. Andersson, “Probabilistic security-constrained AC optimal power flow,” in *2013 IEEE Grenoble Conf.* Grenoble, France: IEEE, jun 2013, pp. 1–6. [Online]. Available: <http://ieeexplore.ieee.org/document/6652374/>



- [12] M. Chamanbaz, F. Dabbene, and C. Lagoa, “AC optimal power flow in the presence of renewable sources and uncertain loads,” *IEEE Trans. Power Syst.*, feb 2017. [Online]. Available: <http://arxiv.org/abs/1702.02967>



- [13] A. Venzke, L. Halilbasic, U. Markovic, G. Hug, and S. Chatzivasileiadis, “Convex Relaxations of Chance Constrained AC Optimal Power Flow,” pp. 1–8, feb 2017. [Online]. Available: <http://arxiv.org/abs/1702.08372>



- [14] A. Y. Lam, B. Zhang, and D. N. Tse, “Distributed algorithms for optimal power flow problem,” in *2012 IEEE 51st IEEE Conf. Decis. Control*. IEEE, dec 2012, pp. 430–437. [Online]. Available: <http://ieeexplore.ieee.org/document/6427082/>



- [15] D. K. Molzahn, J. T. Holzer, B. C. Lesieutre, and C. L. DeMarco, “Implementation of a Large-Scale Optimal Power Flow Solver Based on Semidefinite Programming,” *IEEE Trans. Power Syst.*, vol. 28, no. 4, pp. 3987–3998, nov 2013. [Online]. Available: <http://ieeexplore.ieee.org/document/6510541/>



- [16] R. Madani, M. Ashraphijuo, and J. Lavaei, “Promises of Conic Relaxation for Contingency-Constrained Optimal Power Flow Problem,” *IEEE Trans. Power Syst.*, vol. 31, no. 2, pp. 1297–1307, mar 2016. [Online]. Available: <http://ieeexplore.ieee.org/document/7065336/>



- [17] G. Andersson, *Modelling and Analysis of Electric Power Systems*. ETH Zurich, 2008.
- [18] S. Frank, I. Steponavice, and S. Rebennack, “Optimal power flow: a bibliographic survey II,” *Energy Syst.*, vol. 3, no. 3, pp. 259–289, sep 2012. [Online]. Available: <http://link.springer.com/10.1007/s12667-012-0057-x>














- [19] M. Cain, R. O’Neill, and A. Castillo, “History of Optimal Power Flow and Formulations,” Federal Energy Regulatory Commission, Tech. Rep., 2012. [Online]. Available: <http://www.ferc.gov/industries/electric/indus-act/market-planning/opf-papers/acopf-1-history-formulation-testing.pdf>

- [20] J. Carpentier, “Contribution a l’étude du dispatching économique,” *Bull. Soc. Fr. des Electr.*, vol. 3, pp. 431–777, aug 1962.

- [21] D. Bienstock, “Progress on solving power flow problems,” *Optima*, no. 93, pp. 1–7, 2013.

- [22] M. Negnevitsky, D. H. Nguyen, and M. Piekutowski, "Risk Assessment for Power System Operation Planning With High Wind Power Penetration," *IEEE Trans. Power Syst.*, vol. 30, no. 3, pp. 1359–1368, may 2015. [Online]. Available: <http://ieeexplore.ieee.org/document/6870479/> 
- [23] M. Lange and U. Focken, "New developments in wind energy forecasting," in *2008 IEEE Power Energy Soc. Gen. Meet. - Convers. Deliv. Electr. Energy 21st Century*. Pittsburgh, PA, USA: IEEE, jul 2008, pp. 1–8. [Online]. Available: <http://ieeexplore.ieee.org/document/4596135/> 
- [24] P. Pinson, "Wind Energy: Forecasting Challenges for Its Operational Management," *Stat. Sci.*, vol. 28, no. 4, pp. 564–585, nov 2013. [Online]. Available: <http://projecteuclid.org/euclid.ss/1386078879> 
- [25] S. Boyd and L. Vandenberghe, *Convex Optimization*. Cambridge University Press, 2004.
- [26] S. Bubeck, "Convex Optimization: Algorithms and Complexity," *Found. Trends® Mach. Learn.*, vol. 8, no. 3-4, pp. 231–357, 2015. [Online]. Available: <http://www.nowpublishers.com/article/Details/MAL-050> 
- [27] Y. Nesterov and A. Nemirovskii, *Interior-Point Polynomial Algorithms in Convex Programming*. Society for Industrial and Applied Mathematics, jan 1994. [Online]. Available: <http://epubs.siam.org/doi/book/10.1137/1.9781611970791> 
- [28] L. Vandenberghe and S. Boyd, "Semidefinite Programming," *SIAM Rev.*, vol. 38, no. 1, pp. 49–95, mar 1996. [Online]. Available: <http://epubs.siam.org/doi/abs/10.1137/1038003> 
- [29] R. D. C. Monteiro, "First- and second-order methods for semidefinite programming," *Math. Program.*, vol. 97, no. 1, pp. 209–244, jul 2003. [Online]. Available: <http://link.springer.com/10.1007/s10107-003-0451-1> 
- [30] R. D. C. Monteiro and P. Zanjácomo, "Implementation of primal-dual methods for semidefinite programming based on Monteiro and Tsuchiya Newton directions and their variants," *Optim. Methods Softw.*, vol. 11, no. 1-4, pp. 91–140, jan 1999. [Online]. Available: <http://www.tandfonline.com/doi/abs/10.1080/10556789908805749> 
- [31] J. F. Sturm, "Using SeDuMi, a MATLAB toolbox for optimization over symmetric cones," 2001.
- [32] G. Venter, "Review of Optimization Techniques," in *Encycl. Aerosp. Eng.* Chichester, UK: John Wiley & Sons, Ltd, dec 2010, pp. 1–12. [Online]. Available: <http://doi.wiley.com/10.1002/9780470686652.eae495> 
- [33] A. Ben-Tal and A. Nemirovski, "Robust Convex Optimization," *Math. Oper. Res.*, vol. 23, no. 4, pp. 769–805, nov 1998. [Online]. Available: <http://pubsonline.informs.org/doi/abs/10.1287/moor.23.4.769> 
- [34] G. Calafiore and M. Campi, "The Scenario Approach to Robust Control Design," *IEEE Trans. Automat. Contr.*, vol. 51, no. 5, pp. 742–753, may 2006. [Online]. Available: <http://ieeexplore.ieee.org/document/1632303/> 

- [35] M. C. Campi and S. Garatti, “The Exact Feasibility of Randomized Solutions of Uncertain Convex Programs,” *SIAM J. Optim.*, vol. 19, no. 3, pp. 1211–1230, jan 2008. [Online]. Available: <http://epubs.siam.org/doi/10.1137/07069821X>
- [36] T. Alamo, R. Tempo, and A. Luque, “On the sample complexity of randomized approaches to the analysis and design under uncertainty,” in *Proc. 2010 Am. Control Conf.*, no. 1. Baltimore, MD: IEEE, jun 2010, pp. 4671–4676. [Online]. Available: <http://ieeexplore.ieee.org/document/5531078/>
- [37] S. Formentin, F. Dabbene, R. Tempo, L. Zaccarian, and S. M. Savaresi, “Scenario optimization with certificates and applications to anti-windup design,” in *53rd IEEE Conf. Decis. Control.* IEEE, dec 2014, pp. 2810–2815. [Online]. Available: <http://ieeexplore.ieee.org/document/7039820/>
- [38] S. Boyd, “Distributed Optimization and Statistical Learning via the Alternating Direction Method of Multipliers,” *Found. Trends® Mach. Learn.*, vol. 3, no. 1, pp. 1–122, 2010. [Online]. Available: <http://www.nowpublishers.com/article/Details/MAL-016>
- [39] R. Glowinski and A. Marroco, “Sur l’approximation, par éléments finis d’ordre un, et la résolution, par pénalisation-dualité d’une classe de problèmes de Dirichlet non linéaires,” *ESAIM Math. Model. Numer. Anal. - Modélisation Mathématique Anal. Numérique*, vol. 9, no. R2, pp. 41–76, 1975. [Online]. Available: <https://eudml.org/doc/193269>
- [40] B. He and X. Yuan, “On non-ergodic convergence rate of Douglas–Rachford alternating direction method of multipliers,” *Numer. Math.*, vol. 130, no. 3, pp. 567–577, jul 2015. [Online]. Available: <http://link.springer.com/10.1007/s00211-014-0673-6>
- [41] J. Morales, A. Conejo, and J. Perez-Ruiz, “Economic Valuation of Reserves in Power Systems With High Penetration of Wind Power,” *IEEE Trans. Power Syst.*, vol. 24, no. 2, pp. 900–910, may 2009. [Online]. Available: <http://ieeexplore.ieee.org/document/4814478/>
- [42] T. F. Gonzalez and T. F., *Handbook of approximation algorithms and metaheuristics*. Chapman & Hall/CRC, 2007.
- [43] K. Lehmann, A. Grastien, and P. Van Hentenryck, “AC-Feasibility on Tree Networks is NP-Hard,” *IEEE Trans. Power Syst.*, vol. 31, no. 1, pp. 798–801, jan 2016. [Online]. Available: <http://ieeexplore.ieee.org/document/7063278/>
- [44] W. Tinney and C. Hart, “Power Flow Solution by Newton’s Method,” *IEEE Trans. Power Appar. Syst.*, vol. PAS-86, no. 11, pp. 1449–1460, nov 1967. [Online]. Available: <http://ieeexplore.ieee.org/document/4073219/>
- [45] A. Bakirtzis, P. Biskas, C. Zoumas, and V. Petridis, “Optimal power flow by enhanced genetic algorithm,” *IEEE Trans. Power Syst.*, vol. 17, no. 2, pp. 229–236, may 2002. [Online]. Available: <http://ieeexplore.ieee.org/document/1007886/>
- [46] Z.-q. Luo, W.-k. Ma, A. So, Y. Ye, and S. Zhang, “Semidefinite Relaxation of Quadratic Optimization Problems,” *IEEE Signal Process. Mag.*, vol. 27, no. 3, pp. 20–34, may 2010. [Online]. Available: <http://ieeexplore.ieee.org/document/5447068/>

- [47] X. Bai, H. Wei, K. Fujisawa, and Y. Wang, "Semidefinite programming for optimal power flow problems," *Int. J. Electr. Power Energy Syst.*, vol. 30, no. 6-7, pp. 383–392, jul 2008. [Online]. Available: <http://linkinghub.elsevier.com/retrieve/pii/S0142061507001378> 
- [48] R. Madani, S. Sojoudi, and J. Lavaei, "Convex Relaxation for Optimal Power Flow Problem: Mesh Networks," *IEEE Trans. Power Syst.*, vol. 30, no. 1, pp. 199–211, jan 2015. [Online]. Available: <http://ieeexplore.ieee.org/document/6822653/> 
- [49] V. Rostampour and T. Keviczky, "Probabilistic Energy Management for Building Climate Comfort in Smart Thermal Grids with Seasonal Storage Systems," in *IFAC World Congr. 2017*, nov 2016. [Online]. Available: <http://arxiv.org/abs/1611.03206> 
- [50] R. Grone, C. R. Johnson, E. M. Sá, and H. Wolkowicz, "Positive definite completions of partial Hermitian matrices," *Linear Algebra Appl.*, vol. 58, no. C, pp. 109–124, apr 1984. [Online]. Available: <http://linkinghub.elsevier.com/retrieve/pii/0024379584902076> 
- [51] L. Vandenberghe and M. S. Andersen, "Chordal Graphs and Semidefinite Optimization," *Found. Trends® Optim.*, vol. 1, no. 4, pp. 241–433, 2015. [Online]. Available: <http://www.nowpublishers.com/article/Details/OPT-006> 
- [52] M. Fukuda, M. Kojima, K. Murota, and K. Nakata, "Exploiting Sparsity in Semidefinite Programming via Matrix Completion I: General Framework," *SIAM J. Optim.*, vol. 11, no. 3, pp. 647–674, jan 2001. [Online]. Available: <http://epubs.siam.org/doi/10.1137/S1052623400366218> 
- [53] A. Ahmadi-Khatir, A. J. Conejo, and R. Cherkaoui, "Multi-Area Unit Scheduling and Reserve Allocation Under Wind Power Uncertainty," *IEEE Trans. Power Syst.*, vol. 29, no. 4, pp. 1701–1710, jul 2014. [Online]. Available: <http://ieeexplore.ieee.org/document/6689354/> 
- [54] R. Madani, A. Kalbat, and J. Lavaei, "ADMM for sparse semidefinite programming with applications to optimal power flow problem," in *2015 54th IEEE Conf. Decis. Control*. Osaka, Japan: IEEE, dec 2015, pp. 5932–5939. [Online]. Available: <http://ieeexplore.ieee.org/document/7403152/> 
- [55] H. Zhu and G. B. Giannakis, "Multi-area state estimation using distributed SDP for nonlinear power systems," in *2012 IEEE Third Int. Conf. Smart Grid Commun.* IEEE, nov 2012, pp. 623–628. [Online]. Available: <http://ieeexplore.ieee.org/document/6486055/> 
- [56] A. Nedić and A. Ozdaglar, "Cooperative distributed multi-agent optimization," in *Convex Optim. Signal Process. Commun.*, D. P. Palomar and Y. C. Eldar, Eds. Cambridge: Cambridge University Press, 2010, pp. 340–386. [Online]. Available: <http://ebooks.cambridge.org/ref/id/CBO9780511804458A099> 
- [57] W. Shi, Q. Ling, K. Yuan, G. Wu, and W. Yin, "On the Linear Convergence of the ADMM in Decentralized Consensus Optimization," *IEEE Trans. Signal Process.*, vol. 62, no. 7, pp. 1750–1761, apr 2014. [Online]. Available: <http://ieeexplore.ieee.org/document/6731604/> 





[58] G. Papaefthymiou and B. Klockl, "MCMC for Wind Power Simulation," *IEEE Trans. Energy Convers.*, vol. 23, no. 1, pp. 234–240, mar 2008. [Online]. Available: <http://ieeexplore.ieee.org/document/4453993/>



[59] M. Vrakopoulou, "Optimal Decision Making for Secure and Economic Operation of Power Systems Under Uncertainty," PhD Thesis, ETH Zurich, 2013.



[60] "Power Systems Test Case Archive," *Univ. Washingt.* [Online]. Available: <http://www.ee.washington.edu/research/pstca>



[61] J. Löfberg, "YALMIP : A Toolbox for Modeling and Optimization in MATLAB," in *CACSD Conf.*, Tapei, Taiwan, 2004.



[62] M. ApS, "The MOSEK optimization toolbox for MATLAB manual," 2016. [Online]. Available: <http://docs.mosek.com/7.1/toolbox/index.html>



[63] Gurobi Optimization Inc., "Gurobi Optimizer Reference Manual," 2016.



[64] R. D. Zimmerman and C. E. Murillo-s, "Matpower 5. 1 User's Manual," p. 168, 2015. [Online]. Available: <http://www.pserc.cornell.edu/matpower>



[65] R. Madani, M. Ashraphijuo, and J. Lavaei, "SDP Solver of Optimal Power Flow User's Manual," pp. 1–8, 2014.



[66] O. Megel, J. L. Mathieu, and G. Andersson, "Scheduling distributed energy storage units to provide multiple services," in *2014 Power Syst. Comput. Conf.* IEEE, aug 2014, pp. 1–7. [Online]. Available: <http://ieeexplore.ieee.org/document/7038358/>



[67] M. A. Ortega-Vazquez, D. S. Kirschen, and Y. Dvorkin, "Wind generation as a reserve provider," *IET Gener. Transm. Distrib.*, vol. 9, no. 8, pp. 779–787, may 2015. [Online]. Available: <http://digital-library.theiet.org/content/journals/10.1049/iet-gtd.2014.0614>



[68] O. Mehanna, K. Huang, B. Gopalakrishnan, A. Konar, and N. D. Sidiropoulos, "Feasible Point Pursuit and Successive Approximation of Non-Convex QCQPs," *IEEE Signal Process. Lett.*, vol. 22, no. 7, pp. 804–808, jul 2015. [Online]. Available: <http://ieeexplore.ieee.org/document/6954488/>



[69] A. S. Zamzam, N. D. Sidiropoulos, and E. Dall'Anese, "Beyond Relaxation and Newton-Raphson: Solving AC OPF for Multi-phase Systems with Renewables," pp. 1–10, dec 2016. [Online]. Available: <http://arxiv.org/abs/1612.07255>